January 2020

Surfactant-Nanoparticle Augmented Systems For Enhanced Oil Recovery: Formula Development And Evaluation

Xun Zhong

Follow this and additional works at: https://commons.und.edu/theses

SURFACTANT-NANOPARTICLE AUGMENTED SYSTEMS FOR ENHANCED OIL
RECOVERY: FORMULA DEVELOPMENT AND EVALUATION

by

Xun Zhong

Bachelor of Science, China University of Petroleum (East China), 2014

Master of Engineering, China University of Petroleum (East China), 2017

A Dissertation

Submitted to the Graduate Faculty

of the

University of North Dakota

In partial fulfillment of the requirements

for the degree of

Doctor of Philosophy

Grand Forks, North Dakota

May

2020

i

This dissertation, submitted by Xun Zhong in partial fulfillment of the requirements for the Degree of Doctor of Philosophy from the University of North Dakota, has been read by the Faculty Advisory Committee under whom the work has been done, and is hereby approved.
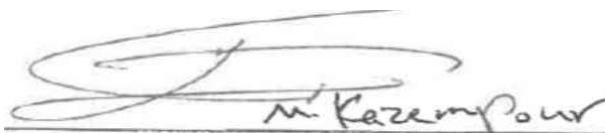
Dr. Hui Pu

Dr. Vamegh Rasouli

Dr. Kegang Ling

Dr. Julia Xiaojun Zhao

Dr. Mahdi Kazempour

This dissertation is being submitted by the appointed advisory committee as having met all of the requirements of the Graduate School at the University of North Dakota and is hereby approved.

Dean of the School of Graduate Studies

04/01/20

Date

ii

PERMISSION

Title   Surfactant-Nanoparticle Augmented Systems for Enhanced Oil Recovery: Formula Development and Evaluation

Department   Petroleum Engineering

Degree   Doctor of Philosophy

In presenting this dissertation in partial fulfillment of the requirements for a graduate degree from the University of North Dakota, I agree that the library of this University shall make it freely available for inspection. I further agree that permission for extensive copying for scholarly purposes may be granted by the professor who supervised my dissertation work or, in his absence, by the Chairperson of the department or the dean of the Graduate School. It is understood that any copying or publication or other use of this dissertation or part thereof for financial gain shall not be allowed without my written permission. It is also understood that due recognition shall be given to me and to the University of North Dakota in any scholarly use which may be made of any material in my dissertation.

Xun Zhong
May 1, 2020

TABLE OF CONTENTS

LISTS OF FIGUTRES

LISTS OF TABLES

LISTS OF SCHEMELS

ACKNOWLEDGEMENTS

ABSTRACT

Surfactant enhanced oil recovery (EOR) technology has received much attraction due to its excellent capability to increase the displacement efficiency by altering the wettability, lowering the oil-water interfacial tension and mobilizing the remaining oil. However, surfactant systems are widely acknowledged to have either low or high adsorption on solid (rock/clay/sediment) surfaces. The adsorption density can be affected by adsorbents, surfactant structure, experimental conditions and some other factors. Also, the driving forces for adsorption vary with different surfactants types. Generally speaking, electrostatic interactions are more prominent for anionic, cationic and zwitterionic surfactants, while chemical interactions are more common for nonionic surfactants.

Proper surfactant adsorption on mineral surfaces can modify interfacial properties and enhance oil recovery while excessive adsorption might result in high cost and limited effectiveness. Economic concerns about chemical flooding should be taken as opportunities to develop new cost-effective formulas that lead to high recoveries. According to the published studies, nanomaterials are good candidates for sacrificial agents or surfactant carriers, meanwhile, some positive synergistic effects produced by mixing surfactants with nanoparticles are favorable for additional oil production. The EOR performance of different nanomaterials together with their limitations were systematically reviewed in Chapter III.

Nonionic surfactants, which occupy over 40.0 % of the global surfactant production, are nonvolatile and benign chemicals widely used in the oil and gas industry. However, their high adsorption loss especially at high temperature and high salinity conditions would limit their large-scale applications. Surfactant MERPOL HCS is a commercial product with cloud point higher than 100 ℃. By integrating hydrophilic silica nanoparticles with surfactant MERPOL HCS, surfactant adsorption was reduced and oil production rate was generally increased. More than 34.0 % OOIP

1

and over 4.0 % OOIP additional oil was recovered compared with 2000 mg/L KCl imbibition and pure surfactant imbibition, respectively. In addition, particles with smaller size turned out to be more effective surfactant carriers and better performance enhancers. However, due to the stability issues of nanoparticles and surfactant, the developed nonionic surfactant-hydrophilic silica nanoparticle augmented system was more suitable for low salinity conditions and the details were shown in Chapter IV.

In order to extend the applications of surfactant-nanoparticle systems to higher salinity conditions, improvements are required. First, the selected surfactant should have higher resistance towards high salinity and elevated temperature. Second, the steric stability of pure nanoparticles should be improved because in normal cases, using surfactant alone as a nanoparticle stabilizer is not enough to overcome the adverse impacts of salts especially when environmental temperature increases. Therefore, in Chapter V, a novel nanofluid formula was developed by integrating a zwitterionic surfactant CAPHS with GLYMO modified silica nanoparticles. According to our experiments, the proposed nanofluid was not sensitive to either monovalent or divalent cations, whose size remained around 10.0 nm in API brine within 8 weeks at 25 ℃ and 4 weeks at 60 ℃. The addition of surfactant into pure nanoparticle systems significantly reduced the concentration of nanoparticles required to induce wettability alteration and the possibility of severe permeability impairment. The presence of nanoparticles also effectively decreased surfactant adsorption loss on rocks and the surfactant concentration needed to produce a low interfacial tension. Moreover, the oil-wet solid surface could be altered to a more water-wet condition beneficial for water imbibition and oil displacement. Core flooding tests showed that the nanofluid composed of 800 mg/L zwitterionic surfactant and 2000 mg/L GLYMO modified silica nanoparticles was able to recover additional 3.12 % and 5.39 % OOIP from Berea sandstone cores in the tertiary recovery mode after

surfactant flooding and pure nanoparticle flooding, respectively.

The total dissolved solids in the API brine is 10.0 wt.% and the highest testing temperature is only 60 °C in our study. These conditions are still less harsh than the salinity of formation brine and reservoir temperature in most unconventional reservoirs. Therefore, some recommendations are proposed in the Conclusions and Recommendations section. The development of surfactant-nanoparticle augmented systems with higher stability should be continued and the emphasis should be put on the new nanomaterials with small size, novel surfactants, low cost and high efficiency.

CHAPTER I

BACKGROUND INTRODUCTION

1. Motivations

Traditional fossil energy including oil and gas sources is anticipated to continue to dominate the energy market and the global energy demand is estimated to increase by another 60.0 % over the next few decades (Hendraningrat et al., 2013; Almahfood and Bai, 2018). Boosting the production of the existing reservoirs and developing new oilfields are believed to be two feasible ways to mitigate the gap between energy demand and energy supply.

However, most of the existing reservoirs have already entered or are entering into their last stages of production encountered with increased water cut and decreased production rate. Meanwhile, searching and developing new oilfields can be difficult and time-consuming. According to Thomas (2008), after conventional recovery methods were exhausted, there was still 0.3×10^{12} m^3 conventional oil and 0.8×10^{12} m^3 of heavy oil remaining in the existing reservoirs worldwide. Given the low recovery factors in most old oilfields and the huge amount of remaining oil, applying enhanced oil recovery (EOR) technologies is of prime importance and meaningful (Kiani et al., 2016). Commonly applied EOR methods are thermal flooding, chemical flooding and miscible flooding, with varying targets for different types of hydrocarbons. The EOR target for light oil reservoirs is around 45.0 % OOIP, compared to that of over 85.0 % for heavy oils and oil sands (Figure 1-1). Chemical methods utilizing chemical formulas as displacing fluids that possess various EOR mechanisms such as interfacial tension reduction, wettability alteration, mobility control etc., are believed to hold the promise for the future thanks to the good results reported in both lab-scale tests and field-scale tests.
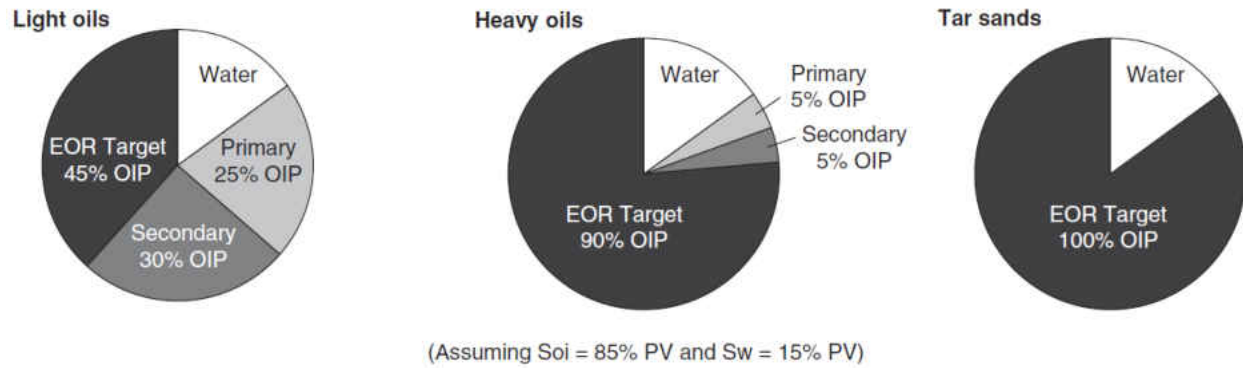
Figure 1-1 EOR target for different hydrocarbons (Thomas, 2008).

The purpose of EOR is to modify the physical and chemical properties of reservoirs (including minerals and fluids), thereby to increase the oil recovery factor (Nieto-Alvarez et al., 2014). Surfactants with excellent capability to reduce the oil-water interfacial tension and/or alter rock wettability are very popular in EOR area, and lab-scale studies have proved their effectiveness to unlock the trapped oil. However, their commercial scale applications are always restrained by excessive surfactant loss due to surfactant adsorption and interactions with formation fluids especially at some incompatible conditions.

Nanotechnology has gained considerable interest in recent decades and gradually developed into the leading-edge EOR technology for oil and gas industry. Nanomaterials usually have a size of 1-100 nm, which is much smaller than the typical pore size of 5-50 μm, thus, ensuring their applicability in low-permeable reservoirs with small pores and narrow pore throats. Commonly-used nanomaterials include metal oxide nanomaterial, carbon-based nanomaterial, and silica-based nanomaterial. Silica-based nanomaterial has long been the most popular one because of its superiority in great marketing potentiality, broad availability, low cost for fabrication, low toxicity and simplicity in surface modification. However, pure silica nanoparticles hardly have any impacts on IFT (Metin et al., 2012) and in most cases relatively high particle concentration (≥ 1.0 wt.%) is required to induce noticeable wettability alteration (Jiang et al., 2017; Jang, et al., 2018).

2

Yuan et al. (2017) reported that even when the applied nanomaterials have super good dispersity in the dispersant, the permeability reduction caused by nanomaterial adsorption and straining was huge, and the adverse effects were observed to increase with increasing nanomaterial concentrations.

Surfactant-nanoparticle augmented systems have been a research focus in recent years because of their synergistic effects, such as increased particle stability, reduced particle dosage, reduced surfactant adsorption loss and enhanced recovery efficiency (Almahfood and Bai, 2018).

2. Research Objectives

An experimental study on the development and evaluation of novel surfactant-nanoparticle augmented systems was conducted. In this study, surfactant-nanoparticle systems suitable for different reservoir conditions (salinity and temperature) are fabricated and the synergistic effects between surfactant and nanoparticles on interfacial properties as well as enhanced oil recovery were systematically evaluated.

3. Dissertation Organization

This dissertation is composed of six chapters. First, the background introduction of this work is provided in Chapter I, which includes the motivations, research objectives and dissertation organization. Chapter III is a review on the applications of nanomaterials in EOR area, Chapters II, IV, V were originated from published journal papers, all of which are my first authorship around the topics of surfactant or surfactant-nanoparticle augmented systems and Chapter VI is the conclusions and recommendations. Details were provided as following.

In Chapter II, we first performed a series of surfactant selection experiments in order to have an overall idea of the applicable conditions of different surfactants. Meanwhile, the adsorption behaviors of different types of surfactants on different kinds of adsorbents were

systematically studied considering the effects of salinity and temperature. By applying Minitab software, a non-linear model with high accuracy was proposed to predict the adsorption density of surfactants at some other conditions.

Chapter III is a review of the most recent publications of nano-EOR. Nanomaterials according to the physical and chemical characters were clarified into three categories: metal oxide nanomaterials, carbon-based nanomaterials and silica-based nanomaterials. Different results were reported in different studies. Nanomaterials can either be used alone or cooperate with other additives such as surfactants and polymers. However, the stability of nanomaterials especially at harsh reservoir conditions is always a great concern, particle retention and aggregation would cause porosity and permeability impairment, and therefore result in reduced efficiency. Meanwhile, deeper theoretical and numerical investigations at nanoscale and the studies on the potential toxicity of nanomaterials to the environment and human body should be continued.

Chapter IV is an intensive study on the development and evaluation of a nonionic surfactant-hydrophilic silica nanoparticle augmented system. The study was conducted at low salinity (0.2 wt.% KCl) and elevated temperature (60 ℃). The adsorption behavior, interfacial properties and EOR performance of the developed nanofluid were systematically studied. Introducing hydrophilic silica nanoparticles into nonionic surfactant system reduced surfactant adsorption loss, rendered further reduction in oil-water interfacial tension and resulted in a more water-wet condition beneficial for oil production process.

Chapter V mainly focuses on the fabrication and evaluation of a zwitterionic surfactant-silica nanoparticle system. Prior to mixing with surfactant, silica nanoparticles were first surface modified with a hydrophilic coupling agent to maintain necessary steric stabilization. Addition of zwitterionic surfactant further increased the electrostatic stabilization. This augmented formula

showed high stability at 60 °C, API brine (8.0 wt.% NaCl + 2.0 wt.% KCl) conditions. Due to synergistic effects between surfactant and nanoparticles, low IFTs could be achieved at surfactant concentrations as low as 10 mg/L. Meanwhile, thanks to their weak interactions, the concentration ratios between surfactant and nanoparticles can be adjusted flexibly to obtain different IFTs and various wetting conditions. The EOR potential of the developed surfactant-nanoparticle augmented system was verified by core flooding experiments in the tertiary recovery mode. Additional oil was recovered by this proposed surfactant-nanoparticle formula after surfactant or pure nanoparticle flooding.

Upon all the efforts and attempts made on the leading role of this research topic, some conclusions were summarized in Chapter VI and besides, both challenges encountered in the way and prospects envisioned in the upcoming years were stated and discussed.

CHAPTER II

COMPARATIVE STUDY ON THE STATIC ADSORPTION BEHAVIOR OF ZWITTERIONIC

SURFACTANTS ON MINERALS IN THE MIDDLE BAKKEN FORMATION

1. Introduction

1.1. The Middle Bakken Formation.

The Bakken Formation occupying nearly 200,000 square miles of the subsurface of the Williston basin, is a huge rock unit from the late Devonian to early Mississippian age. It is one of the most significant contiguously deposited tight oil and gas play in the United States that has been developed through the last decade (Geri et al., 2019). The distribution map of the Bakken Formation is given in Figure 2-1, which spreads over Montana, North Dakota and Saskatchewan. In North Dakota, the Bakken Formation is a thin and clastic unit straddles the Devonian-Mississippian boundary and has a maximum thickness of around 46 meters in the central part of the basin (Lefever et al., 1991). The rock unit is mainly composed of three members, the Lower Shale Member, the Middle Bakken Member and the Upper Shale Member (Table 2-1). The three members show an onlapping relationship with each successively higher member exhibiting wider areal distribution and greater converge towards the marginal shelf areas of Williston Basin (Lefever et al., 1991). Different from the Lower and Upper Members, the mineralogy of the Middle Bakken Member is highly variable, which ranges from clastics (silt and sandstone) to carbonates (primarily dolomite). The detailed geomechanical properties of each layer were compared in Table 2-1 (Deri et al., 2019; Li et al., 2015a).

The first time when oil was discovered within the Bakken Formation was in 1951, but its large-scale production was restricted by the technical conditions at that time. The applications of

6

hydraulic fracturing and horizontal drilling technologies have boosted the Bakken oil production since year 2000 and the production rate reached 1,517,796 barrels per day by October 2019. The United States Geological Survey (USGS) estimates that there are around 7.4 billion barrels of undiscovered, technically recoverable oil in the Bakken Formation.
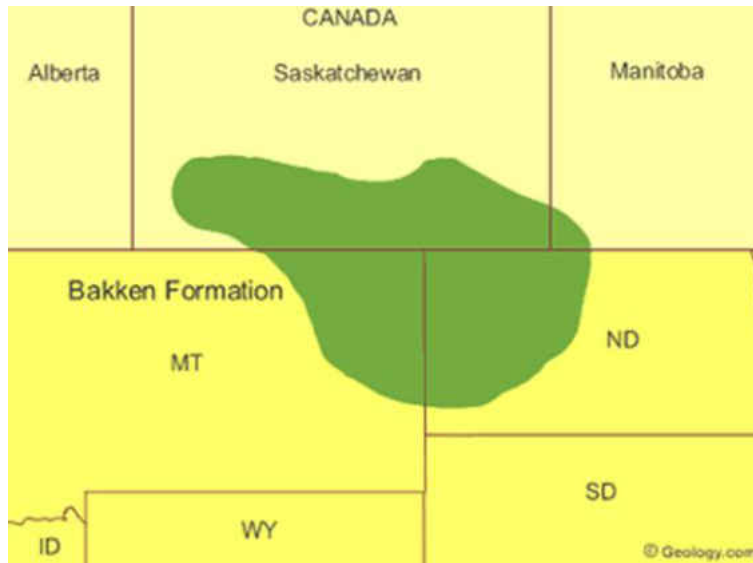
Figure 2-1 Distribution map of the Bakken Formation (Geology.com)

Table 2-1 Lithology of the Bakken Formation (Deri et al., 2019)

Zone name	Lithology	Maximum thickness, m	Description
Upper Bakken	Dark grey to brownish-black to black, fissile, noncalcareous, carbonaceous and bituminous shale	2 ~ 18	Lithologically uniform Fossiliferous
Middle Bakken	Light grey to medium dark grey of siltstones and sandstones, massive or finely laminated	4 ~ 27	Lithologically variable
Lower Bakken	Dark grey to brownish-black to black, non-calcareous, fissile, slightly to highly organic-rich shale	6 ~ 17	Lithologically uniform Rich in pyrite

The Middle Bakken Member, which favorably positioned with respect to excellent source and seal units, has been a research focus since its early exploration. However, the geological heterogeneity, completion methods and fluids as well as depletion strategy all have impacts on its

production. The Middle Bakken Member is characterized as a typical unconventional liquid reservoir (ULR) with narrow pores, low porosity (< 8.0 %), low permeability (< 0.1×10^{-3} μm^2), high salinity (TDS= 150 ~ 300 g/L) and high reservoir temperature (80 ~ 120 ℃). Meanwhile, its primary oil recovery is fairly low, which is lower than 10.0 % of original oil in place (OOIP). The great challenge that petroleum engineers encounter is how to extract the remaining crude oil from this low-permeability pay zones efficiently and economically. In this point, EOR technologies are necessary (Sonnenberg et al., 2011; Rui et al., 2018; Wang et al., 2018). The main purpose of EOR technologies is to modify the physical and chemical properties of the reservoirs (including minerals and fluids), thereby to increase the oil recovery factor (Nieto-Alvarez et al., 2014).

1.2. Surfactant EOR.

Either discovering new oilfields or increasing the production rate from existing oilfields can help to relieve the growing global demand for oil and gas. However, given the facts that searching and developing new reserves can be difficult and time-consuming and there is still about two-thirds of oil remains unrecovered in those existing oilfields, application of EOR technologies turns out to be an important and hot research area (Kamal et al., 2017). Commonly applied EOR technologies are thermal flooding, chemical flooding and miscible flooding with varying targets for different types of hydrocarbons. The major functional mechanisms of thermal methods are to reduce oil viscosity and improve the mobility ratio, hence, this EOR technology is the best choice for heavy oils with API gravity of 10 ~ 20° and oil sand with API gravity lower than 10°. Non-thermal methods are more suitable for light oils with viscosity lower than 100 cp. By injecting miscible gases into the formation, miscible flooding is able to maintain the reservoir pressure and reduce oil viscosity. Meanwhile, the interfacial tension can be hugely decreased due to the disappearance of interfaces. However, its commercial applications are limited by the low sweep

efficiency, high cost, resulted asphaltene precipitation and some other problems related to gas availability and separation. By injecting some chemicals like surfactants, alkaline or polymers into the formation, chemical flooding serves the EOR purpose through different mechanisms such as interfacial tension reduction, wettability alteration, mobility control etc. Laboratory reports show that chemical EOR is able to recover 20.0 ~ 30.0 % additional oil compared to that of around 12.0 ~ 30.0 % in the field tests (Pope, 2011; Kamal et al., 2015). Chemical flooding is therefore believed to hold the promise for the future. Generally speaking, the objective of EOR technologies is to increase the volumetric sweep efficiency (macroscopic efficiency) and/or the displacement efficiency (microscopic efficiency). Usually, sweep efficiency is related to the effectiveness of displacing fluids contacting the reservoir volume, while displacement efficiency is related to the oil displacement at pore scale. Sometimes even though the sweep efficiency is high, the displacement efficiency can be low because oil would be trapped by capillary forces due to unfavorable wetting conditions, therefore, capillary number (Equation 2-1, dimensionless) is applied to describe the relationships between the viscous forces and capillary forces.

$$N_c = \frac{Viscosity\ force}{Capillary\ force} = \frac{\mu v}{\gamma cos\theta} \tag{2-1}$$

Where N_c is the capillary number, μ is the dynamic viscosity of the displacing fluid, v is the displacement velocity, γ is the oil/aqueous interfacial tension (IFT), and θ is the contact angle. When the formation is oil-wet, larger capillary number favors oil production process, which can be achieved by increasing the viscosity of the displacing fluid (sweep efficiency), decreasing capillary force or reducing the IFT. However, when the formation becomes water-wet, capillary force turns to be the driving force, at which case intermediate IFT may be better. Intermediate IFT is beneficial for the penetration of displacing fluid into the highly oil-saturated matrix or natural

fracture regions and accelerate the extraction of the oil in place by rapid imbibition (Kamal et al., 2017).

Surfactant, composed of a polar part (hydrophilic head) and a non-polar part (hydrophobic tail) is a kind of classical chemicals, which enjoys great popularity in chemical EOR area and has been a sustained subject in the past few decades (Song et al., 2016). The amphiphilic nature of surfactant molecules endows them excellent capability to change interfacial properties such as oil/water IFT and rock wettability. Oil/water IFT is the result of imbalanced inter-molecular forces at the interface between oil and water, which is closely related to oil/brine properties, pH and temperature (Ge and Wang, 2015). Different recovery technologies have different requirements for IFTs. While wettability is the tendency of one fluid to spread on a solid surface in the presence of another immiscible fluid, which may affect the capillary pressure, relative permeability and residual oil saturation (Anderson, 1986). Depending on the nature of surfactants, crude oil and rock compositions, surfactants can change rock wettability through physical/chemical adsorption, micellar solubilization (Kumar et al., 2005) and ion-pair formation (Standnesm and Austad, 2000). Several laboratory studies illustrated that a more water-wet reservoir condition can lead to significantly higher oil recovery factor during the water flooding process thanks to the positive effects of capillary force (Hirasaki and Zhang, 2004; Gupta et al., 2009). Ge and Wang (2015) also reported that surfactants with good wetting properties usually have low IFT, but surfactants that were able to result in low IFT may not be good wetting agents.

Based on the charges of their polar head groups, surfactants can be divided into four categories, cationic surfactants (quaternary ammonium salt, pyridine halide, etc.), anionic surfactants (carboxylate, sulfonate, etc.), nonionic surfactants (polyoxyethylene derivatives, polyether, polyhydric alcohols, etc.) and zwitterionic surfactants (betaine type, amino acid type,

10

imidazoline type, etc.). (Zhao et al., 2005) Most surfactants are stable and applicable at normal conditions with low salinity and low temperature. However, when it comes to high temperature and high salinity conditions like the Middle Bakken Formation, cationic surfactants may possibly suffer from Hoffman elimination process, normal nonionic surfactants would precipitate due to weakened hydrogen bonding with water molecules, and those frequently used anionic surfactants such as petroleum sulfonate, alpha olefin sulfonate and sodium dodecyl benzene sulfonate can hardly perform effectively and efficiently at temperature over 90 °C and salinity higher than 100 g/L (Da et al., 2018).

Zwitterionic surfactant, containing both positive and negative charges in its hydrophilic part, recently has become a hot topic in chemical EOR especially for harsh reservoir conditions because of its excellent water solubility, insensitiveness towards salt and temperature, good biodegradation, low toxicity and remarkable interfacial activity at low concentrations (Li et al., 2011; Zhang et al., 2014; Song et al., 2016; Zhao, et al., 2015). Wang et al. (2010) found that zwitterionic surfactant alone with the concentration of 50 ~ 3000 mg/L was able to generate ultralow IFTs when in the presence of over 200 g/L salts. Meanwhile, zwitterionic surfactants have good compatibility with various ionic and nonionic surfactants, contributing to improved salt tolerance and strengthened interfacial properties. Li et al. (2012) and Zhao et al. (2012) showed that with proper addition of betaine, nonionic surfactant Triton X-100, anionic surfactants AOS_{16-18} and cationic surfactant quaternary ammonium salt all could produce desirable foams with higher stability. Moreover, betaine could lower the critical micelle concentration and the Krafft temperature of anionic surfactants (Prajapati and Bhagwat, 2012). Most importantly, there are many indications showing their great potential in EOR areas, for example, by injecting 0.5 PV 500 mg/L zwitterionic surfactant solution, Kamal et al. (2018) were able to obtain an 8.0 % increase in

oil recovery. Also, through the mechanisms of IFT reduction and wettability alteration, a lab synthesized zwitterionic surfactant was able to recover an additional 27.03 % of oil (Kumar and Mandal, 2017). When used with polymer, alkyl-hydroxyl-sulfobetaine zwitterionic surfactant can extract extra 18.6 % more oil after water flooding (Guo et al., 2015). By injecting a small pore volume of zwitterionic surfactant-alkali-polymer slug, Kumar and Mandal (2018) obtained an additional oil recovery of 30.82% of original oil in place (OOIP) in a sandpack coreflooding experiment.

A suitable surfactant candidate for EOR purpose should have the following features, such as good compatibility with reservoir fluids and reservoir temperature, ability to lower IFT or alter rock wettability, low retention on reservoir rocks, and commercial availability at an acceptable cost (Kamal et al., 2017). Favorable surfactant formula with lower surfactant adsorption loss is critical to the economic success of any surfactant projects (Patil et al., 2018). Excessive surfactant adsorption onto rock surfaces leads to low efficiency and may possibly cause irreversible formation damage. Therefore, quantifying surfactant adsorption density is of key importance.

1.3. Surfactant Adsorption.

Surfactant retention due to precipitation, chemical degradation and adsorption is a critical factor that affects the cost-efficiency of surfactant-involved EOR technologies. By selecting proper surfactant formulas and application conditions, the precipitation and degradation issues can be eliminated. While surfactant adsorption is unavoidable. Surfactant adsorption would be affected by various factors and can be more complicated when being applied in harsh reservoir conditions. Proper surfactant adsorption on rock surfaces may be favorable for wettability alteration, but high adsorption especially at near wellbore area might render the surfactant flooding economically and technically unfeasible. Commonly, the requirement of surfactant adsorption loss in ASP (Alkaline-

Surfactant-Polymer) flooding should be lower than 1.0 mg/g (Jian et al., 2016), and the adsorption

threshold for carbonate reservoirs at high temperatures was 1.0 mg/m^2 (Da et al., 2018).

A number of studies has been conducted on the adsorption behaviors of traditional anionic,

cationic and nonionic surfactants onto formation rocks under the influences of salinity, different

cations and temperature in the past several decades with either positively or negatively charged

adsorbents (Koopal et al., 1995; Xu et al., 2008; Ahmadi and Shadizadeh, 2013; Amirianshoja et

al., 2013; Duran-Alvarez et al., 2016), and there is scarce information about the adsorption

isotherms and kinetics of zwitterionic surfactants, except Li et al. (2011) studied the adsorption

behavior of betaine-type surfactant on quartz sand. Alvarez et al. (2014; 2018) and Wang et al.

(2015) figured out the adsorption characteristic of sulfobetaine on limestone. Jian et al. (2018)

investigated the adsorption of betaine type surfactants on carbonates surfaces. However, most

experiments were done at relatively ideal conditions, with either simple mineral composition, low

temperature or low salinity brine. Total surfactant adsorption is the cumulative effects of

electrostatic interactions, chemical interactions (covalent bonding), hydrogen bonding, lateral

associative interactions, solvation and desolvation. The driving forces can be easily influenced by

the physicochemical properties of solutions, surfactants and adsorbents (Ball and Fuerstenau, 1971;

Paria and Kartic, 2004; Cui et al., 2018a; 2018b; Wei et al., 2016). Small changes in certain factors

such as surfactant structure and concentration, salinity, temperature and pH may lead to significant

differences in adsorption density. Anionic surfactants have higher adsorption on positively charged

rocks while cationic surfactants prefer to adsorb on negatively charged rocks (Lv et al., 2011). In

addition, surfactants with greater hydrophobicity shows higher adsorption (Wu et al., 2010). To

quantify the adsorption density, proper methods should be adopted to determine surfactant

concentration. The commonly used techniques are conductivity measurement, surface tension

measurement, titration, UV/vis spectroscopy, high-performance liquid chromatography (HPLC), total organic carbon analysis (TOC), etc.

1.4. Motivations.

Most of the surfactant formulas perform pretty well at mild conditions, but most unconventional reservoirs are high-temperature and high-salinity reservoirs. Therefore, zwitterionic surfactants with good compatibility towards high temperature and high salinity offer a great opportunity to boost the oil production in unconventional reservoirs with harsh reservoir conditions. Acquiring a good knowledge of the adsorption behaviors of zwitterionic surfactants can be beneficial to offer cost-effective choices for future development of surfactant formulas with high thermal and salt resistance.

1.5. Innovation.

So far, to the best of our knowledge seldom has anyone done any researches on the adsorption behavior of zwitterionic surfactants on adsorbents with complex mineral compositions at salinity higher than 250 g/L (with divalent ions) and temperature higher than 100 ℃. In this study, spectrophotometric iodine method using KI-I_2 solution as the color developing agent (Halt and Moulik, 2001) was applied to study and compare the adsorption behaviors of different zwitterionic surfactants on the Middle Bakken samples at the Bakken conditions. This method owns the advantages of high accuracy, easy operation, wide linear detection range with large regression coefficient, high stability in acid condition and low cost.

2. Experimental Section

2.1. Materials.

Five surfactants including three zwitterionic surfactants (BW, CA, CS-50), one nonionic

14

surfactant (HCS, cloud point >100 °C) and one anionic surfactant (964, neutralization required) were used without further purification, detailed information is tabulated in Table 2-2 with some details remaining undisclosed owing to confidential issues. Sodium chloride (NaCl), potassium chloride (KCl), magnesium chloride (MgCl$_2$) and calcium chloride (CaCl$_2$) were used to prepare the Bakken Formation brine (Dong et al., 2011. Table 2-3, density= 1.17 g/cm^3, pH=6.2±0.3). The four metal chlorides together with the iodine (I$_2$) and potassium iodide (KI) purchased from VWR International were all of ACS grade.

Table 2-2 Details of surfactants

Surfactants	Type	Active, %	Manufacture	Molecular formula
BW	Zwitterionic	35.9	Lubrizol	$C_{12}H_{25}N^+(CH_3)_2CH_2COO^-$
CA	Zwitterionic	29.4	Stepan	$C_{11}H_{23}CO-NH-(CH_2)_3N^+(CH_3)_2CH_2COO^-$
CS-50	Zwitterionic	43.5	Stepan	$C_{11}H_{23}CO-NH-(CH_2)_3N^+(CH_3)_2CH_2CH(OH)CH_2SO_3^-$
HCS	Nonionic	60.0	Stepan	$CH_3(CH_2)_m-O-(CH_2CH_2O)_nH$
964	Anionic	86.8	Sasol	$CH_3(CH_2)_m-O-(CH_2CH(CH_3)O)-$ $(CH_2CH_2O)_nCH_2COOH$

Table 2-3 Compositions of Bakken Formation brine

Ions	Concentration, g/L
Na$^+$	85.3
K$^+$	5.64
Ca^{2+}	13.2
Mg^{2+}	1.18
Cl$^-$	184.5
TDS	289.82

The main adsorbents are rock powders prepared by crushing the Bakken rocks (The Middle Bakken Formation, Mountrail County, Ross Field) and Berea sandstones (Kocurek Industries, Inc.,

USA) with a ceramic mortar and pestle. Then, the crushed particles were sieved through 120 mesh (≤125 μm) steel wire screens. Other minerals including calcite (≤20 μm, Alfa Aesar) and clay (≤20 μm, Sigma-Aldrich) were also used for comparison.

2.2. Characterization of Adsorbents.

Scanning electron microscopy (HITACHI SU 8010) with minerals mounted on carbon tape was applied to study the surface morphology of different adsorbents. X-ray diffraction (Rigaku Smartlab) which is based on observing the scattered intensity of an X-ray beam hitting a sample as a function of incident and scattered angle, polarization, and wavelength or energy, was used to analyze the mineral compositions. The Brunauer-Emmett-Teller (BET) surface areas of different absorbents were compared with a nitrogen adsorption-based surface analyzer (Quantachrome Instruments Autosorb). Samples were first dried at 200 °C under the vacuum pressure ($<$20.0 mTorr) for about 4.0 hrs. The analysis was conducted at the boiling temperature of N_2 (77.0 K). Zeta potentials were also obtained through a light scattering Zetasizer (Malvern).

2.3. Spectrophotometric Iodine Method.

2.3.1. Preparation and Characterization of KI-I_2 Solution.

In this research, 0.2 mM KI-0.1 mM I_2 solution was adopted as the color developing agent. The absorbance spectra at different salinities in the wavelength range of 300 ~ 500 nm were recorded via a temperature compensated UV/vis/NIR spectrophotometer (Lambda 1050, PerkinElmer, USA) with a pathlength of 1 cm at the temperature of 298.0±0.2 K, ambient pressure. Pure saline or deionized water with the absence of KI-I_2 were used as the blank control. The operation temperature was around 25 °C.

2.3.2. Preparation of Calibration Curves.

To plot the calibration curves of different surfactants, 5 ~ 6 surfactants standards of known concentrations were first prepared by serial dilution of stock solutions, then KI-I$_2$ solution (with final concentrations of 0.2 mM and 0.1 mM, respectively) was added to start the reaction. The absorbance spectra were measured within 2 mins and the exact absorbance at specific characteristic peaks was recorded.

2.4. Static Adsorption.

Static adsorption of surfactant on rocks is determined by batch equilibrium tests on crushed rock powders. Thirty milliliter surfactant solutions prepared by diluting the bulk solutions with the Bakken Formation brine (initial surfactant concentration = 100 ~ 1000 mg/L) is mixed with 2.0 g rock materials in a 40 mL glass vial. After 1.0 hr stirring at room temperature, samples were transferred to ovens with temperature of 20, 80 or 105 °C, separately. Subsequently, after 24 hrs reaction, the solution was centrifuged for 20 min at 2500 rpm to separate the rock powders. Each sample was triplicated analyzed and the average value was used to calculate the equilibrium residue surfactant concentration.

The exact adsorption amount (Γ, mg/g) was calculated by Equation 2-2.

$$\Gamma = \frac{(c_i - c_{eq})V_{surf}}{m_{ads}} * 10^{-3} \qquad (2\text{-}2)$$

Where c_i is the initial surfactant concentration (mg/L), c_{eq} is the equilibrium surfactant concentration (mg/L), V_{surf} is the volume of the surfactant solution (mL), and m_{ads} is the total mass of the adsorbent (g). The adsorption density was also converted to mg/m^2 based on the specific surface area of each absorbent.

2.4.1. Stability of Surfactants.

The compatibility of surfactants with the Bakken Formation brine was assessed at the concentration of 1000 mg/L, ambient pressure and various temperatures (20, 80 and 105 °C). The surfactants whose concentrations did not undergo sharp decrease within one week were labelled as stable chemicals.

2.4.2. Fitting of Adsorption Models.

Adsorption models are necessary to predict the loading on the adsorption matrix at a certain concentration of the component. Langmuir isotherm and Freundlich isotherm are two commonly used equilibrium adsorption models to correlate the equilibrium adsorption density (Γ_e, mg/g) and concentration (c_e, mg/L). (Ahmadi and Shadizadeh, 2012)

Langmuir isotherm (Equation 2-3) describes the adsorption behavior of adsorbates on an ideal homogeneous adsorbent surface (Langmuir, 1916). Usually a linear relationship between $1/\Gamma_e$ and $1/c_e$ can be observed if Langmuir isotherm is applicable to depict the adsorption equilibrium. Values of Γ_{max} (maximum adsorption, mg/g) and K_L (equilibrium constant, L/mg) can be obtained through curve fitting from the slope and the intercept, separately.

$$\Gamma_e = \frac{\Gamma_{max}K_L c_e}{1 + K_L c_e} \tag{2-3}$$

Freundlich assumed that the adsorbent has a heterogeneous surface composed of different classes of adsorption sites (Rosen, 1989) and proposed Freundlich isotherm. Generally, it was applied to predict reversible adsorption and was not limited to monolayer adsorption, as expressed by Equation 2-4, where K_F and n are Freundlich constants.

$$\Gamma_e = K_F c_e^{1/n} \tag{2-4}$$

3. Results and Discussions

3.1. Physico-Chemical Properties of Adsorbents

XRD (Figure 2-2) and SEM (Figure 2-3) analysis were performed to characterize the basic physico-chemical properties of various adsorbents.
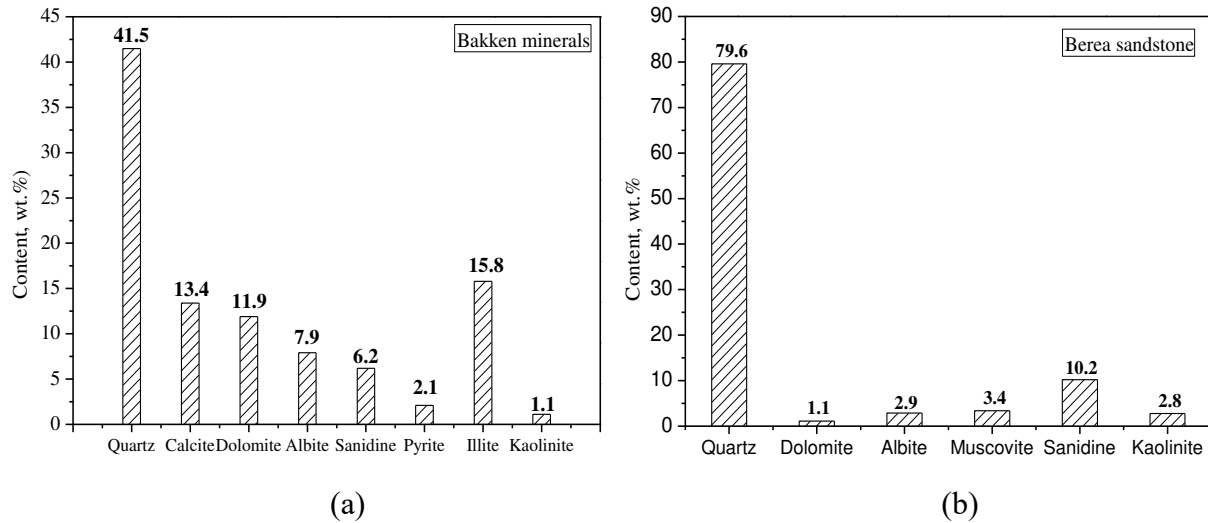
Figure 2-2 Compositions of the Bakken minerals and Berea sandstone. (a) The Bakken minerals. (b) Berea sandstone.

Berea rock is a typical sandstone with quartz as the most abundant mineral (79.4 wt.%) while the composition of the Bakken rock is more complicated, containing 41.5 wt.% quartz, 16.9 wt.% clay (illite and kaolinite), 14.1 wt.% feldspar (albite and sanidine), 12.2 wt.% calcite, 11.5 wt.% dolomite and relatively low pyrite content. Moreover, small silty fines are common on larger particle surfaces, which provide more adsorption sites for chemicals. Laminated clay particles have the largest BET specific surface area (18.63 m^2/g), followed by the Bakken minerals (7.54 m^2/g), Berea sandstone (2.85 m^2/g) and calcite (2.12 m^2/g). Usually, quartz and clay are negatively charged while carbonate minerals (calcite and dolomite) are positively charged.

19
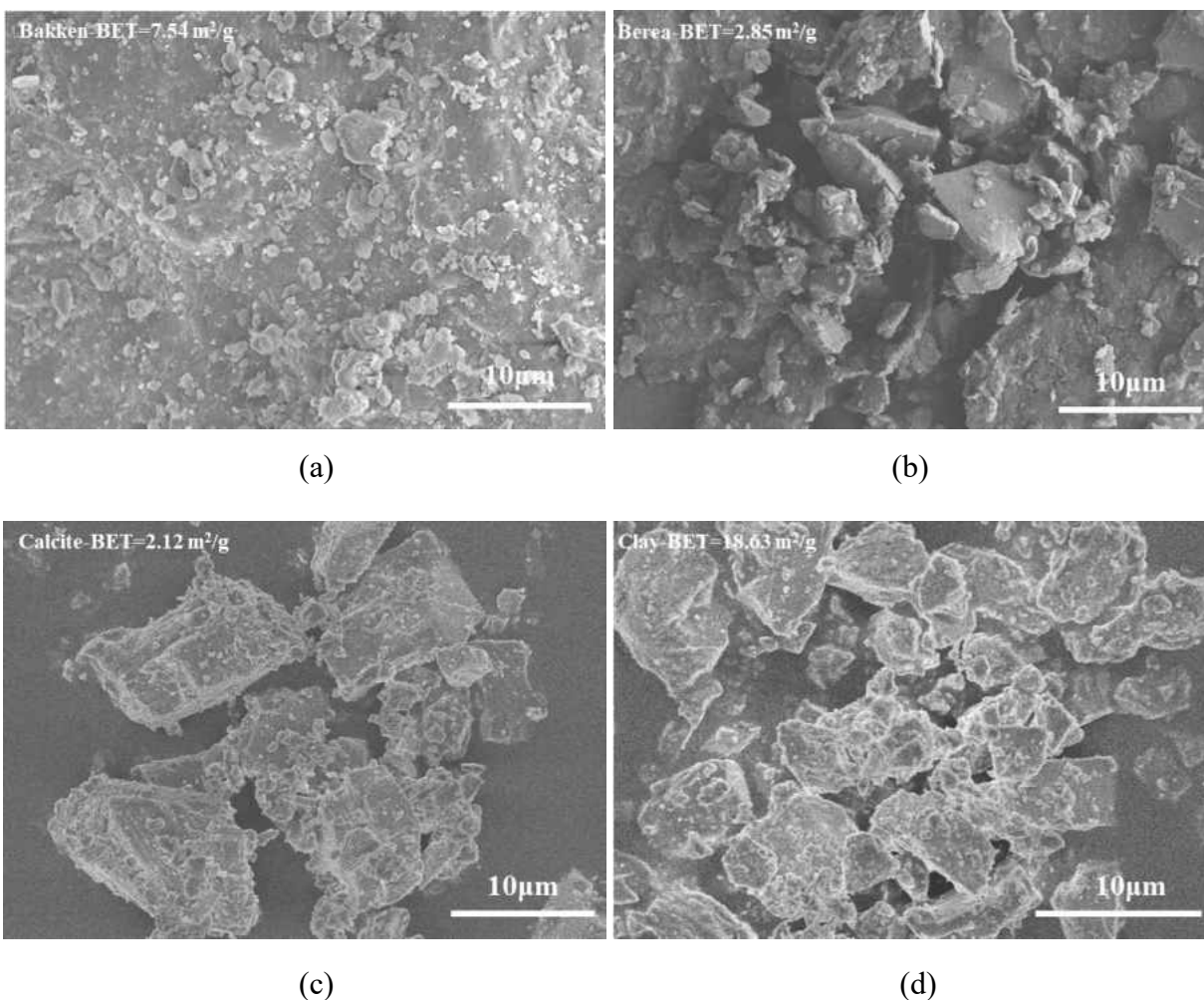
Figure 2-3 SEM images of various adsorbents, scale bar=10.0 μm. (a) The Bakken minerals. (b) Berea sandstone. (c) Calcite. (d) Clay.

3.2. Characterization of KI-I$_2$ Solution.

The color developing agent is composed of 0.2 mM KI and 0.1 mM I$_2$. The absorption spectra of the KI-I$_2$ mixture in the wavelength range of 300 ~ 500 nm are shown in Figure 2-4a, where the absorption peaks at wavelength of 351 nm and 460 nm can be attributed to the characteristic absorption of I$_3^-$ and I$_2$, respectively (Halt and Moulik, 2001). However, when the high salinity Bakken Formation brine was used, the typical I$_3^-$ peak at 351 nm would be replaced by a new peak at 433 nm, which could be explained by the equilibrium shift of the reversible

reaction between KI and I_2 ($KI+I_2 \rightleftharpoons KI_3$), resulting in increasing free iodine and decreasing triiodide ions.
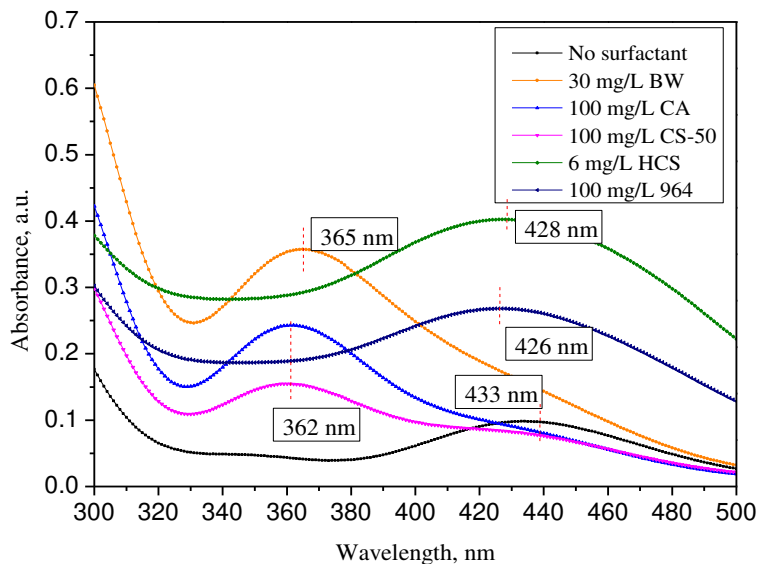
Figure 2-4 Absorption spectra of KI-I_2 mixtures in the presence of the Bakken Formation brine and different surfactants.

3.3. Static Adsorption.

3.3.1. Preparation of Calibration Curves.

Calibration curves are necessary to quantify surfactant concentration in certain solutions. Therefore, the absorbance at wavelength of 365 nm for surfactant BW (12 ~ 50 mg/L), 362 nm for surfactants CA ((10 ~ 100 mg/L)) and CS-50 ((5 ~ 250 mg/L)), 427 nm for surfactant HCS (0.16 ~ 8 mg/L) and 426 nm for surfactant 964 (5 ~ 250 mg/L) were recorded to prepare the calibration curves at the Bakken salinity (Figure 2-5). The absorbance at characteristic wavelengths for different surfactants all showed good linear relationships towards surfactant concentration, with regression coefficients higher than 0.99.
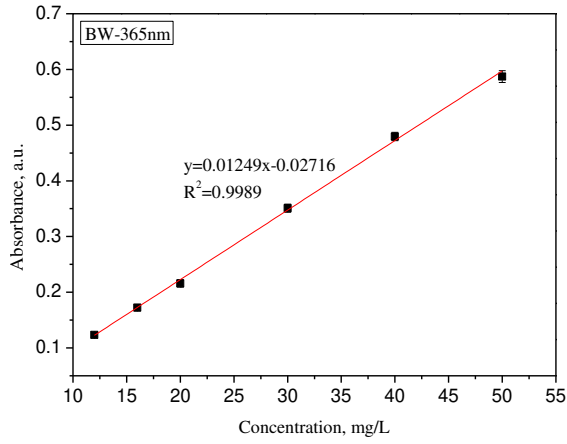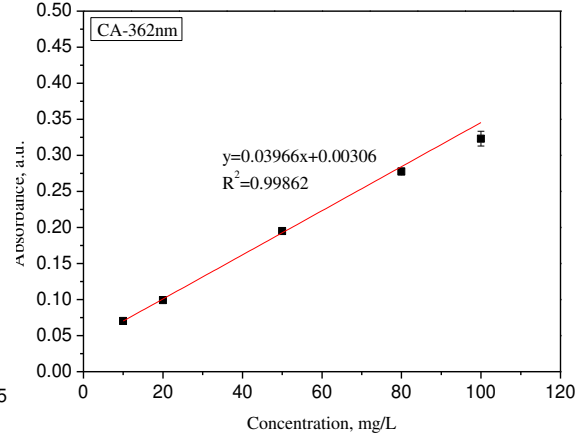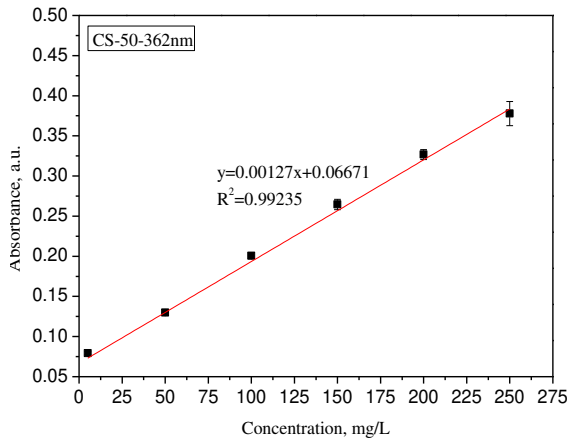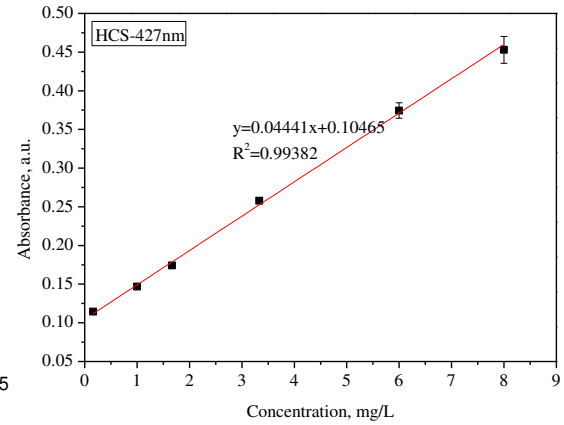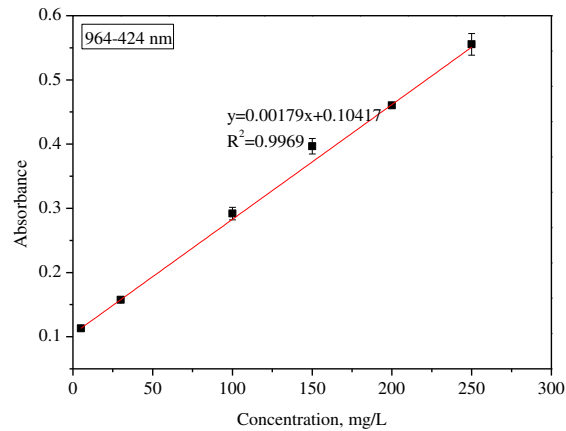
Figure 2-5 Calibration curves (Bakken Formation brine). (a) BW. (b) CA. (c) CS-50. (d) HCS.

(e) 964.

3.3.2. Stability of Surfactants.

The concentration change of active components in different surfactant samples versus time was measured according to the pre-plot calibration curves, as given in Figure 2-6. The stability of nonionic surfactant (HCS) and anionic surfactant (964) were only tested at room temperature due to their stability issues. Surfactants BW and CA showed higher stability than surfactant CS-50, and no precipitation or phase separation was observed within 60 days, which satisfies the long-term stability requirement for field applications.
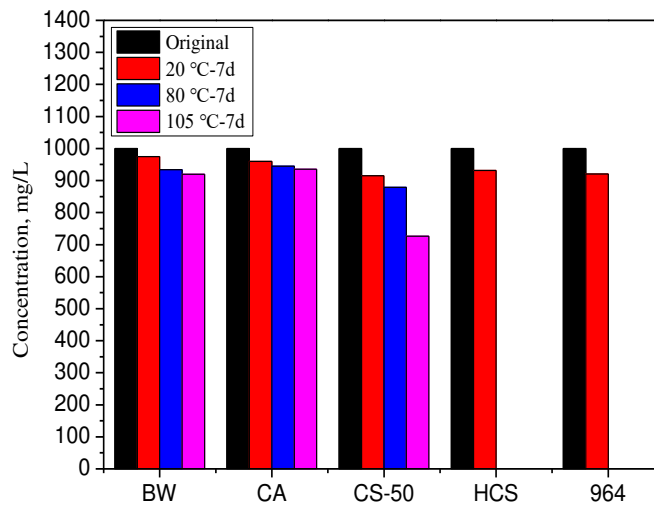
Figure 2-6 Effective surfactants concentrations after aging in given conditions for 7 days.

3.3.3. Optimization of Adsorption Parameters.

Suitable liquid/solid ratio and adsorption cycle are important to study the equilibrium adsorption density. Thus, the adsorption of surfactant BW (1000 mg/L) was first measured at different liquid/solid (Berea sandstone) ratios ranging from 4:1 to 20:1 after 24 hrs at 20 ℃, the Bakken Formation brine, as illustrated in Figure 2-7a. When the liquid/solid ratio is lower than 8:1, a sharp increase in adsorption density was observed, then the increasing rate decreased with a further increase in this ratio. Once the liquid/solid ratio was higher than 15:1, the adsorption

density remained nearly unchanged, indicating an equilibrium adsorption state. Thus, liquid/solid ratio of 15:1 was used in the following experiments.

The aging time also has an impact. In this part, BW concentration and liquid/solid ratio were 1000 mg/L and 15:1, respectively, and the aging time varied from 1 hr to 50 hrs, as shown in Figure 2-7b. The adsorption of BW on Berea sandstone in the first 5 hrs showed a linear increase, then reached a plateau at around 24 hrs, therefore, 24 hrs was selected as an adsorption cycle.

(a)

(b)
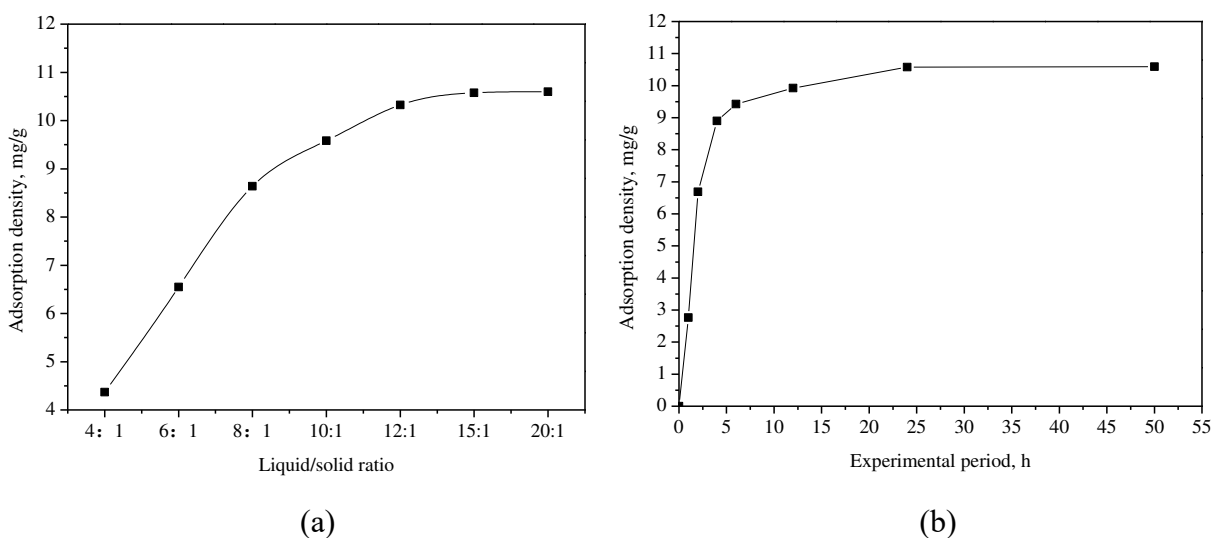
Figure 2-7 Optimization of static adsorption parameters. (a) Liquid/solid ratio. (b) Experimental period.

3.3.4. Effects of Salinity.

In this part, the influence of salinity on adsorption density of zwitterionic surfactants on the Middle Bakken minerals were studied at 20 °C, ambient pressure, as shown in Figure 2-8. All the three surfactants experienced a sharp increase when initial surfactant concentration is relatively low, followed by a reduced slope when surfactant concentration increases further and then gradually reached the adsorption equilibrium. To further study the adsorption equilibrium of surfactants BW and CA in the presence of deionized water and surfactant CS-50 in the presence

of both deionized water and the Bakken Formation brine, the initial surfactant concentration was increased up to 2000 mg/L considering the cost. The difference between the adsorption density of 1000 mg/L surfactant and equilibrium adsorption density was measure to be less than 1.0 mg/g.

(a)   (b)
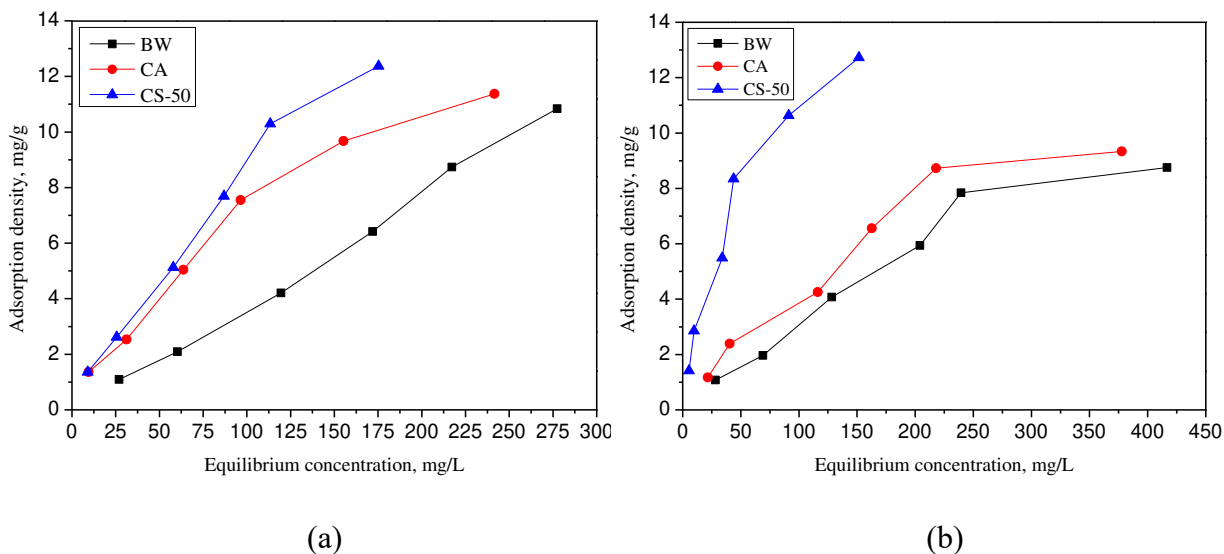
Figure 2-8 Effects of salinity on adsorption density. (a) Deionized water. (b) The Bakken Formation brine (TDS=289.82 g/L).

The adsorption of surfactant CS-50 on the Middle Bakken minerals in deionized water and the Bakken Formation brine were similar, both around 12.5 mg/g (1.66 mg/m^2) for a 1000 mg/L surfactant solution. Because of the differences in steric factors of different functional groups, the adsorption was slightly higher when the interactions between sulfonic groups and positively charged sites on rock surfaces take place. While the adsorption density of surfactants BW and CA in the presence of the Bakken Formation brine were 8.75 mg/g (1.16 mg/m^2) and 9.33 mg/g (1.24 mg/m^2), respectively, both were around 2.06 ± 0.02 mg/g lower than those of 10.83 mg/g (1.44 mg/m^2) and 11.37 mg/g (1.51 mg/m^2) in deionized water condition. It is worth mentioning that the zeta potential of the Bakken minerals reversed to 1.6 ± 0.5 mV from -21.2 ± 0.5 mV when the Bakken Formation brine was applied due to the presence of abundant Ca^{2+} and Mg^{2+} cations.

Different from surfactant CS-50, the acidic parts of surfactants BW and CA are carboxylate

groups, which have higher tendency to gain protons in acidic solutions and generally turn the original zwitterionic form into a fully protonated form, leaving the cationic part plays the dominate role. Herein, both deionized water and the Bakken Formation brine are slightly acidic, as a consequence, part of carboxylate groups would be deprotonated, implying basic groups (cationic parts) partially overweigh the acidic groups (anionic parts). Thus, comparing with positively charged adsorbents, surfactants BW and CA have higher adsorption on negative charged minerals. Though a decrease in adsorption density was observed in high salinity conditions, the equilibrium adsorption densities of surfactants BW and CA were still higher than the threshold adsorption density proposed at high temperatures (1.0 mg/m^2). A possible explanation for this higher adsorption might be the large clay and quartz contents in adsorbents, and details were illustrated in the subsequent paragraphs. Feasible strategies to reduce the surfactant adsorption are to use sacrificial agents like polymers (Da et al., 2018) or nanoparticles (Wu et al., 2017) with surfactants.

Table 2-4 Parameters of Langmuir adsorption model

Surfactants	Correlation	R^2	K_L, $*10^2$ L/mg	Γ_{max}
BW	$1/\Gamma_e = \dfrac{25.495}{c_e} + 0.0555$	0.9818	0.22	18.02
CA	$1/\Gamma_e = \dfrac{16.806}{c_e} + 0.0527$	0.9888	0.31	18.98
CS-50	$1/\Gamma_e = \dfrac{3.4583}{c_e} + 0.0516$	0.985	1.49	19.38

Table 2-5 Parameters of Freundlich adsorption model

Surfactants	Correlation	R^2	K_F	1/n
BW	$\Gamma_e = 0.062c_e^{0.8248}$	0.9658	0.062	0.8248
CA	$\Gamma_e = 0.1345c_e^{0.7444}$	0.9684	0.1345	0.7444
CS-50	$\Gamma_e = 0.5618c_e^{0.6522}$	0.9633	0.5618	0.6522

The experimental data at 100 ~ 1000 mg/L initial surfactant concentration and the Bakken

salinity were also matched by Langmuir and Freundlich adsorption model, separately, and relevant parameters are listed in Table 2-4 and Table 2-5. Considering the values of regression coefficient (R^2) and mean square error, Langmuir model is slightly better fitted and can be more accurate to describe the adsorption isotherm of zwitterionic surfactants on the Middle Bakken minerals. Although high salinity is reported to be favorable for vesicle formation, the relatively low initial surfactant concentration used gave no similar vesicle induced variation trend (Nieto-Alvarez et al., 2014) in our study.

3.3.5. Effects of Temperature.

The adsorption at higher temperatures (80 °C and 105 °C) were also studied (Figure 2-9). The equilibrium adsorption density at 80 °C is slightly smaller than that at 20 °C when the original surfactant concentration is low (100 mg/L), and the difference is more prominent at higher concentration of 1000 mg/L.

(a)   (b)
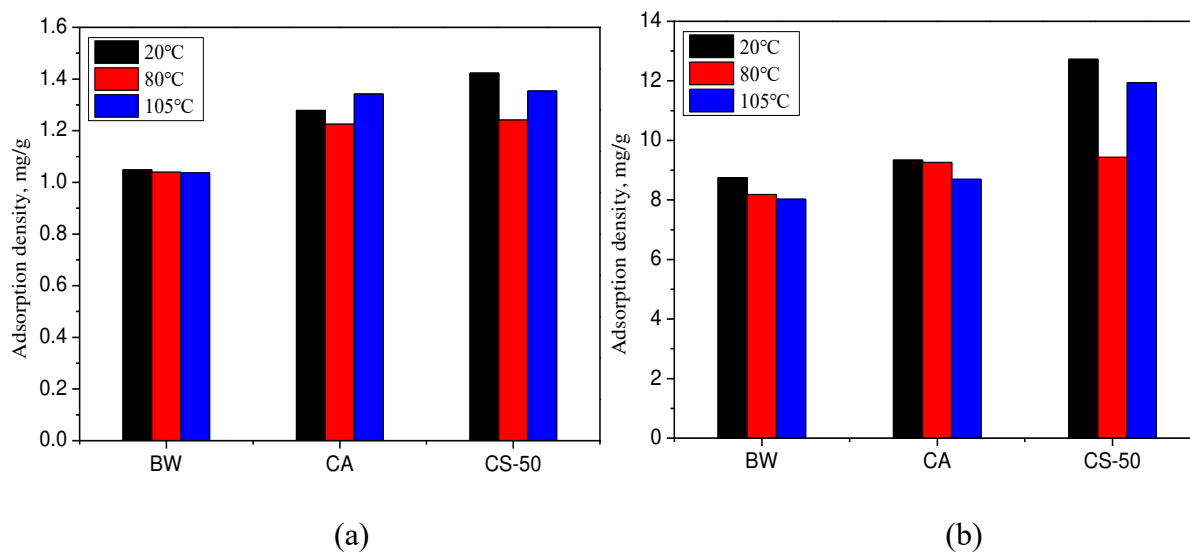
Figure 2-9 Effects of temperature on adsorption density. (a) Original surfactant concentration=100 mg/L. (b) Original surfactant concentration=1000 mg/L.

Adsorption is an exothermic process, so in ideal conditions when active surfactant components remain constant, the adsorption density of zwitterionic surfactants at higher temperatures should be lower. However, for our case, surfactant degradation and/or solubility change at temperature as high as 105 °C and salinity around 290 g/L are inevitable and noticeable especially for surfactant CS-50, so the variation trend in the temperature range of 80 ~ 105 °C was more complicated.

3.3.6. Effects of Mineral Types.

The compositions of the Middle Bakken minerals are complex, which can be divided into three types, quartz, carbonate and clay. Herein, Berea sandstone, calcite and clay were used to represent different mineral groups, and the adsorption of 1000 mg/L surfactant solutions on individual mineral group was studied separately (Figure 2-10). The zeta potential of different minerals at different salinities are presented in Table 2-6. Experimental results showed that the surfactant adsorption on clay minerals in this case is far away from the equilibrium state.
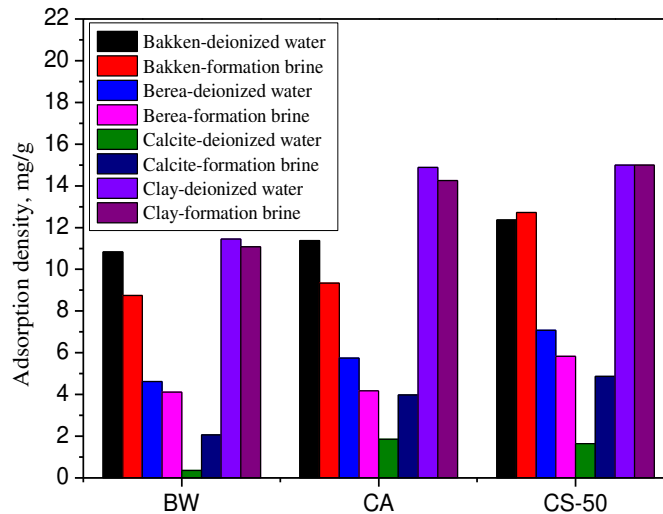
Figure 2-10 Effects of mineral types on adsorption density.

Zwitterionic surfactants have higher loss on clay and quartz than on calcite surfaces

regardless of the salinity, which was just in accordance with the trend of specific surface area, clay has the largest surface area of 18.63 m^2/g, followed by Berea sandstone of 2.85 m^2/g and calcite of 2.12 m^2/g. Results demonstrate that the adsorption of zwitterionic surfactants on the Bakken minerals are strongly influenced by clay and quartz ratios. Surfactant loss in the Bakken Formation due to adsorption might increase with increasing clay and quartz contents.

Table 2-6 Zeta potentials of different minerals

Minerals	Zeta potential, mV	
	Deionized water	Bakken Formation brine
Bakken minerals	−21.2±0.5	1.6±0.5
Berea sandstone	−30.5±0.9	2.4±0.4
Calcite	6.1±0.5	10.7±0.3
Clay	−17.2±0.78	−6.2±0.8

Apart from large clay and quartz contents, the configuration of surfactant molecules also matters. Normally, zwitterionic molecules have three possible configurations, 1) when mineral is strongly negatively charged, the cationic quaternary nitrogen group would orient to the surfaces with anionic part moves away (Mode 1). 2) when surface negative charge is reduced by the adsorption of cations, oblique configuration appeared with sulfonate or carboxylate group getting closer to the mineral surfaces (either because of reduced repulsion interactions or increased attraction interactions with the absorbed Ca^{2+} and Mg^{2+}) and cationic parts remain attracted by the net negatively-charged sites (Mode 2), and 3) vertical configuration when minerals become absolute positively charged. Cationic parts are repulsed and anionic parts are attracted (Mode 3). Therefore, oblique configuration contributes to the minimum adsorption because of the largest contact area of a single molecule (Duran-Alvarez et al., 2016; Nieto-Alvarez et al., 2018), as illustrated in Figure 2-11. In addition, sulfobetaine with sulfonate group was observed to have

higher adsorption than betaine with carboxylate group, which was contrary to the observations of Li (2011). The main reason lies in the surfactant structures. Different structures have different interaction energies and higher negative interaction energies result in higher adsorption.

| (a) | (b) | (c) |
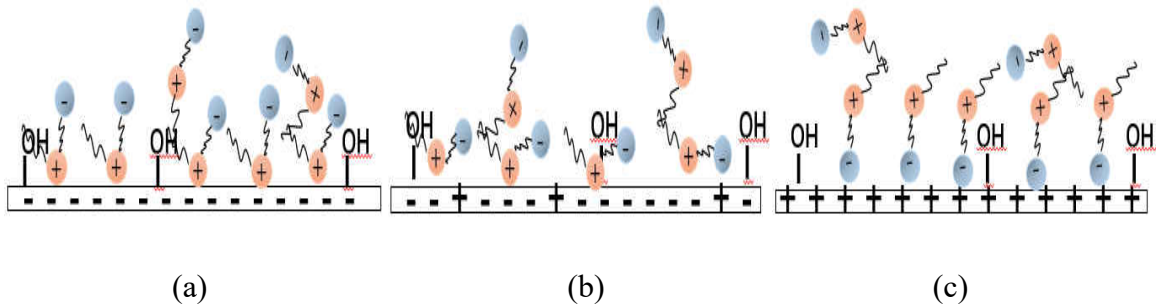
Figure 2-11 Schematic models of suggested adsorption mechanism of zwitterionic surfactants at different salinities. (a) Deionized water. (b) Low salinity with few divalent cations. (c) High salinity with abundant divalent cations.

Obviously, the salinity of the Bakken Formation brine is very high, and the adsorption configuration shifts to mode 3 from mode 1 directly, which offers a good opportunity for later research on finding out the optimal salinity so as to minimize the adsorption of zwitterionic surfactants.

3.3.7. Effects of Surfactant Types.

Besides zwitterionic surfactants, nonionic surfactants and anionic surfactants are also popular in unconventional reservoirs. In this section, the nonionic surfactant HCS and the anionic surfactant 964 were also applied for comparison (Figure 2-12). Relevant experiments were implemented at room temperature, ambient pressure with initial surfactant concentration of 1000 mg/L.

Zwitterionic surfactants have higher adsorption than either nonionic or anionic surfactant on the Middle Bakken minerals with large clay and quartz contents regardless of the salinity. The

Middle Bakken mineralogy is known to vary from dolomitic sandstone to silty dolostone, so according to our results, zwitterionic surfactants may be more suitable to be used as the main component in a surfactant flooding formula for dolostone formations while used as an additive in sandstone formations to help increase the salt tolerance, thermal tolerance and efficiency of other surfactants. The main driving force varies with surfactants structures. For ionic surfactants (Figure 2-13), electrostatic interactions play the leading roles, therefore, the adsorption of ionic surfactants might be easily affected by environmental salinity and other factors that would change the surface charge of adsorbents. While for nonionic surfactants (Figure 2-14), hydrogen bonding and hydrophobic interactions are believed to be the main adsorption mechanisms. Under such circumstance, salinity will not significantly affect the distribution of surface hydroxyl but may contribute to a more compact adsorption pattern. Surfactant adsorption is closely related to chemical structures, environmental salinity and temperature, adsorbents, etc. Small changes in these factors can result in huge differences.
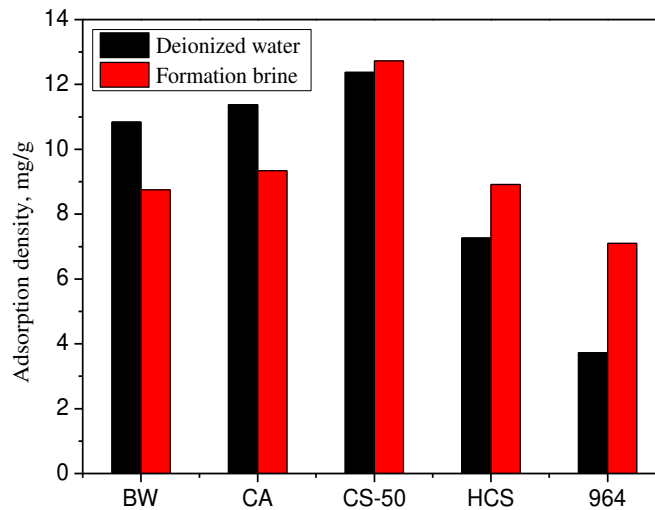
Figure 2-12 Effects of surfactant types on adsorption density.

(a)   (b)
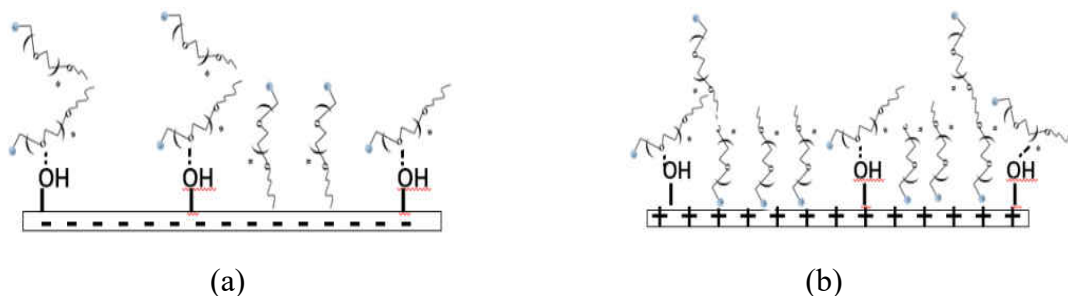
Figure 2-13 Schematic models of suggested adsorption mechanism of ionic surfactant at different

salinities. (a) Deionized water. (b) High salinity with abundant divalent cations.

(a)   (b)
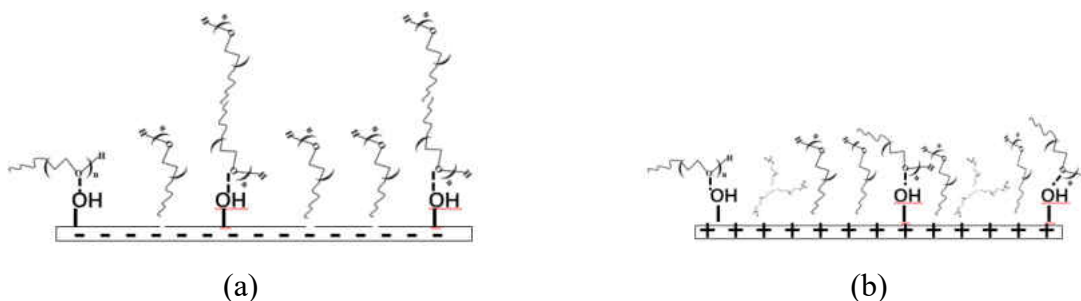
Figure 2-14 Schematic models of suggested adsorption mechanism of nonionic surfactant at

different salinities. (a) Deionized water. (b) High salinity with abundant divalent cations.

Table 2-7 Details of the randomized full factorial design

Factors	Low value	High value
Surfactant	1 (BW)	2 (CA)
Concentration, mg/L (Set 1)	100	600
Concentration, mg/L (Set 2)	600	1000
Temperature, °C	20	105
Mineral	1 (Bakken)	2 (Berea)

Surfactant adsorption can be affected by initial surfactant concentration, salinity, temperature, chemical structures, as well as mineral types. But which factor is the most influential one is still obscure. Sometimes, studying the effects of a single factor while fixing other parameters is not sufficient to draw professional conclusions. So, in this paper, a thoroughly statistical analysis

was done on Software Minitab 2016 (a data processing software). To be more specifical, the 2^k full

factorial design was applied. The salinity was set to be the Bakken salinity and other details are

shown in Table 2-7. In order to make more accurate predictions, the initial surfactant concentration

range was divided into two parts, 100 ~ 600 mg/L and 600 ~ 1000 mg/L considering the different

impacts of surfactant concentration on the adsorption density. Herein, surfactants BW and CA were

selected because of higher stability. After primary screening, only one-way interaction and some

two-way interactions (interactions between two correlated factors) were studied. Their ranking was

clarified in Table 2-8.

Table 2-8 Ranking of different influencing factors

Factors	Set 1	Set 2
	Ranking	Ranking
Surfactant	5	6
Concentration	1	2
Temperature	4	3
Mineral	2	1
Surfactant * Temperature	6	5
Surfactant * Mineral	3	4

Either in Set 1 or Set 2, the top two influential factors remain to be initial surfactant

concentration and mineral (adsorbents). In addition, other interaction effects such as surfactant and

mineral also matters. For Set 2, when initial surfactant concentration is relatively high, the impacts

of temperature was enlarged while the effects surfactants were weakened. In this paper, the

influence of surfactant structure is not that obvious for surfactants BW and CA. To predict the

approximate adsorption densities at some other conditions, the contour plots of adsorption versus

mineral, concentration, and temperature for different simulation sets were plotted, as presented in

Figures 2-15 and 2-16. The x and y axials of the red dots shown on the plot represent the experimental conditions and the values are experimental data (real values), which are consistent with the predicted ranges.

(a)   (b)
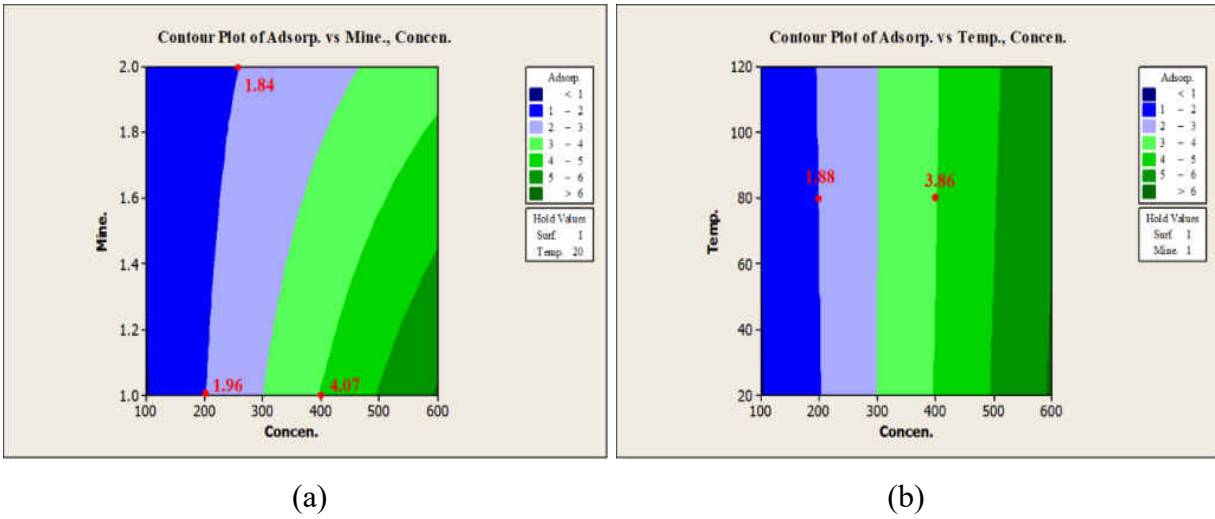
Figure 2-15 Representative contour plots for simulation Set 1. (a) Adsorption vs. Mineral and Concentration. (b) Adsorption vs. Temperature and Concentration.

(a)   (b)
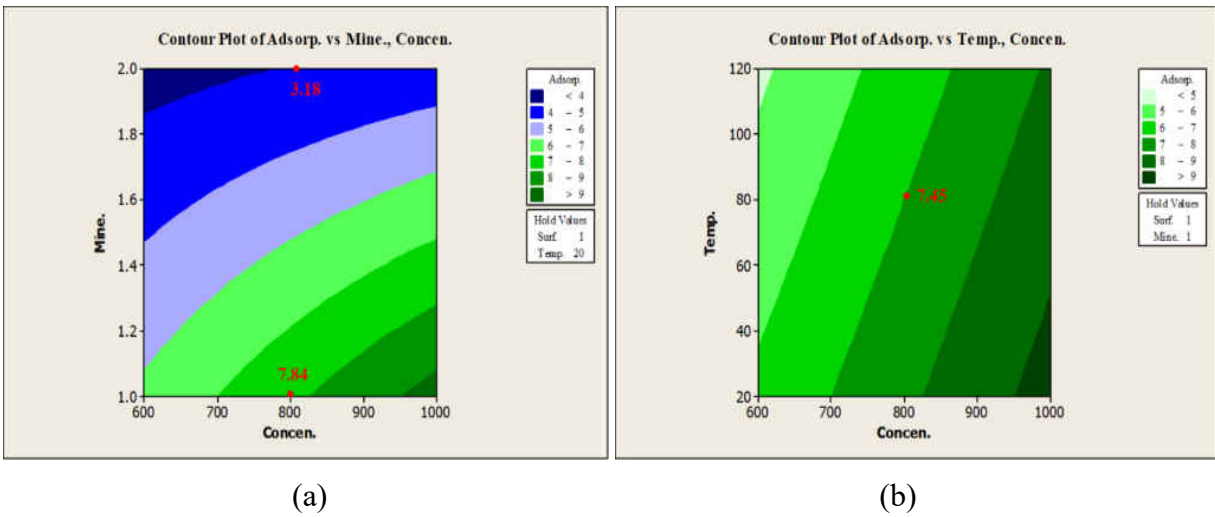
Figure 2-16 Representative contour plots for simulation Set 2. (a) Adsorption vs. Mineral and Concentration. (b) Adsorption vs. Temperature and Concentration.

4. Summary

(1) When the Bakken Formation brine was used, the adsorption of surfactants BW and CA both showed a 2.06 ± 0.02 mg/g decrease while surfactant CS-50 increased a little bit compared with those in deionized water.

(2) The adsorption density of zwitterionic surfactants increases with increasing surfactant concentration at a restrained range. All of the three researched zwitterionic surfactants showed higher increasing rate in the range of $100 \sim 600$ mg/L than that of $800 \sim 1000$ mg/L at the Middle Bakken conditions.

(3) Higher temperature leads to decreased adsorption of zwitterionic surfactants, but considering the degradation phenomenon and/or solubility difference at elevated temperatures, the trend is not that obvious for the temperature range of $80 \sim 105$ ℃.

(4) Compared with nonionic surfactant HCS and anionic surfactant 964, zwitterionic surfactants have higher adsorption on the Middle Bakken minerals with large clay and quartz contents.

(5) Zwitterionic surfactants have higher adsorption loss on clay and quartz than calcite. The high adsorption of the researched zwitterionic surfactants on the Middle Bakken minerals regardless of salinity may be ascribed to the fairly large clay and quartz contents.

(6) The main driving force for zwitterionic surfactants adsorption is electrostatic interaction.

CHAPTER III

REVIEW ON THE APPLICATIONS OF NANOMATERIALS IN ENHANCED OIL

RECOVERY

1. Introduction

Hydrocarbon is predicted to remain to be the primary source energy in the coming decades (Agista et al., 2018). However, the production rates of the existing oilfields are facing a declining trend with a large portion of oil reserves yet to be recovered due to the limitations of production techniques. Therefore, applying enhanced oil recovery (EOR) technologies to unlock the remaining oil is a meaningful and urgent task.

Various EOR technologies including thermal recovery, miscible flooding, chemical methods, and microbial methods have been widely researched and were proven to be efficient in enhancing hydrocarbon recovery. However, these technologies suffered different drawbacks such as high cost, possible formation damage, low utilization rate, early breakthrough and corrosion. Nanotechnology may provide solutions to address these challenges. The size of nanomaterials is in the range of 1 to 100 nm, thanks to their tiny size compared to pore throats, they are able to penetrate into the sedimentary rocks and modify the reservoir properties without causing severe formation damage, therefore, creating more favorable conditions for oil production (Hendraningrat and Torsæter, 2015; Guo et al., 2016; Li, 2016). Nanoparticles (NPs) are environmentally friendly and their cost for field-scale applications is much lower than other chemicals like polymers and surfactants (Sun et al., 2017).

Nanomaterials-based EOR agents include nanofluids, nanoemulsions and nanocatalysts. In this chapter, our main focus was laid on nanofluids EOR. NPs can be used alone (Li et al., 2018;

36

Kiani et al., 2016b) or be integrated with surfactants (Mohajeri et al., 2015; Suleimanov et al., 2011) or polymers (Maghzi et al. 2014; Zeyghami et al., 2014) to prepare augmented systems.

Numerous laboratory experiments using nanomaterials for EOR purpose were conducted in the past few decades. Generally speaking, the most commonly used nanomaterials are metal oxide, organic, and inorganic materials. The functional mechanisms of nano-EOR vary from disjoining pressure, interfacial tension (IFT) reduction, wettability alteration to mobility control, etc. and the EOR performance of NPs is found highly depend on the nanomaterial sizes and concentrations, aqueous salinity, reservoir temperatures and porous media, etc. (Hendraningrat et al., 2012; Onyekonwu and Ogolo, 2010)
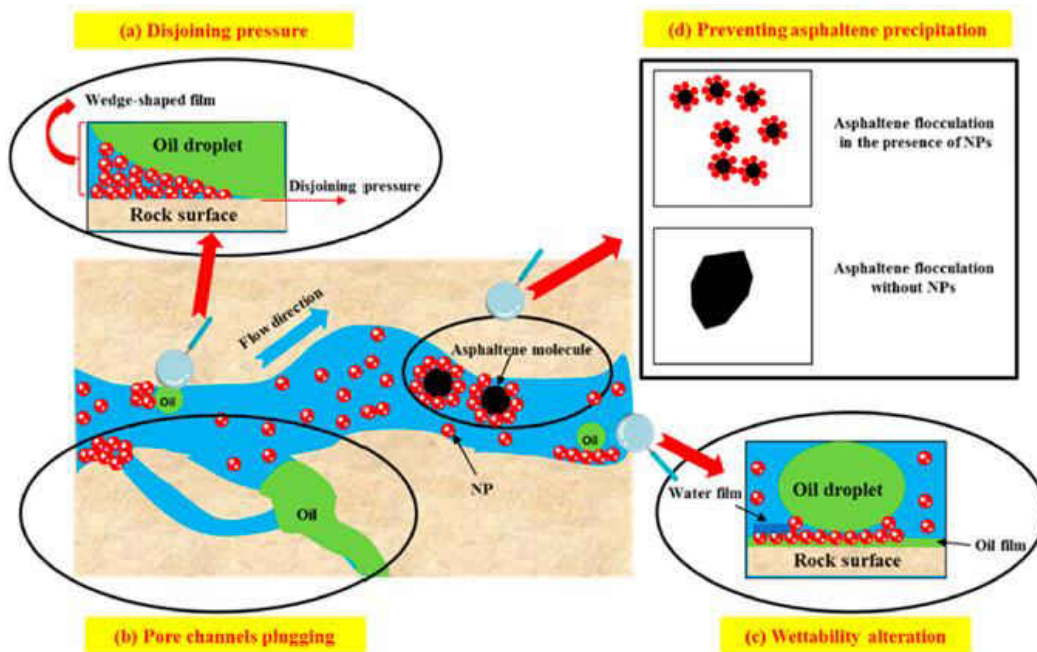
Figure 3-1 Possible EOR mechanisms of nanofluids (Sun et al., 2017).

2. Classification of Nanomaterials

2.1. Metal Oxide Nanomaterials.

Aluminum oxide (Al_2O_3), copper oxide (CuO), iron oxide (Fe_2O_3), tin oxide (SnO_2), magnesium oxide (MgO), nickel oxide (NiO/Ni_2O_3), titanium dioxide (TiO_2), zinc oxide (ZnO) and zirconium oxide (ZrO_2) are commonly studied metal-oxide nanomaterials.

2.1.1. Aluminum oxide (Al_2O_3).

Al_2O_3 finds wide use in the mining, ceramic, and materials science communities. Nano-alumina could be synthesized by flame spray pyrolysis (Kiani et al., 2016b), modified plasma arc (Chang and Chang, 2008) and mechanochemical methods (Tsuzuki and McCormick, 2004). The morphology of aluminum oxide is shown in Figure 3-2. The applications of Al_2O_3 NPs in EOR area are summarized in Table 3-1 in APPENDIX.
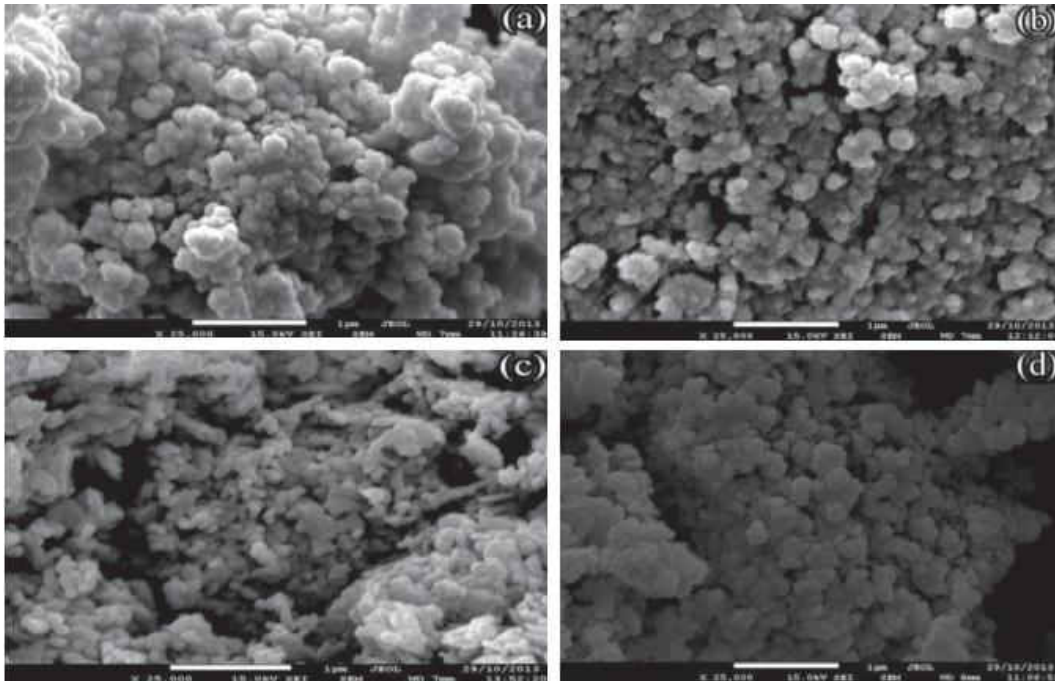
Figure 3-2 FE-SEM images of (a) titanium oxide, (b) aluminum oxide, (c) nickel oxide and (d) silicon oxide (Alomair et al., 2015).

Joonaki et al. (2014) reported that when Al_2O_3 NPs (0.035 ~ 0.3 wt.%) flooding was conducted, an oil recovery of 76.8 % OOIP (an increase of 20.2 % compared to water flooding)

could be achieved due to wettability alteration and IFT reduction. Alomair et al. (2015) found that the combined mechanisms of emulsion viscosity reduction, displacing fluid viscosity increase and asphaltene precipitation reduction could help recover another 6.0 % OOIP when 0.01 ~ 0.1 wt.% of Al_2O_3 NPs were used. In addition, other possible functional mechanisms such as oil viscosity reduction (Ogolo et al., 2012) and clay swelling inhibition (Kiani et al., 2016b) were also reported to be favorable for the oil production process.

| (a) | (b) |

Figure 3-3 Contact angles of oil/air/rock systems treated by 100 mg/L Al_2O_3 NPs. (a) Before treatment, (b) After treatment (Giraldo et al., 2013).
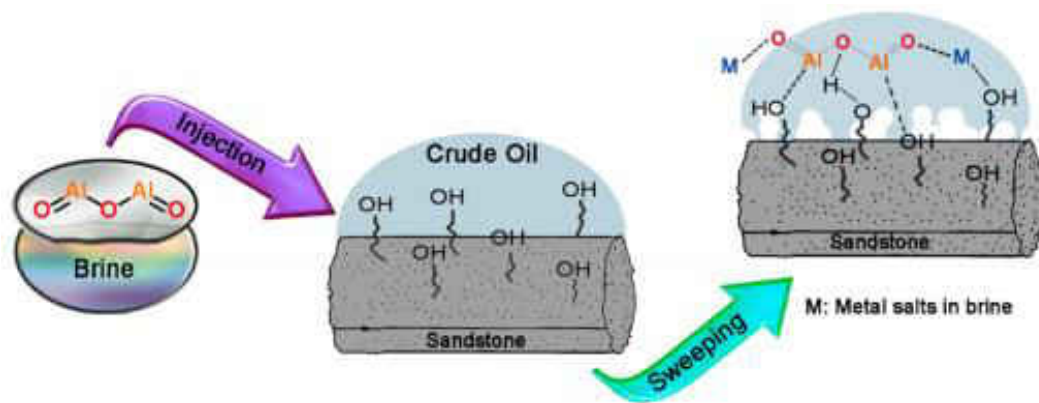
Figure 3-4 Possible mechanism for NGA particle adsorption on the sandstone rocks (Kiani et al., 2016b).

Using surfactant-Al_2O_3 NP mixtures for EOR was also popular. According to Moslan et al. (2016), Al_2O_3 NP has higher stability than ZrO_2 NP considering its lower retention. Due to the

synergistic effects between cationic surfactant CTAB and Al_2O_3 NPs, the IFT was reduced to a smaller value of 1.65 mN/m from 8.46 mN/m and contact angle was reduced to 40° from original 128°, compared to those of 1.85 mN/m and 47° for ZrO_2 NPs at the same conditions. When Al_2O_3 NPs were mixed with anionic surfactant SDS, 10.0 ~ 30.0 % more oil was recovered than SDS alone though a small increase in IFT was noticed. In addition, smaller Al_2O_3 NPs were able to yield an oil recovery 63.0 % higher than that of larger NPs. While for ZnO NPs, the impacts of NP size showed an opposite trend, larger ZnO NPs gave an increase of 145.0 % in the final recovery as compared with the formula with smaller NPs (Zaid et al., 2012).

2.1.2. Copper oxide (CuO).

CuO is a black solid, which can be produced by pyrometallurgy in a large scale. It is a significant product of copper mining and the precursor to many other copper-containing products and chemical compounds (Hernando et al., 2014), as shown in Figure 3-5.

(a)   (b)
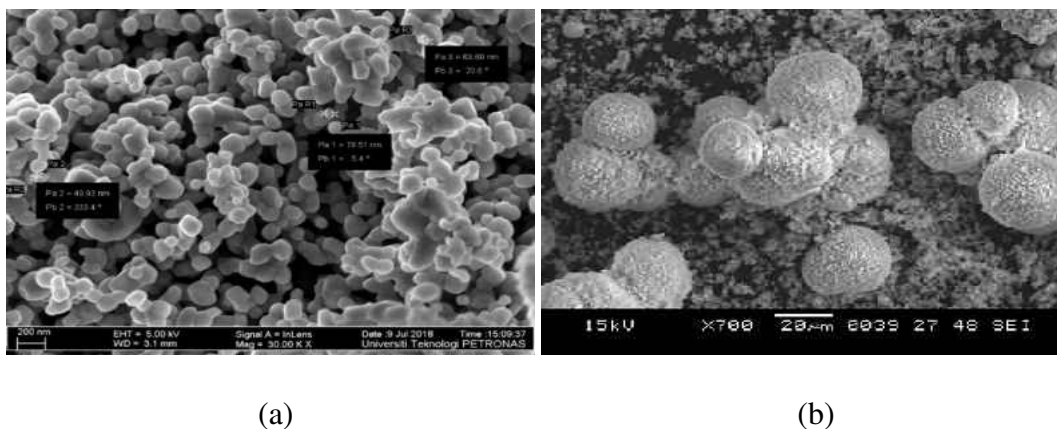
Figure 3-5 FE-SEM images of CuO NPs. Figures were obtained from (a) GNM.com. (b)

(Ugwekar and Lakhawat, 2014)

So far there are only limited information related to CuO NPs application in EOR field except Shah (2009) found that 1.0 wt.% CuO NPs when dispersed in PDMS and CO_2 mixture could reduce heavy oil viscosity and thicken the displacing fluid, therefore, recovered another 13.3 %

OOIP. Meanwhile, CuO NP also showed similar potential to change carbonate rock wettability just as Fe_2O_3 and NiO NPs did (Shah, 2009).

2.1.3. Iron oxide (Fe_2O_3/ Fe_3O_4/ $CoFe_2O_4$).

Iron oxides and oxyhydroxides are widespread in nature and play important roles in many geological and biological processes for sensing, imaging and data storage because of their unique magnetic and electric properties (Negin et al., 2016). There were also some studies related to the applications of iron oxide NPs in increasing oil recovery, as illustrated in Table 3-2 in APPENDIX.
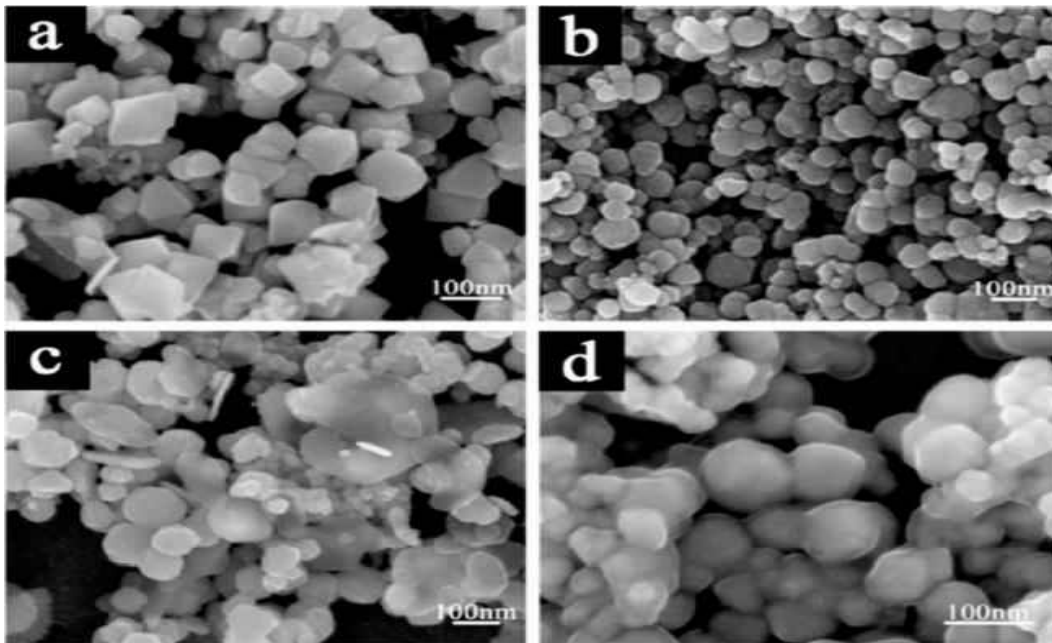
Figure 3-6 SEM images of Fe_3O_4 NPs prepared with different alkali sources. (a) NaOH, (b) $NH_3 \cdot H_2O$, (c) mixed alkali, (d) sodium oleate (Shekhawat et al., 2016).

Haroun et al. (2012) found that using Fe_2O_3 NPs could obtain a recovery of 57.0 %, but Ogolo et al. (2012) reported that the efficiency of Fe_2O_3 NPs was lower than other metal oxide NPs such as CuO, NiO ($\leq$ 85.0 %) and Al_2O_3. Ferrofluids (Fe_3O_4/$CoFe_2O_4$) were also proposed for magnetic oil recovery. Shekhawat et al. (2016) and Kothari et al. (2010) both reported that Fe_3O_4 NP was a good viscosity modifier and a promising EOR agent for heavy oil reservoirs. In

addition, the EOR efficiency of ferrite nanoparticles could be enhanced by electromagnetic waves, where oil recovery increased by 22.88 % in Yahya's case (Yahya et al., 2012).

2.1.4. Magnesium oxide (MgO).

Fine migration is a worth-noting problem in oil production process. Detachment of fine particles from sand surfaces would plug pores and throats, therefore, resulting in an adverse impact on the ultimate oil recovery. MgO NPs with or without surfactant (Huang et al., 2010; Ahmadi et al., 2013) were reported to be effective in reducing fine migration. In addition, MgO NPs showed higher efficiency in attaching fines and changing their surface properties compared with Al_2O_3 and SiO_2 NPs. The potential of MgO NP in EOR was also evaluated by Ogolo et al. (2012), an increment of 1.7 % was obtained when using MgO nanofluids prepared by deionized water.

(a)   (b)
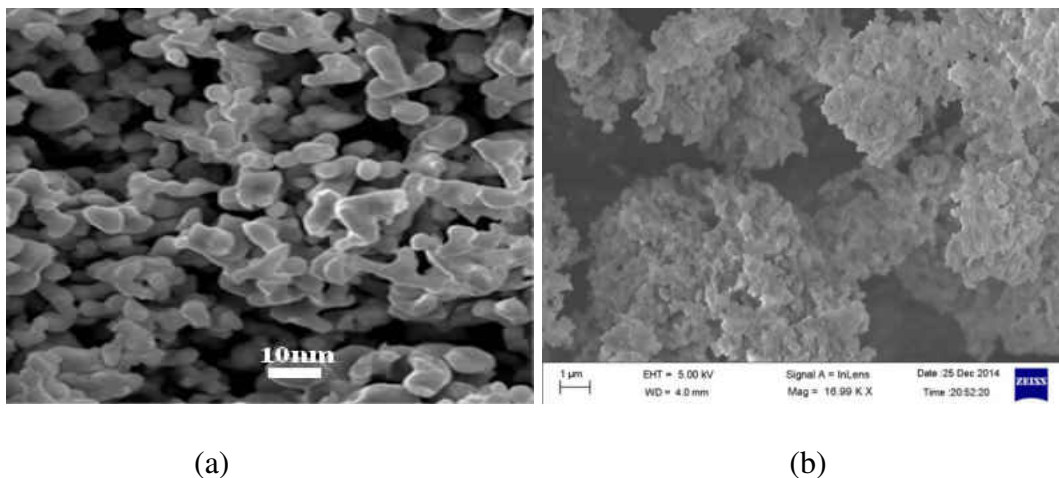
Figure 3-7 FE-SEM images of MgO NPs. Figures were obtained from (a) US-Nano.com. (b) (Kandiban et al. 2015)

2.1.5. Nickel oxide (NiO/Ni₂O₃).

The potential use of nickel oxide for EOR has been proposed by several researchers, as shown in Table 3-3 in APPENDIX. Compared with other metal oxide such as ZrO_2 (Nwidee et al., 2017), Al_2O_3 (Ogolo et al., 2012), and CuO (Haroun et al., 2012), NiO does not possess superior

properties, but it still demonstrates the capabilities to alter rock wettability, reduce oil viscosity as well as remove heavy oil components (Nassar et al., 2008). Moreover, NiO NPs were reported to be able to improve the efficiency of thermal recovery process (Shokrlu et al., 2011).

(a)   (b)
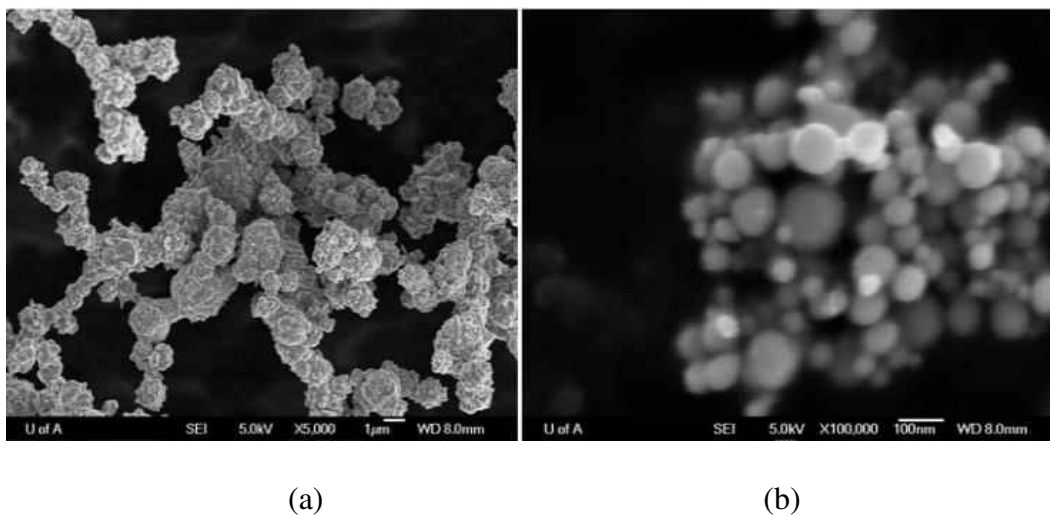
Figure 3-8 FE-SEM images of nickel particles. (a) Microparticles, (b) nanoparticles (Shokrlu et al. 2011).

2.1.6. Tin oxide (SnO₂).

Tin (IV) oxide NPs can be synthesized through chemical precipitation method, sol-gel method, spray pyrolysis, thermal evaporation of oxide powders, chemical vapor deposition (Naje et al., 2013), and hydrothermal method (Patil et al., 2012). SnO_2 nanoparticles are commonly used as electrocatalysts (Jiang et al., 2005) and there was only limited information of SnO_2 NPs in EOR except Ogolo et al. (2012) showed that when being dispersed in deionized water, the performance of SnO_2 in increasing oil recovery from sandstone cores was comparable with ZrO_2 NPs.

<center>(a)   (b)</center>
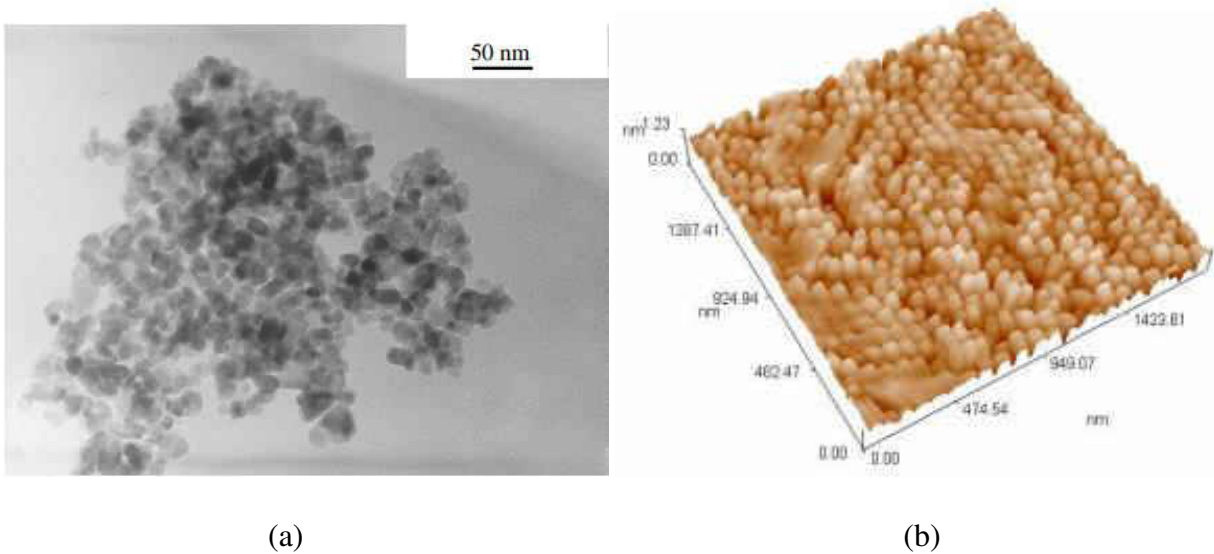
Figure 3-9 Surface characterization of SnO_2 NP. (a) TEM image (Wang et al., 2005), (b) SPM

<center>image (Naje et al. 2013).</center>

2.1.7. Titanium Oxide (TiO₂).

Titanium oxide, sourced from ilmenite, rutile, and anatase (Goresy et al., 2001), is widely

used in painting, sun screening and food coloring. Recently, the potential of TiO_2 NPs in EOR has

been proposed by some researchers, as summarized in Table 3-4 in APPENDIX.

Ehtesabi et al. (2013) used nano TiO_2 to enhance heavy oil recovery from sandstone rocks.

0.01 wt.% TiO_2 alone was able to yield an oil recovery of 80.0±10 %, which was 31.0 % higher

than that of water flooding. However, when NP concentration increased to 1.0 wt.%, pore blockage

would happen due to particle accumulation and the ultimate recovery factor would decrease.

Hendraningrat et al. (2014; 2015) compared the performance of TiO_2, Al_2O_3 and SiO_2 NPs, due to

the more water-wet condition created by TiO_2 NPs, TiO_2 NP flooding demonstrated the highest

efficiency in recovering oil from Berea sandstone when used in the tertiary mode, followed by

Al_2O_3 and SiO_2 NPs. However, compared with SiO_2 NPs, untreated hydrophilic metal oxide NPs

with lower surface conductivity were much easier to aggregate in brine solutions. Therefore, to

<center>44</center>

obtain nanofluids with higher stability and lower the possibility of serve formation damage, dispersants like PVP (Povidone K30) should be applied.
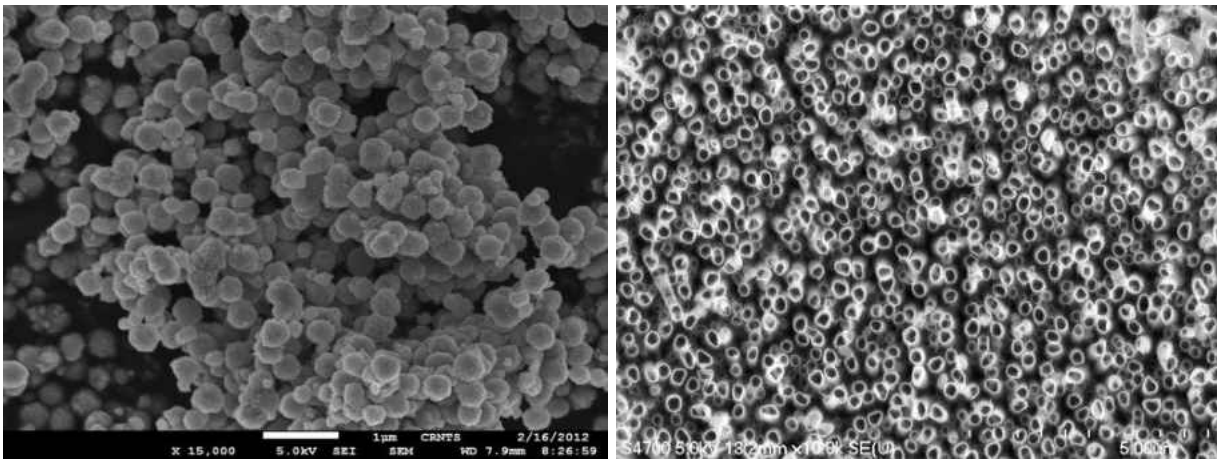
(a)   (b)

Figure 3-10 SEM images of TiO_2 based nanomaterials. (a) TiO_2 NP, (b) TiO_2 nanotube (Indiamart.com).
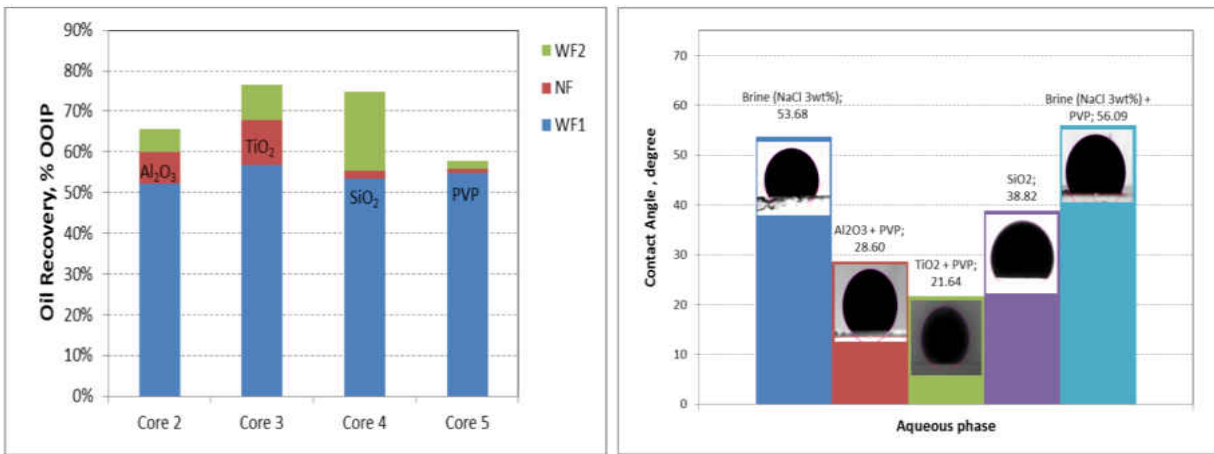
(a)   (b)

Figure 3-11 Comparison between Al_2O_3 NP, TiO_2 NP and SiO_2 NP. (a) Oil recovery, (b) contact angle (Hendraningrat et al., 2014).

TiO$_2$ NPs also have the capability to enhance the efficiency of surfactant or polymer flooding. Cheraghian (2016a) found that the oil recovery by SDS/TiO_2 (2.2 wt.%) mixture was

45

around 50.5 %, compared to that of 46.0 % for pure surfactant. While in the case of polymer flooding, an increase of 3.9 % was obtained when NPs were introduced because of displacing fluid viscosity increase (Cheraghian, 2016b).

2.1.8. Zinc oxide (ZnO).

ZnO nanomaterials are popular additives for various materials and products like plastics, rubbers, cement, lubricants, batteries, tapes, etc. (Hernández-Battez, 2008). ZnO nanostructures with different morphologies and sizes can be prepared via a simple hydrothermal process of zinc nitrate (Zhu et al., 2018; Peng et al., 2016).
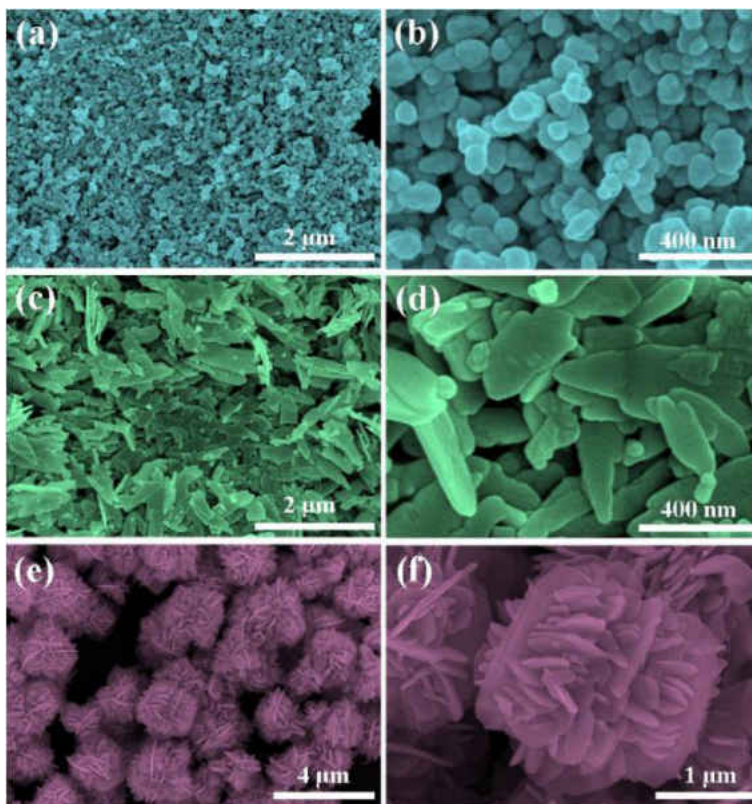
Figure 3-12 SEM images of ZnO nanomaterials. (a-b) Nanoparticles, (c-d) nanoplates, (e-f) nanoflowers (Zhu et al., 2018).

In the past few years, researchers have spent many efforts in developing novel EOR agents and ZnO NPs turned out to be a promising production enhancer (Table 3-5 in APPENDIX). Latiff

et al. (2011) successfully recovered another 26.2 % of the residual heavy oil (μ=16.31 cp, 25 °C) from a glass micromodel when 0.1 wt.% ZnO flooding (prepared by 3.0 wt.% synthetic brine, room temperature) was conducted under electromagnetic wave radiation due to IFT reduction. Also, ZnO NPs are good wettability alteration agents and oil viscosity reducers (Tajmiri et al., 2015). With the help of 0.2 wt.% ZnO NPs, additional 13.27 ~ 17.18 % OOIP and 8.89 % OOIP (heavy oil, μ=16000 cp) could be recovered from water-wet or intermediate-wet sandstone and oil-wet carbonate rocks at 50 °C, respectively. Meanwhile, stabilizers such as anionic surfactants SDS and SDBS could be introduced to prepare more homogeneous ZnO nanofluids, and Adil et al. (2016) reported that the most stable system at 95 °C was composed of 0.1 wt.% ZnO NPs and 0.025 wt.% SDBS at pH=2.0. The dispersion showed a hydrodynamic diameter of 240.9 nm and the viscosity of which was 11.0 % higher than the brine. Additional 5.0 ~ 50.0 % OOIP could be recovered by SDS-0.05 wt.% ZnO mixture due to emulsification (Zaid et al., 2012).

However, Feng (2012) and Ogolo et al. (2012) both found that injecting ZnO NPs into formation might cause permeability impairment.

2.1.9. Zirconium Oxide (ZrO_2).

ZrO_2 is widely used as catalyst, raw material for ceramic production, protective coating agent, refractory material, etc. (Negin et al., 2016). ZrO_2 NPs are commercially available and can also be synthesized through a facial sol-gel method using zirconium oxychloride as a source material (Thammachart et al., 2001). In recent years, the potential of ZrO_2 NPs in EOR area has been exploited (Table 3-6 in APPENDIX). Using 0.05 wt.% ZrO_2 alone in deionized water, the intermediate-wet calcite substrates can be altered water-wet within 2.0 hrs and a more water-wet condition could be achieved by increasing NP concentration (0 ~ 0.05 wt.%), aging time or solution

salinity (3.0 ~ 20.0 wt.% NaCl) (Karimi et al., 2012). Also, ZrO_2 NPs are proved to be good asphaltene precipitation inhibitors and mobility modifiers (Rezvani et al., 2018).

In addition, ZrO_2 NPs are compatible with both nonionic and cationic surfactants. Karimi et al. (2012) conducted an experimental study on the effects of ZrO_2 NP-nonionic surfactant augmented system on changing the wettability of carbonate rocks. Due to the adsorption of NPs and the formation of nanotextures (Figure 3-13) on rock surfaces, strongly oil-wet rock samples were rendered strongly water-wet, resulting in additional oil recovery of 48.0 % and 58.0 % OOIP, respectively when 5.0 wt.% and 10.0 wt.% ZrO_2 NPs were added in spontaneous imbibition tests at 70 ℃.
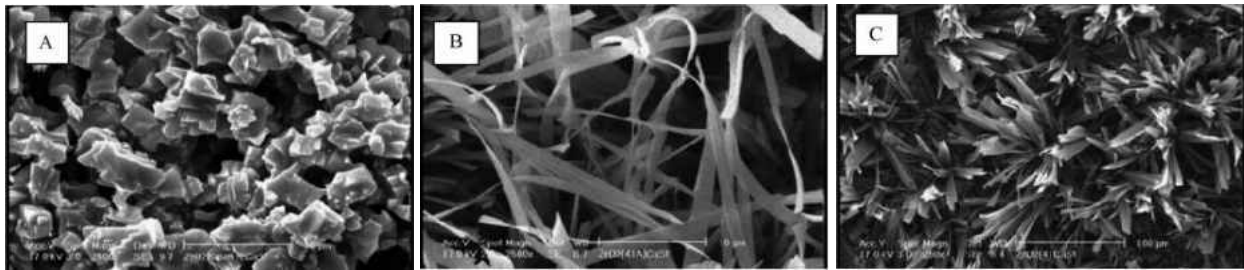
Figure 3-13 SEM images of an oil-wet carbonate rock aged in different fluids (pH=2.0 ~ 3.0). (A) Tween 80+Span 85+glycerin+LA2, (B) Tween 80+Span 85+glycerin+LA2+5 wt.% NP, (C) Tween 80+Span 85+glycerin+LA2+10 wt.% NP (Karimi et al., 2012).

2.2. Carbon-Based Nanomaterials.

Carbon NPs, carbon nanotubes and graphene nanosheets all belong to the family of carbon-based nanomaterials. They are very popular in the scientific community and engineering area because of their extraordinary physical, chemical, optical, mechanical, thermal properties. In recent years, their applications in oil production also attracted some attention, the details are given in Table 3-8 in APPENDIX.
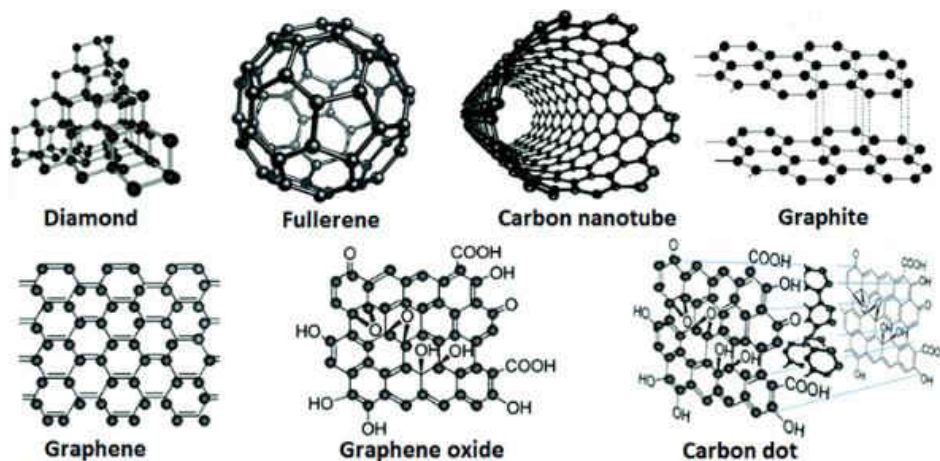
Figure 3-14 The schematics of the representative carbon-based nanomaterials (Yan et al., 2016).

2.2.1. Carbon Nanoparticle.

Spherical shape carbon nanoparticles with unique properties are generally synthesized by hydrothermal method, which are widely used in different applications (Cassagnau, 2015) including EOR. Li et al. (2017a) prepared a novel and stable nanofluid by dispersing lab-synthesized carbon NPs into 3.0 wt.% NaCl brine. Experimental results demonstrated that with the addition of 0.1 wt.% carbon NPs, the oil-water IFT could be reduced to 13.4 mN/m from 26.2 mN/m, oil contact angle would increase to 120° from 36° and an increase of 26.1 % in ultimate oil recovery was obtained at 60 °C. Meanwhile, Kanj et al. (2011) reported similar results in the field tests. When used in high temperature (> 100 °C) and high salinity (≥ 12.0 wt.%) condition, carbon NP A-Dots yielded an oil recovery as high as 86.0 %.

However, reducing particle retention in the reservoir is also important to minimize formation damage. Yu et al. (2010) studied the transportation behaviors of carbon NPs in either carbonate or sandstone porous mediums. They found that the increasing ionic strength would significantly delay the breakthrough time of carbon NPs and increase particle retention due to the

charge interactions between NPs, salt ions and porous mediums. To mitigate particle retention, conducting NPs surface modification is necessary.

2.2.2. Carbon Nanotube.

Carbon nanotubes, applicable for emulsion and foam preparation and stabilization, as well as drug delivery, have attracted great research interests thanks to their interfacial activeness.

(a)   (b)   (c)
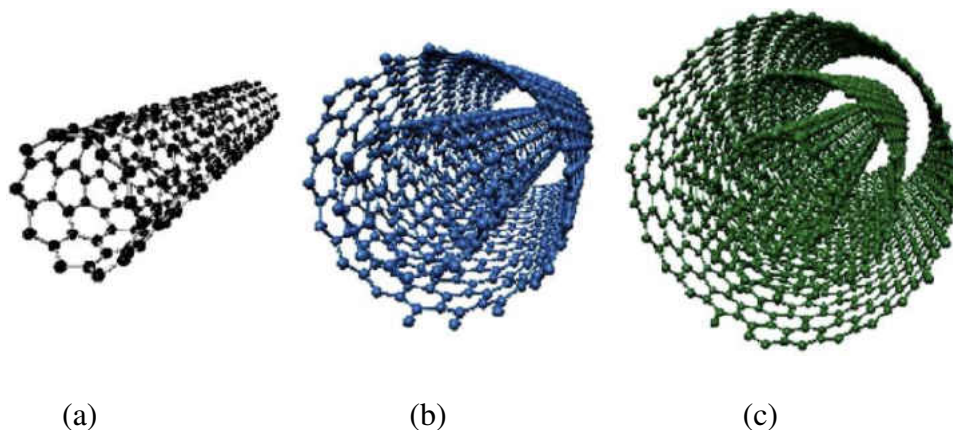
Figure 3-15 Ball and stick illustrations of (a) single, (b) double, (c) triple-walled carbon nanotubes (IOP, 2013).

However, their low stability especially at high salinity conditions has limited their applications to a certain extent. Therefore, different additives including polymers and surfactants were added. Bai et al. (2010) tried to use Triton X-series nonionic surfactant with different hydrophilic polyethoxylated chain lengths to improve the dispersion stability of MWCNTs through hydrophobic and π–π interactions. However, the retention of CNTs in the formation is unavoidable and the adsorption rate was closely related to formula stability, CNT concentration and oil saturation (Kadhum, 2015). CNTs increase oil recovery mainly through IFT reduction (AfzaliTabar, 2017) and wettability alteration. Alnarabiji et al. (2016) compared the impacts of CNT concentration on ultimate oil recovery and found that the highest recovery rate of 31.8 % was

achieved by 0.05 wt.% CNT in deionized water. In addition, when nano flooding was conducted at a proper injection rate under the impacts of electromagnetic wave, 36.67 % residual oil in place (ROIP) could be extracted by 0.01 wt.% of MWNT (Chandran, 2013).

2.2.3. Graphene Nanosheet.

Graphene nanosheet is the product of chemical oxidation and exfoliation of graphite powders and it is widely used in water treatment, battery, and other industries (Cote et al., 2010; You et al., 2018). With an edge-to-center distribution of hydrophilic and hydrophobic domains, graphene oxide is considered as an unconventional surfactant which is less active than the conventional ones (Lian et al., 2017). Therefore, conducting surface modification to improve graphene performance and stability is very important. An amphiphilic graphene-based nanosheet synthesized by Luo et al. (2016) could spontaneously accumulate at the heptane/brine interface and change the interfacial properties. With excellent stability in the presence of salts, the graphene nanosheets (0.005 ~ 0.01 wt.%) recovered additional 6.7 ~ 15.2 % oil in the tertiary mode. Similar phenomenon was also observed by Chen et al. (2018) and Radnia et al. (2018).
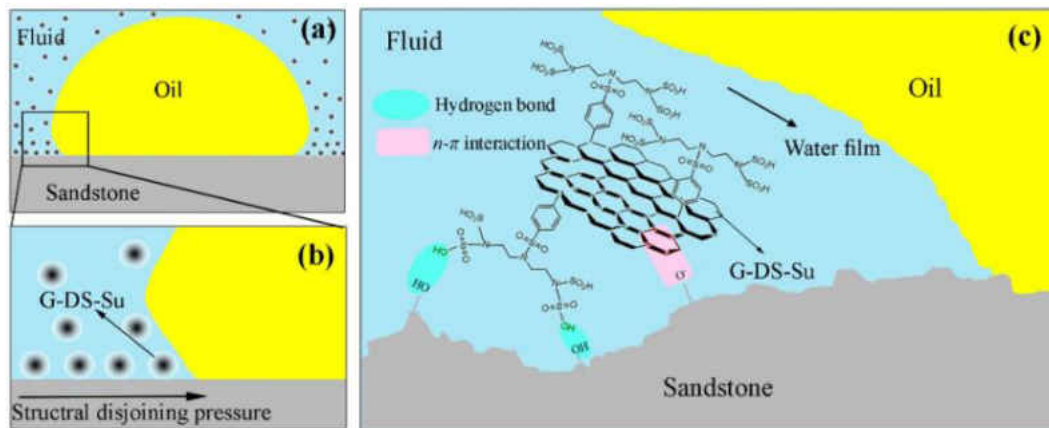
Figure 3-16 The sandstone wettability alteration due to: (a)-(b) structural disjoining pressure mechanism and (c) adsorption of G-DS-Suonto the sandstone (Radnia et al., 2018).

Moreover, to extend the application of graphene nanosheet to harsher reservoir conditions with even higher temperature and salinity, Zuniga et al. (2016) connected a zwitterionic polymer to the base nanomaterials and obtained an excellent formula stable for over 140 days at 90 °C, API brine (8.0 wt.% NaCl + 2.0 wt.% CaCl$_2$).

2.3. Silica-Based Nanomaterials.

Silica nanoparticles (SiNPs) are the most commonly used inorganic nanomaterials because of their wide availability, low cost for fabrication and surface modification. What's more, they can be produced with a good degree of control, and the physical-chemistry properties of silica surfaces and interfaces are among the most well-known (Miranda, 2012). By connecting different terminal groups onto particle surfaces, SiNPs with a wide range of hydrophilicity can be obtained. Herein, SiNPs EOR with or without other additives like surfactants and polymers were discussed systematically, details were shown in Table 3-9 in APPENDIX.

2.3.1. Pure SiNPs.

Using silica nanofluid prepared by bare SiNPs or surface modified SiNPs in the absence of other additives for EOR has been reported by some researchers. Different SiNPs involved formulas were tested for sandstone and carbonate reservoirs, but the additional oil recovery was not guaranteed and the performance varies in different situations.

Hendraningrat et al. (2013a) and Xu et al. (2015) found that IFT showed a decrease tend when hydrophilic NPs were introduced into the brine and higher NPs concentration resulted in lower IFT and higher oil mobilization efficiency. But Roustaei and Bagherzadeh (2015) reported a higher IFT in their case when hydrophilic SiNPs were added and Jiang (2017) found that SiNPs barely have any impacts on IFT. However, the majority of the related studies including these three reached an agreement on the capability of SiNPs to alter rock wettability to a more water-wet

condition, but the underlying mechanisms differ for different porous mediums. For sandstone reservoirs, NP adsorption-induced nonuniform rock roughness change is believed to be the possible mechanism (Li et al., 2016; Lu et al., 2017), while for carbonate reservoirs, the partial release of carboxylate groups from the oil-wet calcite surface and their replacement with hydrophilic SiNPs was suggested to be the functional mechanism (Monfared, 2016). Contact angle is an important parameter to characterize rock wettability, but Jiang et al. (2017) found that the contact angle measurement on quartz plates had relatively large uncertainty, while the changing trend was clearer for calcite plates and the smaller the NP size and the higher the NP concentration, the smaller the water contact angle (more water wet).

Wettability alteration is beneficial for the oil recovery process (Al-Anssari et al., 2018; Li et al., 2017b; Youssif et al., 2018). The nanofluid prepared by 1.0 wt.% surface modified SiNPs and 5.0 wt.% NaCl brine (pH=10.0) was able to recover approximately 38.0 % OOIP through spontaneous imbibition, compared to that of 6.0 % for pure brine (Dai et al., 2017). Xu et al. (2018) also reported that hydrophilic SiNPs in an aqueous phase could lead to dramatic swelling, dewetting, and disjoining of crude oil, and therefore resulted in approximately 11.0 % incremental oil recovery in a completely homogeneous porous micromodel when 0.2 wt.% NPs (prepared by seawater) flooding was conducted.

The type of terminal groups, NP size, rock permeability, initial rock wettability, injection rate as well as temperature all have influences on an oil recovery process. Miranda et al. (2012) conducted molecular dynamic simulation to compare Silanized (H-passivated), PEGlyated, and sulfonated functionalized SiNPs. They concluded that PEG chain presented the highest values for the desirable characteristics of NPs to be used for EOR. Meanwhile, increasing the number of PEG monomers was conductive to increase NP's mobility, which was consistent with Lara's (2016)

work. Hendraningrat et al. (2013b) showed that Nano-EOR was applicable in a wide range of reservoir permeability and the initial rock wettability significantly affected incremental oil recovery. When residual oil saturation is similar, increasing NP size and nanofluid injection rate might decrease the efficiency but increasing the temperature would be advantageous to the oil production process. NP adsorption is always irreversible (Al-Anssari, 2016), and the breakthrough of the injected NPs will be delayed when NP concentration increases. Worse still, the pressure drop would increase more rapidly due to porosity and permeability impairment (Yuan, et al., 2016; Zallaghi et al., 2018), and the adverse impacts were more obvious for nano-structure particles compared with colloidal NPs (Li et al., 2015).

(a)   (b)
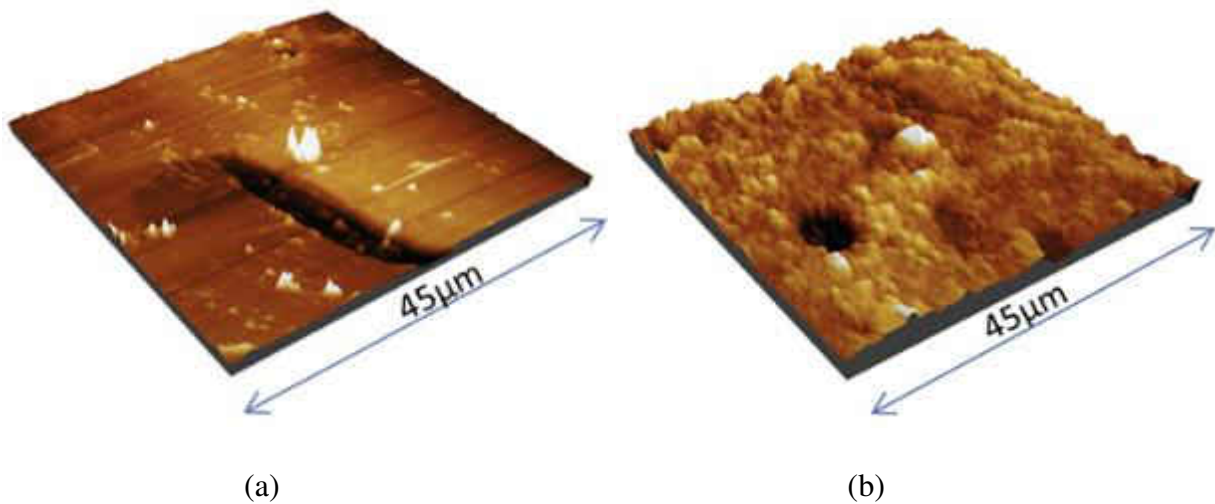
Figure 3-17 AFM images of a calcite surface used in the experiments before (a) and after (b) nano-modification (Al-Anssari, 2016).

2.3.2. SiNPs with Surfactant.

SiNPs have been widely studied for EOR. In recent years, the combinations of silica NPs and surfactants with improved stability and more controllable mobility were tested to have great potential in low permeability reservoirs (MeElfresh, 2012a; 2012b).

| (a) | (b) | (c) |
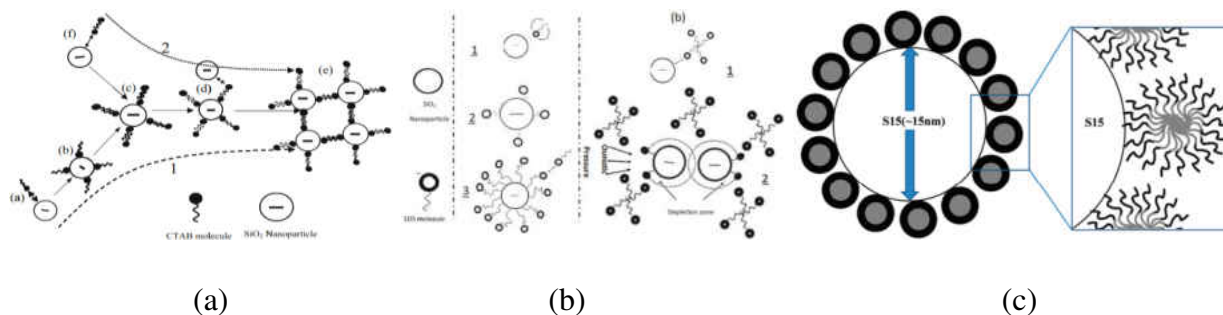
Figure 3-18 Schematic of surfactant adsorption on hydrophilic SiNP surface. (a) Cationic surfactant (Songolzadeh, 2017), (b) anionic surfactant (Songolzadeh, 2017), (c) nonionic surfactant (Sharma et al., 2010).

2.3.2.1. SiNPs with Cationic Surfactant.

The most commonly used collaborative cationic surfactant for SiO_2 is cetyltrimethyl ammonium bromide (CTAB). It is a quaternary ammonium surfactant widely used in biology, medicine, protein electrophoresis, DNA extraction, nanoparticle synthesis, etc.

The addition of surfactant CTAB into SiNPs dispersion modifies the hydrophobic/lipophilic character of NPs and increases their affinity to the interfaces (Ravera, 2008). While adding SiNPs into CTAB systems increases IFT and renders the originally oil-wet rocks more water-wet. Additional 46.7 % and 10.0 % oil were recovered compared with brine and surfactant imbibition in Roustaei's (2013) study. In addition, the surface modulus that defines the dilational viscoelasticity and surface strength also rises with increasing NP concentration, which is beneficial for stable foam and emulsion preparation (Jiang et al., 2016).

However, due to the opposite charge of surfactant and NPs, the negative charge on SiNPs surfaces would be gradually neutralized with increasing CTAB concentration, thus, particle would coagulate to form a white interconnected network (Ma et al., 2010; Songolzadeh et al., 2017), which is more likely to cause pore plug and formation damage.

2.3.2.2. SiNPs with Anionic Surfactant.

Owing to their similar charge, anionic surfactant shows the capability to increase the stability of SiNPs through supercharging effects (Ahmed et al., 2017), therefore, SiNP-anionic surfactant systems are more widely used in oil and gas industry. However, it is worth mentioning that more attention should be paid to SiNP/surfactant concentration ratios in order to prepare a stable and applicable formula, because sometimes when surfactant concentration is higher than its CMC (critical micelle concentration), osmotic depletion would produce adverse effects. SiNPs alone nearly have no impacts on IFT. But ultra-low ITFs or expanded ultra-low IFT region can be obtained when SiNPs were used together with anionic surfactants (Le et al., 2011; Xu et al., 2018).

Adding anionic surfactant into SiNPs can also intensify NPs' performance in altering wettability (Jha et al., 2019). Cheraghian et al. (2017) reported that an oil recovery of 45.0 % was obtained for SDS near its CMC. Addition of 2.2 wt.% fumed SiNPs enables a more water-wet condition and a 13.0 % increment in ultimate recovery. SiNPs with anionic surfactant SY can even alter the reservoir wettability from a liquid-wet state to a gas-wet state, therefore increases the mobility of liquid. As a result, the oil recovery increased from 46.6 % to 78.4 % and the residual oil saturation reduced from 29.2 % to 17.8 % (Franco-Aguirre et al., 2018).

However, the hydrophilicity of SiNPs might affect the overall performance. Zargartalebi et al. (2014) compared the interfacial properties of hydrophilic and slightly hydrophobic fumed silica nanoparticles when in conjunction with SDS. They found that the reduction in IFT was much more considerable for hydrophobic particles at all surfactant concentrations and the efficiency of SDS was significantly improved, resulting in additional oil recovery of 15.86 ~ 20.41% (Zargartalebi et al., 2015).

2.3.2.3. SiNPs with Nonionic Surfactant.

Nonionic surfactants are inexpensive, easily available, mild and environmental-friendly chemicals with uncharged hydrophilic head, and have been applied in different applications. The cooperation between nonionic surfactant and SiNPs in EOR is also a worth-studying area.

Through small-angle X-ray scattering (SAXS) and contrast matching small angle neutron scattering (SANS) analysis, Sharma et al. (2010) found that the adsorption of nonionic surfactant on hydrophilic SiNPs gives a rise to the short-range interparticle repulsion that makes particle aggregation thermo-reversible. In addition, the adsorption density of nonionic surfactant on carbonate rocks can be reduced more by hydrophobic SiNPs than hydrophilic ones (Ahmadiand Shadizadeh, 2012). By integrating hydrophobic SiNPs with nonionic surfactant Triton X-100, Zhao et al. (2018) developed a nanofluid with excellent anti-temperature and anti-salinity property. Moreover, the spontaneous imbibition tests showed that the proposed formula can improve oil recovery to about 16.0 %, comparing with about 8.0 % for Triton X-100 solution because of more noticeable wettability alteration. Kuang et al. (2018) compared the synergistic effects between SiNPs and different additives including oleic acid, polyacrylic acid, cationic surfactant (n-Alkyl dimethyl benzyl ammonium chloride), anionic surfactant (ammonium alkyl, C_{6-10}, Ether Sulfate) and nonionic surfactant (linear alcohol, C_{9-11}, Ethoxylate) in EOR. They concluded that the nanofluids with nonionic surfactant were the most effective colloidal solutions for oil recovery in both sandstone and carbonate core samples due to IFT reduction.

2.3.3. SiNPs with Polymer.

Chemical loss due to adsorption, precipitation, and other reasons reduces the efficiency of polymer flooding schemes. The addition of SiNPs can help resolve such problems and enhance polymer performance. Cheraghian et al. (2014) found that SiNPs could decrease polymer

adsorption better than clay particles. Zhu et al. (2014) reported that HAHPAM (hydrophobically associating hydrolyzed polyacrylamide)/silica hybrids exhibited better shear resistance and long-term thermal stability than HAHPAM alone in synthetic brines. In addition, adding SiNPs into HAHPAM system significantly increased the apparent viscosity and the elastic modulus of the original system, and resulted in a higher oil recovery factor of 10.57 %, compared to that of 5.44 % for pure polymer solution. Sharma et al. (2016) showed that SiO_2 nanofluids significantly increased oil recovery, particularly at higher temperatures, mainly due to IFT reduction, displacing fluid viscosity increase, and wettability alteration. Additional 11.99 % and 19.25 % OOIP was recovered by polymer-SiNPs and surfactant-polymer-SiNPs systems compared with water flooding, respectively. Similar results were also published by Choi et al. (2017) and Saha et al. (2018).
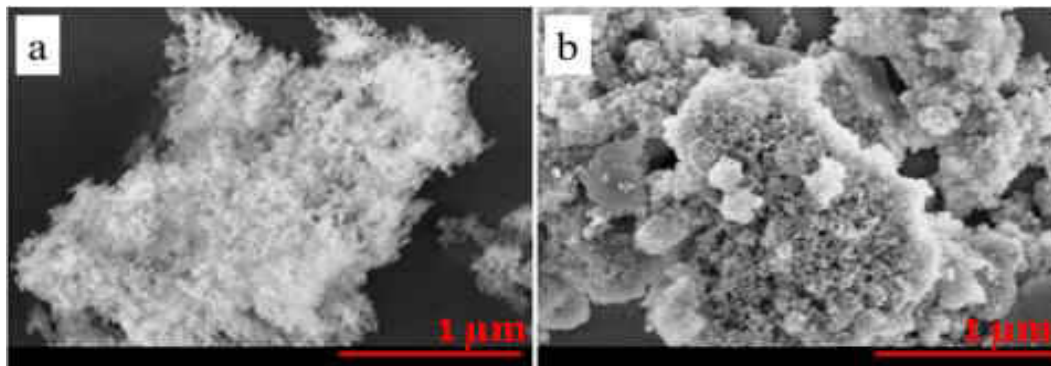
Figure 3-19 SEM images of (a) SiNP-PAM and (b) SiNP-PAM-SDS nanofluids (1.0 wt.% SiO_2) at 30 °C (Sharma et al., 2016).

3. Nanoparticle Stability

Though promising results have been obtained for nano-EOR, NP stability is always a worth-noticing problem, which is also a major challenge to extend its applications. According to our review, most previous studies that evaluated NP performance were conducted either in deionized water, low salinity brine or low temperatures. The published studies also seldomly

address the NP size change when environmental condition changes and there are no specific criteria to characterize particle stability (MeElfresh et al., 2012b; Hamad et al., 2016). However, in fact, NP dispersions become unstable and agglomerated when they are subjected to changes in pH, NP concentration, salinity, temperature, etc. (MeElfresh et al., 2012b) Divalent cations like Mg^{2+}, Ca^{2+}, and Ba^{2+} are more effective in causing NP aggregation than the monovalent cation such as Na^+ and K^+, where the critical salt concentration (CSCs) of monovalent cations are about 100 times higher than those of divalent cations. However, the CSCs of monovalent cations experiences a sharper decrease than divalent cations when temperature increases (Metin et al., 2011). Other factors including initial particle size and particle type also strongly affect the kinetics of particle aggregation (Metin et al., 2014).

NP aggregation and precipitation decrease the effectiveness of the nanofluids and could cause severe formation damage. To ensure the long-distance transportation and long-term stability of NPs and to reduce their retention and aggregation, conducting NP surface modification or adding additives is necessary. Due to different surface modification methods, particle size varies a lot. Though in normal cases, larger particles show higher stability than smaller particles, smaller particles with better injection and transportation ability are better preferred especially for formations with small pores and narrow throats.

The retention rate of large NP aggregates is much higher than non-aggregated NPs (Kim, et al., 2015). SiNP aggregation can be prevented by lowering the pH according to "H^+ protection" theory (Sofla et al., 2018). By using hydrochloric acid as the stabilizer, SiNPs were found to free from aggregation at high salinity and high temperature conditions (3.8 wt.% synthetic brine, 60 ℃).

Other stabilizers or modification methods are also effective. Ranka et al. (2015) used antipolyelectrolyte based stabilizers (polyzwitterion chain incorporated within a polymeric

stabilizer) for either hydrophilic silica or hydrophobic polystyrene NPs. Long-term colloidal stability was achieved at a salinity up to 12.0 wt.% at 90 °C. In a similar way, Zuniga et al. (2016) modified the partially reduced graphene oxide (prGO) with a zwitterionic polymer and obtained a new material with excellent dispersibility and long-term stability in high salinity brines including standard API brine and Arab-D brine. The dispersions remained stable for over 140 days at 90 °C. Xue et al. (2014) grafted random copolymers onto the iron oxide to provide colloidal stability in API brine. However, particles coated or modified with polymers usually have larger size, which is unfavorable for their transportation in the narrow pore throats. Replacing copolymer by low molecular weight ligands solves this problem. By covalently connecting a hydrophilic ligand onto SiNPs surfaces, Worthen et al. (2016) prepared a novel and highly stable SiNP nanofluid, whose hydrodynamic diameter remained essentially constant at room temperature and up to 80 °C for over 30 days at acidic conditions. Moreover, there was no huge size difference between the surface modified NPs and the original NPs. With this surface-modified SiNPs alone, Griffith and Daigle (2018) successfully prepared stable O/W emulsions with zero shear elastic storage modulus.

4. Challenges and Recommendations

There are still some other challenges for the future development and large-scale applications of nano-EOR, mainly including the limitations of technologies, cost, environmental and health issues (Agista et al., 2018; Sun et al., 2017; Negin et al., 2016; Almahfood and Bai, 2018).

4.1 Challenges

(1) The lack of theoretical and numerical investigation into nano scale and large-scale pilot tests have limited the thorough understanding of nano-EOR technologies.

(2) The relationships between nanomaterial adsorption, wettability alteration capability and permeability impairment should be figured out to prepare suitable EOR formulas.

(3) According to the research of Archer et al. (2012), nanomaterials may cause damage to DNA, chromosomes and lung diseases. Long time exposure to nanomaterial could pose a significant risk. Therefore, integrated research on the health and safety of NPs must be done to prevent the risk to human beings and the environment.

4.2 Recommendations

(1) Development and preparation of homogeneous and highly stable nanofluid is still a tough and challenging work. The cost-efficiency property should also be considered.

(2) Nanofluids mixtures composed of different kind of nanomaterials for EOR is a new and promising research area.

(3) When preparing augmented systems, a small change in concentration ratio, particle type, particle surface group and surfactant or polymer structure can result in great variety.

5. Summary

In this chapter, a critical review of the most recent research progress in nano-EOR is presented. This review shows great potential of either pure nanofluids or compound nanofluids, indicating that nano-EOR with IFT reduction, wettability alteration and viscosity modification capability as well as disjoining pressure mechanism is a good substitute for the traditional chemical EOR methods. However, the porosity and permeability impairment caused by NPs adsorption and retention, the difficulty in preparing stable nanofluids with high tolerance towards increasing temperature and salinity and its possibility in causing health problems all would limit its large-scale applications. Future researches should combine the theoretical and numerical investigations in nano-scale with the experimental work.

APPENDIX

Table 3-1 Applications of aluminum oxide nanomaterials in enhanced oil recovery

NP	Dispersant	C(NP), wt.%	T, °C	Oil viscosity, cp/API, °	Porous media	Recovery method	EOR mechanism	EOR, %	Reference
Al_2O_3 (MgO, Fe_2O_3, Ni_2O_3, ZnO, ZrO_2, SnO, SiO_2)	DI water	0.3	25	53.3 cp	Sandpack	Flooding	Oil viscosity reducer	5.0~12.5	(Ogolo et al., 2012)
Al_2O_3	Anionic surfactant (PRNS) DI water	0.01~1.0	50	64 cp (25 °C) 19.2°	Sandstone Sandpack (2.19 D)	Imbibition Flooding	Wettability alteration	N/A	(Giraldo et al., 2013)
Al_2O_3 (ZnO)	Anionic surfactant (SDS) 3.0 wt.% brine	0.05	60	N/A	Glass beads pack	Flooding	Emulsification	9.5~30.0	(Zaid et al., 2013)

Al$_2$O$_3$, (Fe$_2$O$_3$ SiO$_2$)	2.5 wt.% brine (+ propanol)	0.035~0.3	25	40.38 cp 29.56°	Sandstone	Flooding	Wettability alteration IFT reduction	20.2	(Joonaki and Ghanaatian, 2014)
Al$_2$O$_3$ (TiO$_2$, SiO$_2$)	Povidone (PVP, 0.1~1.0 wt. %) 3 wt.% brine	0.05	25~80	5.1 cp 39.80°	Berea sandstone (118~330 mD, 15.2%)	Flooding	Wettability alteration	13.34	(Hendraningrat and Torsæter, 2014)
Al$_2$O$_3$ (TiO$_2$, SiO$_2$)	0.3~2.5 wt.% brine	0.005	26~60	21.7 cp (26 °C) 32.46°	Limestone	Flooding	Wettability alteration IFT reduction Oil viscosity reducer	4.5~9.9	(Bayat et al., 2014)
Al$_2$O$_3$ (NiO, TiO$_2$, SiO$_2$)	3.0 wt.% brine	0.01~0.1	25	17.45°, heavy oil	Berea sandstone (150~210 mD, 20%)	Flooding	Displacing fluid thicker, IFT reduction, asphaltene precipitation inhibitor	6.06	(Alomair et al., 2015)
γ-Al$_2$O$_3$	0.2~20.0 wt.% brine	0.1	25~ 80	N/A	Berea sandstone	Flooding	Clay swelling inhibitor	7.0~10.0	(Kiani et al., 2016)

					(32 mD, 23.28%)				
Al_2O_3 (ZrO_2)	Cationic surfactant (CTAB, 0.12 wt.%) 2.0 wt.% brine	0.5	N/A	6.4 cp (40 °C) 28.6°	Carbonate dolomite (100 mD, 21%)	N/A	Wettability alteration IFT reduction	N/A	(Moslan et al., 2016)
Al_2O_3 (SiO_2, TiO_2, Fe_2O_3, CuO SiO_2 + Al_2O_3, SiO_2 + TiO_2, Al_2O_3 + TiO_2)	Surfactants (PVP, PEG, SDS, 1.0 wt.%, stabilizers) DI water 0~20.0 wt.% NaCl	0.01~5.0	20~80	1527 cp (50 °C) 14.98°	Sandstone	N/A	Wettability alteration	N/A	(Sun et al., 2018)

Table 3-2 Applications of iron oxide nanomaterials in enhanced oil recovery

NP	Dispersant	C(NP), wt.%	T, °C	Oil viscosity, cp/API, °	Porous media	Recovery method	EOR mechanism	EOR, %	Reference
Fe_3O_4 (Magnetic NP)	Surfactants (oleic acid, tetramethylammonium	15.0~20.0	≤140	N/A	Sand trays	Flooding	Displacing fluid thicker (in a magnetic field)	N/A	(Kothari et al., 2010)

	hydroxide, citric acid, soy lecithin) Hydrocarbon oil						Oil viscosity reducer		
Fe$_2$O$_3$ (CuO, NiO)	4.0% NH$_3$.H$_2$O in DI water	5.0	25	28.4°	Carbonate (77~149 mD, 10~24%)	Flooding	Wettability alteration	9.0~14.0	(Haroun et al., 2012)
Fe$_2$O$_3$ (MgO, Ni$_2$O$_3$, SnO$_2$, ZrO$_2$, Al$_2$O$_3$, ZnO, SiO$_2$)	DI water	0.3	25	53.3 cp	Sandpack	Flooding	Oil viscosity reduction	9.2	(Ogolo et al., 2012)
CoFe$_2$O$_4$ (Magnetic NP)	Anionic surfactant (SDS, stabilizer, 0.1~1.0 wt.%) 1.0 wt.% brine With electromagnetic waves (Antenna)	N/A	N/A	3.37 cp 42.1°	N/A (158~560 mD, 18~21 %)	Flooding	N/A	22.88	(Yahya et al., 2012)
Fe$_3$O$_4$ (Magnetic NP)	Sodium oleate coated NPs (hydrophobic) DI water	N/A	N/A	N/A	N/A	Flooding	Penetrate into small capillaries and deep formation, increase	N/A	(Shekhawat et al., 2016)

NP	Dispersant	C(NP), wt.%	T, ℃	Oil viscosity, cp/API, °	Porous media	Recovery method	EOR mechanism	EOR, %	Reference
	Magnetic field						the sweep efficiency		

Table 3-3 Applications of nickel oxide nanomaterials in enhanced oil recovery

NP	Dispersant	C(NP), wt.%	T, ℃	Oil viscosity, cp/API, °	Porous media	Recovery method	EOR mechanism	EOR, %	Reference
NiO	Toluene	1.0~5.0	N/A	Heavy oil	N/A	N/A	Asphaltenes remover	N/A	(Nassar et al., 2008)
NiO	Polymer (Xanthan gum) DI water	0.05	N/A	Heavy oil/bitumen	Glass bead micromodels (6 D)	Flooding	N/A	N/A	(Shokriu and Babadagli, 2011)
NiO (CuO, Fe$_2$O$_3$)	4.0 % NH$_3$.H$_2$O in DI water	5	25	28.4°	Carbonate (77~149 mD, 10~24%)	Flooding	Wettability alteration	9.0~14.0	(Haroun et al., 2012)
Ni$_2$O$_3$ (MgO, SnO$_2$, ZrO$_2$, Al$_2$O$_3$, Fe$_2$O$_3$, ZnO, SiO$_2$)	DI water	0.3	25	53.3 cp	Sandpack	Flooding	Oil viscosity reducer	2.0	(Ogolo et al., 2012)

NiO (ZrO₂)	3.0~20.0 wt.% brine	0.004~0.05	N/A	Oil-wet rendered by dodecyltriet hoxysilane	Limestone	N/A	Wettability alteration	N/A	(Nwidee et al., 2017)
NiO	Polymer (Xanthan gum, 0.005~0.04 wt.%) CSBK medium (pH=7.2~7.4)	N/A	30	Heavy oil	Sand pack	Flooding	Displacing fluid thicker	5.98	(Rellegadla et al., 2018)

Table 3-4 Applications of titanium dioxide nanomaterials in enhanced oil recovery

NP	Dispersant	C(NP), wt.%	T, ℃	Oil viscosity, cp/API, °	Porous media	Recovery method	EOR mechanism	EOR, %	Reference
TiO₂	0.5 wt.% brine	0.01~1.0	N/A	41.21 cp 22.3°	Carbonate (Φ =23.7%)	Flooding	Wettability alteration	14.0~31.0	(Ehtesabi et al., 2014; 2015)
TiO₂ (Al₂O₃, SiO₂)	0.3~2.5 wt.% brine	0.005	26~60	21.7 cp (26 ℃) 32.46°	Limestone	Flooding	Wettability alteration, IFT reduction, Oil viscosity reducer	3.0~6.6	(Bayat et al., 2014)

TiO$_2$ (Al$_2$O$_3$, SiO$_2$)	Povidone (PVP, 0.1~1 wt. %) 3.0 wt.% brine	0.05	25~80	5.1 cp 39.80°	Berea sandstone (118~330 mD, 15.2%)	Flooding	Wettability alteration	20.0	Hendraningrat and Torsæter, 2014; 2015)
TiO$_2$ (Al$_2$O$_3$, NiO, SiO$_2$)	3.0 wt.% brine	0.01~0.1	25	17.45° heavy oil	Berea sandstone (150~210 mD, 20%)	Flooding	Displacing fluid thicker, IFT reduction, asphaltene precipitation inhibitor	1.8	(Alomair et al., 2015)
TiO$_2$	Anionic surfactant (SDS, 0.16~0.2 wt.%) 2.0 wt.% brine	2~2.4	N/A	1320 cp (25 ℃) 17°	Five-spot glass micromodels	Flooding	Surfactant adsorption reducer	4.85	(Cheraghian et al., 2016a)
TiO$_2$	Polymer (HPAM, 0.12~0.42 wt.%) 2.0 wt.% brine	1.9~2.5	N/A	1320 cp (25 ℃) 17°	Sandstone (282 mD, 18.3%)	Flooding	Displacing fluid thicker	1.3~4.2	(Cheraghian et al., 2016b)
TiO$_2$ (SiO$_2$)	Anionic surfactant (SDS, 0.2 wt.%)	0.1	N/A	68 cp (22 ℃)	Micromodels	Flooding	Wettability alteration	6.0	(Sedaghat et al., 2016)

				19.4°	(1600 mD, 52.48%)					
	Polymer (HPAM, 0.12 wt.%)									
TiO$_2$	Anionic surfactant (AAS, 0.3 wt.%) Nonionic surfactant (EA, 0.3 wt.%) 4.0 wt.% brine	0.05~0.2	40	24 cp (40 ℃)	Sand pack	Flooding	Surfactant adsorption reducer, IFT reduction	7.81	(Nourafkan et al., 2018)

Table 3-5 Applications of zinc oxide nanomaterials in enhanced oil recovery

NP	Dispersant	C(NP), wt.%	T, ℃	Oil viscosity, cp/API, °	Porous media	Recovery method	EOR mechanism	EOR, %	Reference
ZnO	Anionic surfactant (SDS) 3.0 wt.% brine	0.1	N/A	16.31 cp (25 ℃)	Glass bead pack (380 mD，28.7%)	Flooding+ electromagnetic wave radiation	EM wave push ZnO NP to oil-water interface	7.54	(Latiff et al., 2011)
ZnO (Al$_2$O$_3$, MgO, Fe$_2$O$_3$, Ni$_2$O$_3$,	DI water	0.3	25	53.3 cp	Sandpack	Flooding	Oil viscosity reducer	3.3	(Ogolo et al., 2012)

ZrO$_2$, SnO$_2$, SiO$_2$)									
ZnO (Al$_2$O$_3$)	Anionic surfactant (SDS) 3 wt.% brine	0.05	60	N/A	Glass beads pack	Flooding	Emulsifier	5.0~50.0	(Zaid et al., 2013)
ZnO	N/A	0.2	50	16000 cp (25 °C) 13°	Sandstone Carbonate	Imbibition	Wettability alteration IFT reduction	8.89~17.18	(Tajmiri et al., 2015)
ZnO	Anionic surfactants (SDS, SDBS, oleic acid) 3.0 wt.% brine	0.01~0.1	95	N/A	N/A	N/A	Displacing fluid thicker	N/A	(Adil et al., 2016)

Table 3-6 Applications of zirconium oxide nanomaterials in enhanced oil recovery

NP	Dispersant	C(NP), wt.%	T, °C	Oil viscosity, cp/API, °	Porous media	Recovery method	EOR mechanism	EOR, %	Reference
ZrO$_2$	Nonionic surfactants (NON-EO4, LA2, LA7, Tween 80, Span	5.0~10.0	70	32.8°	Carbonate	Imbibition	Wettability alteration	48.0~ 58.0	(Karimi et al., 2012)

	20, Span 80, Span 85), pH=2.0~3.0								
ZrO$_2$ (Al$_2$O$_3$, MgO, Fe$_2$O$_3$, Ni$_2$O$_3$, ZnO, SnO$_2$, SiO$_2$)	DI water	0.3	25	53.3 cp	Sandpack	Flooding	Oil viscosity reducer	4.2	(Ogolo et al., 2012)
ZrO$_2$	Anionic surfactant (SDS, 0.1~0.3 wt.%) Cationic surfactant (CTAB, 0.1~0.4 wt.%)	0.01	N/A	130.4 cp 23.99°	5-spot glass micromodel	Flooding	IFT reduction, Wettability alteration, Displacing fluid thicker	8.0.~ 14.0	(Mohajeri et al., 2015)
ZrO$_2$	3.0~20.0 wt.% brine	0~0.05	N/A	Oil-wet rendered by dodecyltriethoxy-silane	Limestone	N/A	Wettability alteration	N/A	(Nwidee et al., 2016)
ZrO$_2$ (NiO)	3.0~20.0 wt.% brine	0.004~0.05	N/A	Oil-wet rendered by dodecyltriethoxy-silane	Limestone	N/A	Wettability alteration	N/A	(Nwidee et al., 2017)

Table 3-7 Applications of other metal oxide nanomaterials in enhanced oil recovery

NP	Dispersant	C(NP), wt.%	T, °C	Oil viscosity, cp/API, °	Porous media	Recovery method	EOR mechanism	EOR, %	Reference
CuO	Polymer (PDMS, 5.0 wt.%) CO_2/VRI 2.2 wt.% brine	0.5~3	50	Heavy oil	Berea sandstone	Flooding	Oil viscosity reducer, displacing fluid thicker	13.3	(Shah, 2009)
CuO (NiO, Fe_2O_3)	4.0 % $NH_3 \cdot H_2O$ in DI water	5	25	28.4°	Carbonate (77~149 mD, 10~24%)	Flooding	Wettability alteration	9.0 ~14.0	(Haroun et al., 2012)
MgO	2.0 wt.% KCl	0.25	N/A	N/A	N/A	Flooding	Fine fixation	N/A	(Huang et al., 2010)
MgO SnO$_2$ (ZrO$_2$, Ni$_2$O$_3$, Al$_2$O$_3$, Fe$_2$O$_3$, ZnO, SiO$_2$)	DI water	0.3	25	53.3 cp	Sandpack	Flooding	Oil viscosity reducer	1.7 ~3.3	(Ogolo et al., 2012)
MgO (Al$_2$O$_3$, SiO$_2$)	Anionic surfactant (SD)	N/A	N/A	N/A	Sandstone (micromodel)	N/A	Fine fixer	N/A	(Ahmadi et al., 2013)

	DI water								
Non-ferrous metal NPs	Anionic surfactant (Sodium 4-alkyl-2ylbenzene-sulfonate, 0.0078~0.05 wt.%)	0~0.001	25	7 cp (25 ℃)	Sand pack (1.0 D, 26%)	Flooding	IFT reduction, Displacing fluid thicker	12.0~17.0	(Suleimanov et al., 2011)
Trimetallic (W, Ni, and Mo) (Nanocataylst)	Pentane (diluent)	N/A	240~340	Bitumen/VGO 7550 /122.3cp (40 ℃)	Oil sands packed bed column (250 D)	Flooding	Catalytic hydrocracking, Oil viscosity reducer	118.0 ~151.0	(Hashemi et al., 2013)

Table 3-8 Applications of organic nanomaterials in enhanced oil recovery

NP	Dispersant	C(NP), wt.%	T, ℃	Oil viscosity, cp/API, °	Porous media	Recovery method	EOR mechanism	EOR, %	Reference
Single-walled-carbon-nanotube (SWNT)/silica nanohybrid	Surfactant (0~0.05 wt.%) Polymer (0~0.2 wt.%) 0~2.5 wt.% NaCl	0.0025~0.1	N/A	Decane	Sandpack sandstone)	Flooding	Emulsion stabilizer	N/A	(Villamizar et al., 2010)

	pH=1~13								
Arab-D Dots (Carbon based fluorescent NPs)	0~23.0 wt.% brine	0.001	25~150	N/A	Carbonate (9.98 mD, 20.3%)	Flooding	N/A	86.0 (ultimate)	(Kanj et al. 2011)
Multiwall Carbon Nanotubes (MWNT)	DI water/0.003 wt.% brine + Electromagnetic waves	0.01~1	60	16.5 cp (60 °C)	Glass beads micromodel	Flooding	N/A	23.0~36.7 (ROIP)	(Chandran, 2013)
Hydrophobic multiwall carbon nanotubes (MWCNT)	DI water	0.01~0.1	60	N/A	Glass micromodels	Flooding	Wettability alteration	23~31.8 (ultimate)	(Alnarabiji et al., 2016)
Graphene-based amphiphilic Janus nanosheets	5.0 wt.% brine (4.0 wt % NaCl + 1.0 wt % CaCl$_2$)	0.005~0.01	N/A	75 cp (25 °C)	Sandstone (44.5~132 mD, 24.8~27.9 %)	Flooding	Interfacial accumulation Elastic interfacial films	6.7~12.5 (ultimate)	(Luo et al., 2016)
MWCNT SWCNT	0.1~1.0 wt.% brine	0.1	25~90	n-decane	N/A	N/A	IFT reduction,	N/A	(AfzaliTabar et al., 2017)

NP	Dispersant	C(NP), wt.%	T, °C	Oil viscosity, cp/API, °	Porous media	Recovery method	EOR mechanism	EOR, %	Reference
SiO₂	pH=7.0~10.0						Wettability alteration		
Carbon NP	3.0 wt.% NaCl	0.001~0.1	60	1 cp (25 ℃) 45.15°	Sandstone (0.6 mD, 14%)	Imbibition	IFT reduction Wettability alteration Disjoining pressure	3.8~26.1	(Li et al., 2017)
Amphiphilic Graphene Oxide	1.5 wt.% brine	0.001~0.1	60	108 cp (60 ℃) 23.82°	Core plug (3.0~5.0 mD) Micromodel (< 100 mD)	Flooding	Emulsifier, IFT reduction Wettability alteration	3.62 ~10.83	(Chen et al., 2018)
Sulfonated graphene (G-DS-Su)	10.0 wt.% NaCl	0~0.2	N/A	35 cp 38.37°	Sandstone (106.18~142.50 mD, 18.11~20.99 %)	Flooding	Emulsifier, Wettability alteration	8~14	(Radnia et al., 2018)

Table 3-9 Applications of silica-based nanomaterials in enhanced oil recovery

NP	Dispersant	C(NP), wt.%	T, ℃	Oil viscosity, cp/API, °	Porous media	Recovery method	EOR mechanism	EOR, %	Reference

SiO$_2$ (Lab-synthesized, 10~12 nm)	Anionic surfactant (XSA-1416D, SS16-47A (16-47A), IAMS-M2-P, 0.1 wt.%) 3.44 wt.% brine	0~0.1	55~91	1.969 cp 34.77°	DSE reservoir rock slice	Imbibition	Ultra-low IFT	N/A	(Le et al., 2011)
SiO$_2$ (Fumed silica, hydrophilic & hydrophobic)	Nonionic surfactant (Zyziphus Spina Christi, 0.1~8.0 wt.%)	0.05~0.2	N/A	N/A	Carbonate (1~10 mD, 12.39 %)	N/A	N/A	N/A	(Ahmadi and Shadizadeh, 2012)
SiO$_2$ (4~20 nm, surfactant modified)	2.0 wt.% KCl	10	25~76	San Andres crude oil	Berea sandstone (160 mD) Indiana limestone (40 mD)	Imbibition Flooding	Disjoining pressure	9.6~23.0	(MeElfresh et al., 2012a; 2012b)
SiO$_2$ (Hydrophilic, 7~40 nm)	3.0 wt.% NaCl	0.05	25~80	Degassed crude oil	Berea sandstone (5~450 mD)	Flooding	Disjoining pressure	2.13~9.78	(Hendraningr at et al., 2013b)

SiO₂ (material)	Brine/additive	Conc.	Temp	Viscosity/contact angle	Rock	Process	Mechanism	Recovery	Reference
SiO$_2$ (7 nm, 300 m^2/g)	3.0 wt.% NaCl	0.01~0.1	N/A	5.10 cp (22 °C) 39.81°	Berea sandstone (Water-wet, 9~35 mD, 13~24 %)	Flooding	IFT reduction, Disjoining pressure	0~14.29	(Hendraningrat et al., 2013a)
SiO$_2$	CTAB, 1.0 wt.% 6.8 wt.% brine	0.1~0.4	23	11.014 cp (22 °C) 33.42°	Carbonate (7 mD, 16%)	Imbibition	Wettability alteration	46.7	(Roustaei, 2014)
SiO$_2$ (7 nm, 395 m^2/g)	Polymer (HAHPAM, 0.05~1.0 wt.%) 3.19 wt.% brine	0.1~1.0	85	39.2 cp (85 °C) 20.65°	Core plug (1.5 D)	Flooding	Rheological properties enhancer	5.13	(Zhu et al., 2014)
SiO$_2$ (Hydrophilic, 20~70 nm, 140 m^2/g)	5.0 wt.% NaCl	0.1~0.6	N/A	11.014 cp (22 °C) 33.42°	Carbonate (7 mD, 16%)	Flooding	Wettability alteration	25.0~29.0	(Roustaei and Bagherzadeh, 2015)
SiO$_2$ (Hydrophilic/hydrophobic)	Anionic surfactant (SDS, 0.2~0.6 wt.%)	0.025~1.0	N/A	26 cp (25 °C) 28.22°	Sandpack (367.96 mD, 21.34%)	Flooding	Surfactant adsorption reducer	15.9~20.4	(Zargartalebi et al., 2015)

Hydrophilic silica nano-structure particles (7 nm, 300 m^2/g) Hydrophilic colloidal SiNP (18 nm, 350 m^2/g)	3.0 wt.% NaCl	0.05~0.5	N/A	N/A	Berea sandstone (365 mD, 19.5 %)	Flooding	Wettability alteration, IFT reduction	4.0~12.0	(Li and Torsæter, 2015; Li et al., 2015b)
SiO$_2$ (Colloidal Silica, 40 nm) LUDOX TM-50	DI water	0.1	N/A	Dodecane (1.364 cp)	Micromodel Sandstone	Imbibition	Wettability alteration	25.0 (ROIP)	(Li et al., 2017)
Zeolite	Polymer (PVP, 1.0 wt.%) 6.7 wt.% seawater 0.1~5.0 wt.% NaCl	0.02~0.05	N/A	32.08°	Limestone	N/A	IFT reduction Wettability alteration	N/A	(Hamad et al., 2016)
SiO$_2$	Polyacrylamide (PAM, 0.1 wt.%)	0.5~2.0	30~90	22.8 cp (25 ℃) 25.57°	Sandpack	Flooding	IFT reduction, displacing fluid thicker,	11.99 ~19.25	(Sharma et al., 2016)

78

	With/without SDS (0.14 wt.%)						wettability alteration		
SiO$_2$ (Fumed, 20~80 nm, 300 m^2/g)	SDS (0.16~0.2 wt.%) 2.0 wt.% brine	1.8~2.2	50	1320 cp 17°	5-spot glass micromodel (4.5 mD, 3.3%)	Flooding	wettability alteration	13.0	(Cheraghian et al., 2017)
SiO$_2$ (Nanofluid, 10~150 nm)	DI water	0.01~1.0	N/A	n-decane	Calcite (220 mD)	Flooding	Wettability alteration	8.7	(Jiang et al., 2017)
SiO$_2$ (< 40 nm, 205.7 m^2/g)	0.75 wt.% NaCl	0.0005 ~0.001	50	20.9 cp (50 ℃) 31.14°	Core plug (0.68~0.95 mD, 9.35~11.95 %)	Imbibition Flooding	Wettability alteration	4.48~10.33	(Lu et al., 2017)
SiO$_2$ (LUDOX CL-X) Grafted with Poly(MPC-co-DVB)	N/A	N/A	25	N/A	N/A	Flooding	IFT reduction	5.0	(Choi et al., 2017)

SiO2 (Powder)	Anionic surfactant (IOS19~23) 3.5 wt.% brine	0.05~0.3	N/A	43.381 cp (STP) 26.37°	N/A	N/A	IFT reduction	N/A	(Ahmed et al., 2017)
SiO2 (Fumed, 7nm, 300 ± 30 m²/g)	Anionic surfactant (SDS, 0.04 wt.%) 3.0 wt.% NaCl	0.05~0.5	26	186.04 cp (19 ℃) 22.2°	Core plugs (138.2~172.1 mD, 16.8~18.2 %)	Flooding	IFT reduction Wettability alteration	4.85~11.7	(Zallaghi et al., 2018)
SiO2 (15~25 nm) γ -Al2O3 (20~50 nm)	SDS CTAB 0~5.0 wt.% NaCl	0.05~0.1	N/A	3.2 cp 42.5°	Carbonate	N/A	IFT reduction Wettability alteration	N/A	(Songolzadeh and Moghadasi, 2017)
SiO2 (Surface modified)	5.0 wt.% NaCl pH=10	0.1	80	5 cp (25 ℃) 44.50°	Core plug (54 mD, 20%)	Imbibition	Wettability alteration Disjoining pressure	26	(Dai et al., 2017)
SiO2 (Hydrophilic, 15 nm)	Polymer (Xanthan gum, 0.1~0.5 wt.%) 0.44 wt.% brine	0.1~2	30~80	20.1 cp (30 ℃) 21.21°	Berea sandstone (746~1002 mD, 25.1~26.5 %)	Flooding	IFT reduction, displacing fluid thicker, emulsion stabilizer,	18.44~20.82	(Saha, et al., 2018)

80

SiO₂	Surfactant/Fluid	Conc.	Temp	Viscosity/Contact angle	Rock	Method	Mechanism	Recovery	Reference
							wettability alteration		
SiO_2 (30.0 % liquid dispersion)	Anionic surfactant (KD, 0.05 wt.%) 3.0 wt.% NaCl 3.0 wt.% brine	0.01~100.05	90	2.73 cp (80 °C) 34.97°	Tight cores (0.2~0.3 mD, 9~12 %)	Flooding	Ultra-low IFT, wettability alteration Emulsifier, Injection pressure reducer	2.31	(Xu et al., 2018)
SiO_2 (Hydrophobic, 8 nm, 380 ± 30 m²/g)	Nonionic surfactant (TX-100, 0.1 wt.%) 3 wt.% NaCl pH=10	0.1	80	5.0 cp (25 °C) 40.39°	Core plug (5 mD)	Imbibition	Wettability alteration	16	(Zhao et al., 2018)
SiO_2 (7 nm, 380 m²/g)	Anionic surfactant (SY, 3.0~7.0 wt.%) DI water	0.05~0.1	25	46.1°/7.2°	Sandstone	Flooding imbibition	Wettability alteration, Surface tension reduction	N/A	(Franco-Aguirre et al., 2018)
SiO_2 (Fumed, 7nm, 100 m²/g)	3.8 wt.% brine pH=2.0~4.87	0.2	60~90	40.6 cp 27.49°	Micromodel (2.5 D, 57%)	Flooding	IFT reduction Wettability alteration	3	(Li et al., 2018)

81

SiO₂ (Dispersion, 10 nm, modified with hexanedioic acid)	3.0 wt.% NaCl	0.001~1.0	60	2.02 cp (60 °C) 48.53°	Sandstone	Imbibition	IFT reduction Wettability alteration Disjoining pressure	10.2~25.0	(Li et al., 2017b)
SiO₂ (10~40 nm)	3.0 wt.% NaCl 0.5 wt.% KCl	0.01~0.5	N/A	14.5 cp 32.5°	Benthemier Sandstone (587~823 mD, 19.4~22.2 %)	Flooding Imbibition	Wettability alteration	20.0	(Youssif et al., 2018)
SiO₂ (7 nm, 389.1 m²/g)	CTAB/SDS/Tween 20 (0.001~0.01 wt.%) 1.0 wt.% NaCl	0.001	25~70	33.2°	Five-spot pattern micromodel	Flooding	N/A	N/A	(Betancur et al., 2018)
SiO₂ (Al₂O₃, TiO₂)	Oleic acid, polyacrylic acid, Different types of surfactants	0.1	N/A	2.804 cp (60 °C) 43.19°	Berea sandstone Edward Carbonate	Imbibition Flooding	IFT reduction	6.2	(Kuang et al., 2018)
SiO₂ (15 nm)	Anionic surfactant (AOT, 11.247 mM)	0.1~0.3	25	28.07 cp (25 °C)	Berea sandstone	N/A	Wettability alteration	N/A	(Jha et al., 2019)

				38.98°	(200 mD)				
Nanopyroxene (Partially coated)	2.0 wt.% NaCl	0.005	25~60	31.30 cp (25 ℃) 31.14°	Sandstone (63 mD, 19~22%)	Flooding	Wettability alteration, IFT reduction, Disjoining pressure	10.57	(Sagala et al., 2019)
Aluminosilicate NP	0.028 wt.% brine	0.0001 ~0.002	25~60	19.97 cp (60 ℃) 30.9°	N/A	Flooding	Wettability alteration IFT reduction	4.44~15.59	(Wijayanto et al., 2019)

CHAPTER IV

INCREASED NONIONIC SURFACTANT EFFICIENCY IN OIL RECOVERY BY

INTEGRATING WITH HYDROPHILIC SILICA NANOPARTICLES

1. Introduction

Most oilfields around the world are experiencing a production rate declining period with recovery factors of primary and secondary production stages lower than 0.45, while the global energy demand is estimated to rise by about 60.0 % over the next few decades (Hendraningrat et al., 2013; Almahfood and Bai, 2018). Given the insufficient primary and secondary production technologies, increased global energy demand and decreased new economic reservoirs, applications of enhanced oil recovery (EOR) techniques are indeed essential (Kiani et al., 2016b). Surfactant EOR is a promising method to unlock remaining oil and reduce residual oil saturation (Kamal et al., 2017). It is estimated that surfactant flooding can yield a recover rate of around 17.0 %, however, the high cost of chemicals, the huge chemical loss and the possible formation damage have limited its commercial implementations (Johannessen and Spildo, 2013; Wu et al., 2008; Shah and Schechter, 2012). Based on the data from U.S. Department of Energy (DOE, Washington, DC, USA), 67.0 % of the total oil in the U.S. will remain in the reservoirs because of the limitations of oil extraction technologies (Kong and Ohadi, 2010). Therefore, novel, advanced and cost-effective EOR techniques become even more necessary.

Nanotechnology, with higher preciseness, effectiveness and reliability, has opened its way in energy production and storage (Elmouwahidi et al., 2017; Randviir and Banks, 2017), agriculture productivity enhancement and food processing (Cerqueira et al., 2017; Duncan and Singh, 2017), air pollution and water treatment, heat transfer enhancement (Dasgupta et al., 2017;

Yu et al., 2017), medicine (Jahangirian et al., 2017; Bayford et al., 2017), construction (Sierra-Fernandez et al., 2017), etc. In recent years, the applications of nanoparticles and nanofluids in EOR have attracted great attention considering their easy penetration into the pore throats and their potentials in changing reservoir properties (Guo et al., 2016). Nanotechnology offers new opportunities to move beyond the current alternatives for EOR purpose.

Nonionic surfactants are nonvolatile and benign chemicals (Puerto et al., 2010; Alvarea et al., 2017; Wan et al., 2007) extensively used in a wide range of industrial applications (Sharma ET AL., 2010). Nonionic surfactants produce no ions in aqueous phase and are less sensitive to electrolytes, making them perfect choices for high salinity saline or hard water. According to the statistics, the market share of nonionic surfactants has noticeably increased during the last few decades, occupying over 40.0 % of the total global surfactant production with polyethoxylated products dominated. Usually the nominal hydrophilic polyEO functional groups within the structures of polyethoxylated nonionic surfactants are not extremely hydrophilic due to the presence of methylene units, thus enabling their solubility in organic solvents, their capability in removing organic compounds from solid samples and their potentials in acting as wetting agents and emulsifiers.

However, polyethoxylated surfactants, when used alone, are acknowledged to have considerable adsorption on sedimentary rocks especially when there are large contents of clay and silica minerals at incompatible conditions thanks to the hydrogen bonding interactions between EO groups and hydroxyl groups on solid surfaces. Therefore, introducing some additives to modify the environmental conditions or act as sacrificial agents might be necessary to mitigate this issue and also do help to produce some unexpected synergistic effects. Both alkali and polymers have been tried, but their efficiency would be hugely restrained if their solubility and stability cannot be

well regulated. Nanoparticles (NPs), because of their small size (1 ~ 100 nm), large surface area and other exclusively properties, have attracted growing attention and showed great potential in oil and gas industry (Nwidee et al., 2017). Commonly used NPs include organic and inorganic types, and silica nanoparticle (SiNP) has long been the most popular one because of its superiority in great marketing potentiality, broad availability, low cost, low toxicity and simplicity in surface modification (Sun et al., 2014).

Though surfactant-SiNP augmented systems have been extensively studied and were reported to have great potentials in oil and gas industry with encouraging laboratory results (Park et al., 2008; Murray and Ettelaie, 2004; Nguyen and Schulze, 2003; Li et al., 2017; Wu et al., 2017; Jung et al., 2018; Bazazi et al., 2017; Qiu, 2010; Binks, et al., 2007), the underlying interactions between different components, crude oil and reservoir rocks are not yet completely well understood and the functional mechanisms could vary for surfactants with different structures and SiNPs with varying hydrophobicity.

In this paper, a polyethoxylated nonionic surfactant MERPOL HCS and two commercial hydrophilic SiNPs (LUDOX Silica) with similar compositions but different sizes were selected to prepare different augmented systems. The adsorption behavior changes of the nonionic surfactant with respect to adsorbents, variations in NP properties together with their synergistic effects on interfacial properties and oil production were systematically studied. Herein, surfactant MERPOL HCS was selected because it is a commercial product ready to use and its cloud point is reported to be higher than 100 °C, therefore, enables the future possibility to extend this work to higher temperature conditions.

2. Experimental Section

2.1. Materials.

Polyethoxylated alcohol surfactant MERPOL HCS with an effective concentration of 60.0 wt. % and critical micelle concertation (CMC) around 100 mg/L (Figure 4-1) was supplied by Stepan Company.
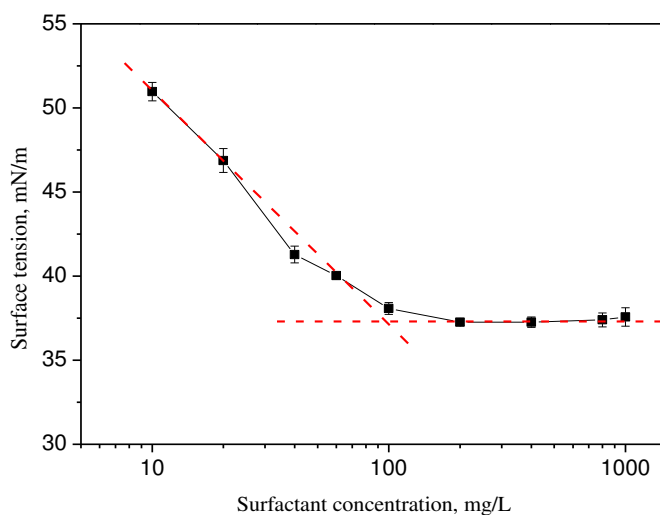
Figure 4-1 Critical micelle concentration of surfactant MERPOL HCS.

Two charge-stabilized SiNPs (Zeta potential ≈ -30 mV), LUDOX SM-30 (30 wt. % suspension in water) and LUDOX TM-50 (50 wt. % suspension in water) with average hydrodynamic diameters about 9.61±0.39 nm and 22.35±0.35 nm, respectively (Figure 4-2) were purchased from Sigma-Aldrich. In terms of the Fourier transform infrared spectra of SiNP powders in Figure 4-3, the compositions of the SiNPs can be regarded as almost identical. Crude oil, with API gravity of 43.2 °API and viscosity around 2.0 cp at room temperature was applied. 0.2 wt.% KCl (analytical grade, Sigma Aldrich) was used as a background electrolyte to decrease the degree of clay swelling.

Adsorbents for static adsorption tests were crushed Bakken (Mountrail County, ROSS Field) and Berea (Kocurek Industries, Inc., USA) rock powders sieved through 120 mesh (≤125 μm) steel wire screens. The results of X-Ray Diffraction (XRD) demonstrate that the Middle

Bakken sample is composed of 41.5 wt.% quartz, 23.7 wt.% carbonate, 16.9 wt.% clay, 14.1 wt.% feldspar and a few pyrite, whereas the Berea sample mainly consists of 79.6 wt.% quartz and 13.1 wt.% feldspar (Zhong et al., 2018; 2019a).

(a)   (b)
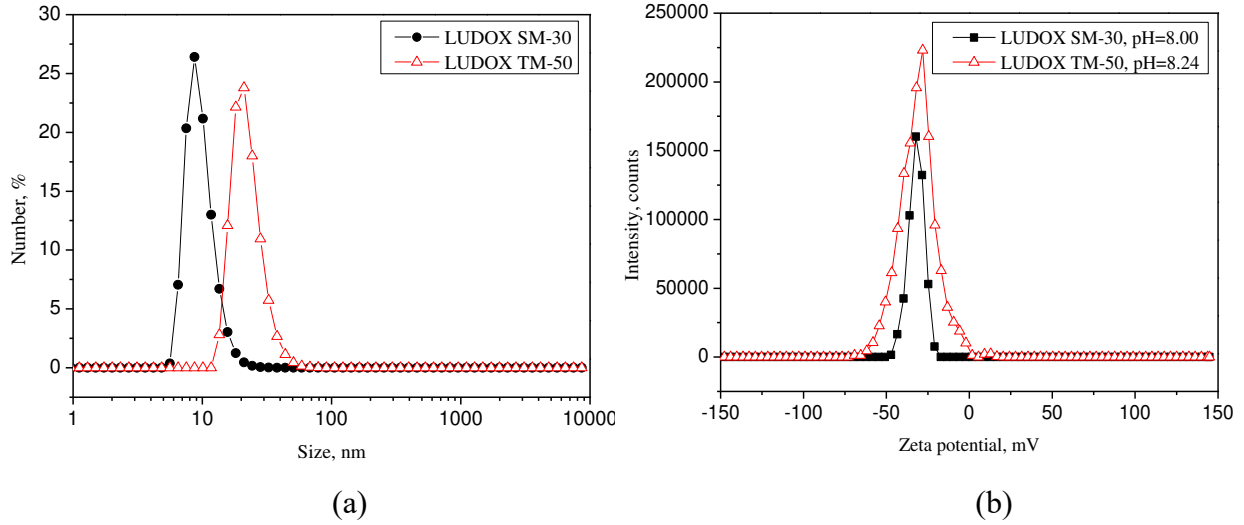
Figure 4-2 Basic properties of the hydrophilic SiNPs. (a) Size distribution. (b) Zeta potential.
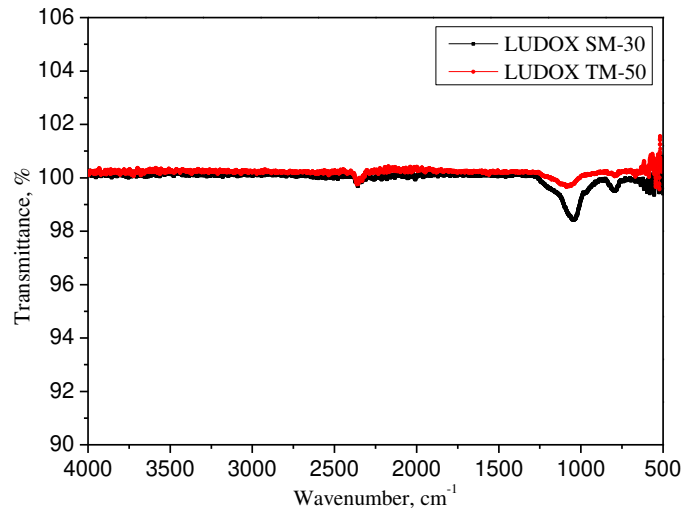
Figure 4-3 Fourier transform infrared spectra of vacuum dried SiNP samples.

2.2. Static Adsorption Test.

The adsorption behaviors of surfactant MERPOL HCS in the absence and presence of SiNPs were studied separately through batch equilibrium tests. Rock samples were first washed

three times with deionized water to remove the fine grains and to ensure the degree of accuracy. Generally, 2.0 g crushed rock samples were mixed with 30 mL surfactant solution (100 ~ 1000 mg/L) or surfactant-SiNP nanofluid (1000 mg/L surfactant + 50 ~ 2000 mg/L SiNPs, pH≈8.0) in a 40 mL vial and aged for 24 hrs to ensure fully interaction. Thereafter, rock powders were removed by centrifugation at 2500 rpm for 15 min and the residual surfactant concentration was analyzed by a temperature compensated UV/vis/NIR spectrophotometer (Lambda 1050, PerkinElmer, USA) (Zhong et al., 2018). Unlike pure surfactant systems, the residual surfactant concentration in surfactant-SiNP augmented system should be divided into two parts, free surfactants and surfactants carried by suspended SiNPs (bonded surfactants) (Ahmadi and Shadizadeh, 2012; Jian et al., 2016). The concentration of free surfactants can be acquired directly when suspended NPs were removed, while the number of bonded surfactants should be calculated based on the ratio of SiNPs remaining suspended (determined by gravimetrical method) after contacting with rock powders.

Surfactant adsorption density (q_e, mg/g) can be calculated by Equation 4-1.

$$q_e = \frac{(c_i - c_{eq})V}{m} \times 10^{-3} \qquad (4\text{-}1)$$

Where c_i and c_{eq} are the initial and equilibrium surfactant concentrations (mg/L), respectively. V is the volume of the surfactant solution or nanofluid (mL), and m is the mass of the adsorbent (g, SiNPs or rock samples).

2.3. Interfacial Properties.

2.3.1 Two-Phase Interface-Interfacial Tension.

Surfactants, consisting of a hydrophilic head and a hydrophobic tail, usually are amphiphilic in nature and are tend to adsorb on the interfacial regions. But pure SiNPs without any

surface modification are usually of high hydrophilicity and are difficult to be held at the water-oil interfaces, hence were reported to barely have any impacts on oil-water interfacial tension (IFT) regardless of size and concentration (Metin et al., 2012). IFT measurement may provide insightful information on the interactions between surfactant and NPs. In this study, IFTs between crude oil and different nanofluids were measured through a spinning drop tensiometer (M6500, Grace Instrument). The volume of oil droplet was about $2.0 \sim 4.0$ μL. Dynamic tracking of the oil radius of cylindrical oil droplet as a function of spinning speed was employed, and the equilibrium width was recorded and used for IFT calculation.

2.3.2. Three-Phase Interface-Contact Angle.

The water contact angle at air/aqueous/Berea sandstone (1.0 *1.0 *0.25 in.) interface and oil contact angle at oil/aqueous/Berea sandstone interface were measured separately after equilibrium using a contact angle device in the sessile drop mode.

2.4. Spontaneous Imbibition Test.

Berea sandstone core plugs with permeability around 0.06 μm^2 and porosity of 16.7 % were first cleaned using Soxhlet extraction apparatus and then saturated with crude oil under pressurized vacuum conditions. After that, the saturated cores were aged in oil for another 30 days at 80 °C. Spontaneous imbibition tests were conducted at 60 °C by placing the oil saturated core plugs into 0.2 wt.% KCl brine, surfactant solution or different surfactant-nanoparticle augmented systems, and the percentage of oil being displaced from the cores versus soaking time was recorded to plot the oil production curves.

3. Results and Discussions

3.1. Surfactant Adsorption on Rocks in the Absence of SiNPs.

The main force drives polyethoxylated nonionic surfactant adsorption on rock surfaces is the hydrogen bonding between ethoxy groups and hydroxyl groups. Usually, there are larger quantities of hydroxyl groups on quartz and clay surfaces, thus, the adsorption of such surfactants on rocks rich in quartz and clay especially clay is noticeable. The adsorption behavior of surfactant MERPOL HCS (100 ~ 1000 mg/L) on the Middle Bakken and Berea samples was studied.
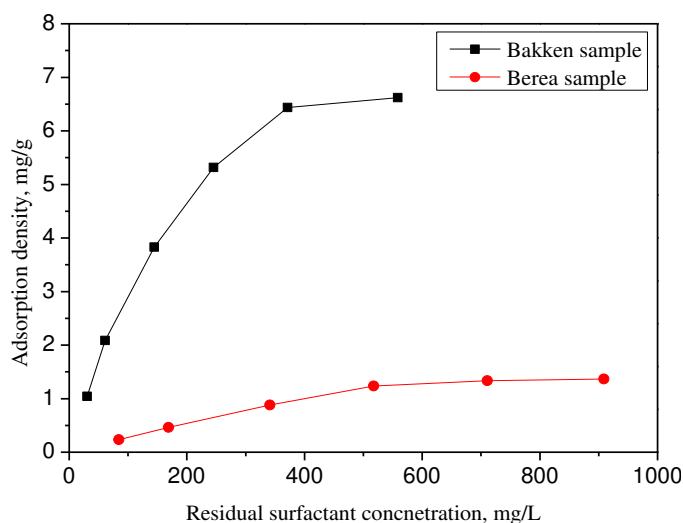
Figure 4-4 Surfactant adsorption on rocks in the absence of SiNPs.

As described in Figure 4-4, surfactant adsorption first increased sharply with increasing surfactant concentration and then generally reached the plateau when the adsorption capacity of rock samples is saturated. The saturated adsorption capacity of surfactant MERPOL HCS on the Middle Bakken and Berea samples in the absence of SiNPs were 6.62 mg/g and 1.37 mg/g, respectively. The huge discrepancy (~ 5.25 mg/g) between the two adsorbents can be explained by the difference in sample compositions. The Middle Bakken sample is a clay-rich adsorbent which provides lots of adsorption sites for surfactant molecules, resulting in higher surfactant loss. Simply from the economical perspective, surfactant MERPOL HCS seems to have broader

application prospects in formations with lower clay content where more surfactant molecules can act effectively at the oil/water interfaces.

However, surfactant loss in the two cases both excessed the threshold value of 1.0 mg/g (Jian et al., 2016) for economical surfactant EOR, therefore, finding an effective method to reduce surfactant loss is necessary and meaningful. SiNPs are good sacrificial agents for anionic surfactants or nonionic surfactants without ethoxy groups (Ahmadi et al., 2012; Jian et al., 2016), but how will the presence of SiNPs affect the adsorption of polyethoxylated nonionic surfactants on varying adsorbents is still ambiguous.

3.2. Surfactant Adsorption on SiNPs.

Surfactants interact strongly with NPs and the adsorption density of surfactant would be affected by NP concentration and size. In this part, the adsorption behaviors of 1000 mg/L surfactant MERPOL HCS on both LUDOX SM-30 and LUDOX TM-50 SiNPs surfaces were studied at room temperature, ambient pressure, as presented in Figure 4-5.

The average surfactant adsorption density on every single SiNP first decreased proportionally with growing SiNPs concentrations at low concentrations (50 ~ 500 mg/L) and then showed a moderate decrease when particle concentration increased further up to 2000 mg/L when surfactant concentration is a constant. 2000 mg/L LUDOX SM-30 with specific surface area about $320 \sim 400$ m^2/g was able to consume all the 1000 mg/L surfactant (adsorption density = 0.5 mg/mg), leaving no free surfactant behind. While the surfactant-bonding capability of LUDOX TM-50 (S=110 ~ 150 m^2/g) was much weaker, where only less than half of the surfactant (~ 412.2 mg/L) successfully turned into the bound state when NP concentration reaches the highest level of 2000 mg/L in our research, suggesting that SiNPs with smaller size are better nonionic surfactant carriers. In addition, the zeta potentials at different SiNP concentrations were measured, as shown in Figure

4-6.
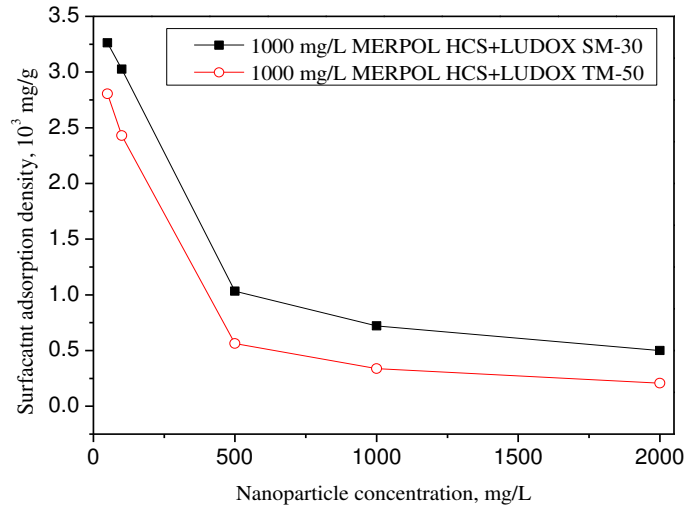
Figure 4-5 Surfactant adsorption on SiNPs.
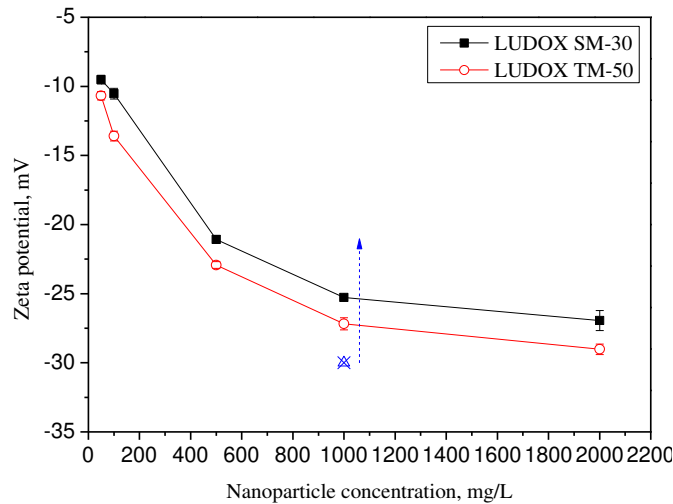
Figure 4-6 Zeta potentials at different SiNP concentrations

With the addition of 1000 mg/L surfactant MERPOL HCS, the zeta potentials of SiNPs (1000 mg/L) increased from around -30.0 mV to -25.3 mV and -27.2 mV for LUDOX SM-30 and LUDOX TM-50, respectively. When the concentration ratio between surfactant and SiNPs further increased to 20:1 (1000 mg/L MERPOL HCS + 50 mg/L SiNPs), the zeta potential reached an approximate value of -10.0 mV due to surfactant adsorption (Sis and Birinci, 2009). Theoretically, SiNPs with less surface charge are more unstable, but owing to the relatively low CMC value of

around 100 mg/L, surfactant MERPOL HCS shows great tendency to form micelles, and the steric repulsion induced by these micelles is conducive to NP stabilization, therefore, no noticeable aggregation or precipitation was observed in this work. Different from cationic surfactants, which would reverse SiNPs surface charge or promote a "Zero Zeta Potential" state due to charge neutralization, the effects of nonionic surfactants are less destructive.

To better explain the interactions between the polyethoxylated nonionic surfactant and hydrophilic SiNPs, Molecular Dynamics (MD) simulation in molecular dimension was performed with the LAMMPS (Plimpton, 1995) package. The configuration snapshots were rendered by OVITO (Stukowski, 2010) software. Simulations were carried out under the NPT ensemble. The long-range electrostatic interactions were calculated using the particle-particle particle-mesh (PPPM) method (Hockney and Eastwood, 1989) with an accuracy of 10^{-4} and a cutoff radius of 12 Å. The temperature was kept constant at 300 K using the Nosé-Hoover (Nosé, 1984; Hoover et al., 1982) thermostat with a relaxation time of 100 fs. The pressure of the system was maintained at 1 atm using the Parrinello-Rahman (Parrinello and Rahman, 1981) method with a time constant of 1000 fs. Fast-moving bonds involving hydrogen atoms were constrained with the SHAKE (Ryckaert et al., 1977) algorithm, and the time step was set to 2 fs. The final configures were obtained after 4 ns simulation.

In the simulation, CLAY force field (Cygan et al., 2004), OPLS-AA force field (Jorgensen et al., 1996) and single point charge/extended (SPC/E) model (Berendsen et al., 1987) were implemented individually to construct hydroxyl functional group covered hydrophilic SiNP (Figure 4-7a), nonionic surfactant (Figure 4-7c) and water (Figure 4-7b) component. Periodic boundary condition was applied in all three directions, and for better visual effect, water molecules were concealed and did not shown in the configuration snaps. According to the simulation results,

94

surfactants adsorbed on SiNPs surfaces through different forms at varying situations. When surfactant concentration is low (Figure 4-8a), surfactant molecules tend to form loose monolayers and render particles partially hydrophobic. When surfactant concentration increases (Figure 4-8b ~ 4-8c), SiNPs surfaces were more likely to be covered by surfactant bilayers or even surfactant micelles, therefore, the hydrophilicity of particles increased again and the resultant steric repulsion force between particles were beneficial for SiNPs stabilization.

(a)   (b)

(c)   (d)
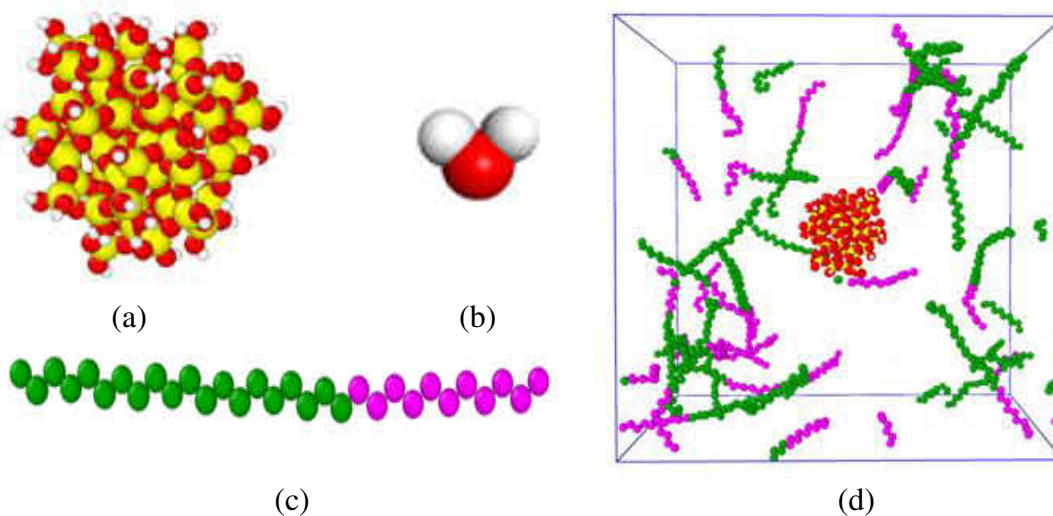
Figure 4-7 (a) SiNP with hydroxyl groups on the surface. (b) Water. (c) Nonionic surfactant (hydrophilic head atoms are represented as green particles hydrophobic tail atoms are represented as magenta particles). (d) Initial simulation configuration. Atom color code: O, red; Si, yellow; H, white.
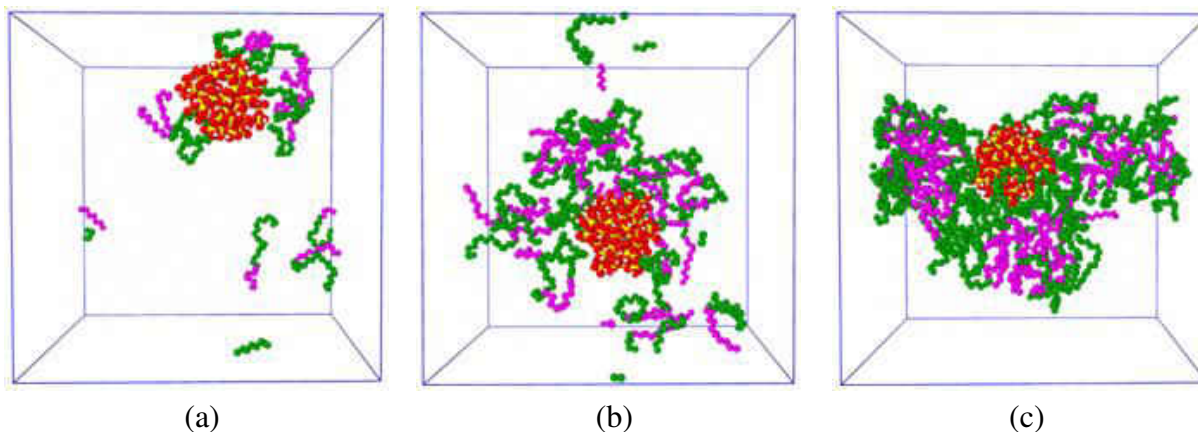
Figure 4-8 Equilibrium configurations for different situations. (a) Low c(surfactant)/c(SiNP) ratio. (b) Medium c(surfactant)/c(SiNP) ratio. (c) High c(surfactant)/c(SiNP) ratio.

3.3. Surfactant Adsorption on Rocks in the Presence of SiNPs.

The adsorption of polyethoxylated nonionic surfactant on SiNPs complicated the interactions between the surfactant, SiNPs and the rock, will SiNPs compete with rocks fighting for MERPOL HCS molecules/micelles and reduce surfactant loss or will SiNPs act as intermediaries and finally promote surfactant loss on rocks? In this paper, series of experiments were carried out to offer an answer.

3.3.1. Effects of SiNP Concentration.

Surfactant-nanoparticle augmented systems composed of 1000 mg/L surfactant MERPOL HCS and 50 ~ 2000 mg/L SiNPs were mixed with different rock powders to study the impacts of SiNPs concentration on surfactant adsorption. The corresponding surfactant adsorption densities at different conditions were measured and summarized in Figure 4-9.

Surfactant adsorption was greatly restrained with the addition of hydrophilic SiNPs. Originally, about 44.1 % surfactant was lost on the Middle Bakken rocks when 1000 mg/L surfactant MERPOL HCS was used. With the inclusion of 2000 mg/L LUDOX SM-30 or LUDOX

TM-50 SiNPs, surfactant adsorption loss on the Middle Bakken samples was reduced to 27.9 %

and 37.3 %, respectively. While for Berea sample, the resultant adsorption densities can be even

less than 1.0 mg/g, which are 0.48 mg/g and 0.91 mg/g, separately. The competitive adsorption of

surfactant on SiNPs and rock samples might be the reason for less surfactant loss when LUDOX

SiNPs present, and LUDOX SM-30 with smaller size and stronger surfactant-carrying capacity

showed higher efficiency. Moreover, the influence of SiNPs also largely depended on the nature

of the adsorbents. For example, when 500 mg/L LUDOX SM-30 NPs were added into 1000 mg/L

surfactant MERPOL HCS solution, surfactant adsorption density showed a 20.1 % decrease for

the Middle Bakken case and a 40.9 % reduction for the Berea sample. A possible interpretation for

this phenomenon is that the relatively high contents of clay and carbonate in the Middle Bakken

samples captured some SiNPs, and then those SiNPs acted as connectors, inducing some surfactant

loss, therefore, shielding parts of the positive effects.
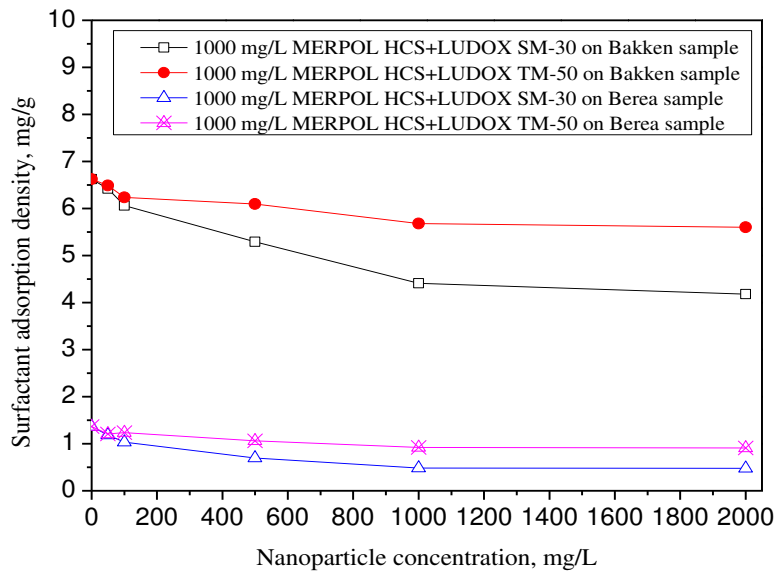
Figure 4-9 Surfactant adsorption on rock samples with the presence of SiNPs.

Furthermore, sensitivity analysis based on factorial design (Minitab 2016) was conducted

to rank the influential factors, figure out the prominent parameters and make predictions.

Table 4-1 Details and results of randomized 2^k full factorial design

	Factor	Low value	High value	Ranking
Main Factors	Surfactant concentration	1000 mg/L (constant)		
	Adsorbent	1 (Bakken)	2 (Berea)	1
	Nanoparticle	1 (LUDOX SM-30)	2 (LUDOX TM-50)	2
	Concentration, mg/L	50	1000	4
Interactions	Adsorbent*Nanoparticle			3

Table 4-1 indicates that for a surfactant HCS-LUDOX SiNP augmented system, SiNP size has more prominent effects than SiNP concentration on surfactant adsorption density. In addition, Figure 4-10 gives the contour plots for surfactant adsorption prediction when 1000 mg/L MERPOL HCS was used together with 50 ~ 1000 mg/L LUDOX SM-30 NPs or LUDOX TM-50 NPs. Values being highlighted in the figure were the experimental data at given conditions. Over 80.0 % of the real data fitted well with the predicted outcomes, revealing the feasibility of the proposed model.

(a)   (b)
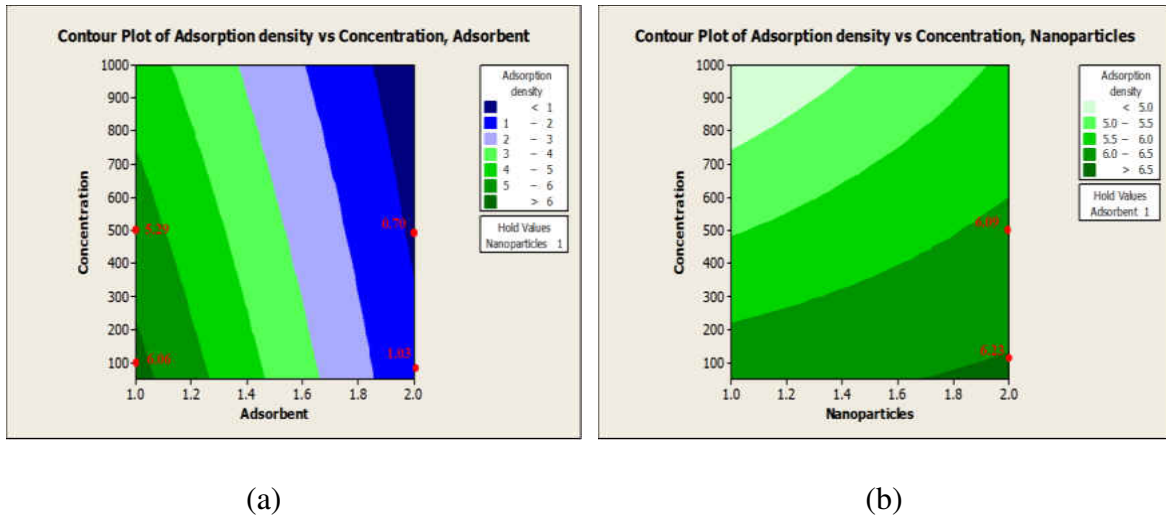
Figure 4-10 Representative contour plots. (a) Adsorption vs. Adsorbent and SiNP Concentration.

(b) Adsorption vs. SiNP type and SiNP Concentration.

3.3.2. Effects of Temperature.

Attributing to the dehydration of ethoxylate functional group (Zhong et al., 2018) in MERPOL HCS structure and the enhanced particle-particle interactions between SiNPs, Figure 4-11 displays a growing trend for MERPOL HCS (1000 mg/L) adsorption in the presence of 2000 mg/L SiNPs at elevated temperatures (20 °C, 60 °C, 80 °C). 0.41 mg/g more surfactant loss was detected for MERPOL HCS - LUDOX SM-30 SiNPs system on the Middle Bakken sample at 80 °C compared to the adsorption density of 4.18 mg/g at 20 °C, and the difference for Berea case at the same conditions was smaller than 0.10 mg/g.
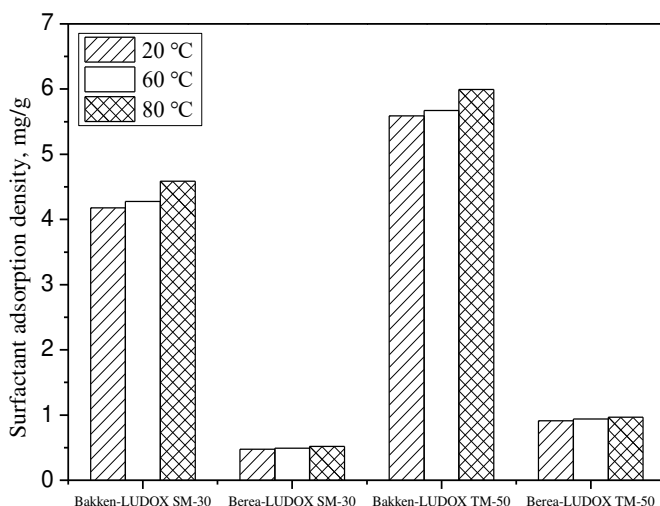
Figure 4-11 The effects of temperature on surfactant adsorption with the presence SiNPs.

3.4. Interfacial Characterization.

3.4.1. Interfacial Tension.

Synergistic effects on IFT reduction were observed for surfactant HCS – LUDOX SiNPs augmented systems, as illustrated in Figure 4-12. The IFTs of 2000 mg/L KCl, 1000 mg/L LUDOX SM-30 and LUDOX TM-50 were 16.4±0.5 mN/m, 14.1±0.5 mN/m and 13.5±0.8 mN/m, respectively. 1000 mg/L surfactant MERPOL HCS alone can reduce the IFT to ~ 3.8 mN/m, with

the help of 2000 mg/L LUDOX SM-30 and LUDOX TM-50, the magnitudes further decrease by another 50.0 % (~ 1.9 mN/m) and 13.2% (~ 0.5 mN/m). The observed IFT reduction, attributing to better interfacial adsorption rendered by surfactant release from the particles or the effect of surfactant-coated particles decreases the capillary forces, promotes water imbibing and favors the oil production process (Omurlu et al., 2016; Ravera et al., 2006).
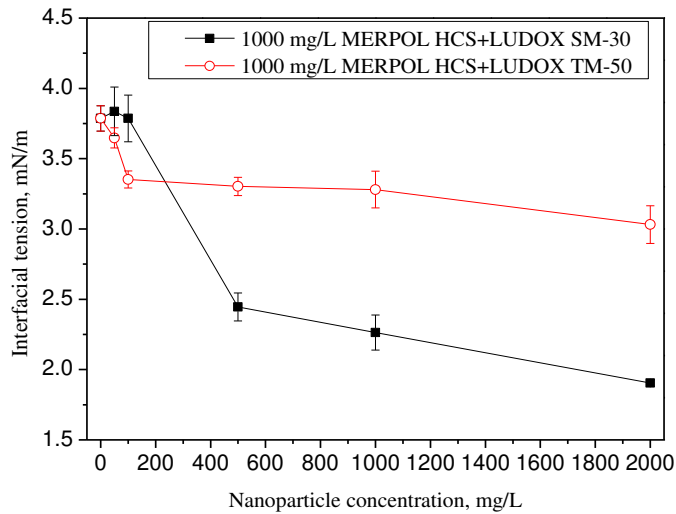
Figure 4-12 Impacts of SiNP concentration on IFT reduction.

3.4.2. Contact Angle.

The wettability alteration capability of different formulas was tested by measuring the contact angles of the aqueous droplet or oil droplet being captured on an oil-wet Berea sandstone slice treated with paraffin (original θ at oil/aqueous/solid interface $\approx 40.5°$).

Rock was rendered intermediate-wet by 1000 mg/L MERPOL HCS ($\theta \approx 81.5°$) alone and could change towards more water-wet when 2000 mg/L LUDOX SM-30 or LUDOX TM-50 was added, showing contact angles of 98.0° and 89.5°, respectively (Figure 4-13). Experimental data were summarized in Figure 4-14.

(a)   (b)

(c)   (d)

Figure 4-13 Oil contact angle. (a) 2000 mg/L KCl brine. (b) 1000 mg/L MERPOL HCS

surfactant. (c) 1000 mg/L MERPOL HCS surfactant + 2000 mg/L LUDOX SM-30 nanoparticle.

(d) 1000 mg/L MERPOL HCS surfactant + 2000 mg/L LUDOX TM-50 nanoparticle.
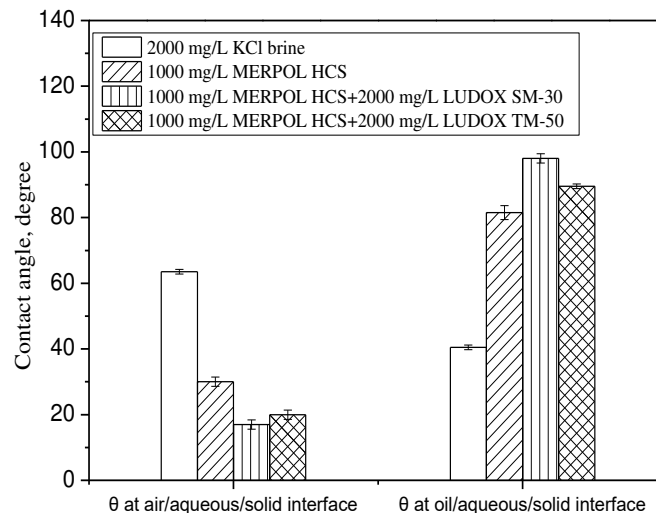
Figure 4-14 Effects of different formulas on contact angles.

3.5. Spontaneous Imbibition.

      To evaluate the efficiency of the proposed nanofluids, spontaneous imbibition tests were

conducted. In this work, nanofluids were adopted either as a secondary oil recovery technology

after brine imbibition or a tertiary oil recovery technology after brine and surfactant imbibition.

Selected formulas for imbibition tests were 0.2 wt.% KCl brine, 1000 mg/L MERPOL HCS

surfactant solution, and two different surfactant-SiNP augmented systems, 1000 mg/L MERPOL

HCS surfactant + 2000 mg/L LUDOX SM-30 SiNPs and 1000 mg/L MERPOL HCS surfactant +

2000 mg/L LUDOX TM-50 SiNPs. The oil recovery curves are plotted in Figure 4-15 with details

being presented in Table 4-2.
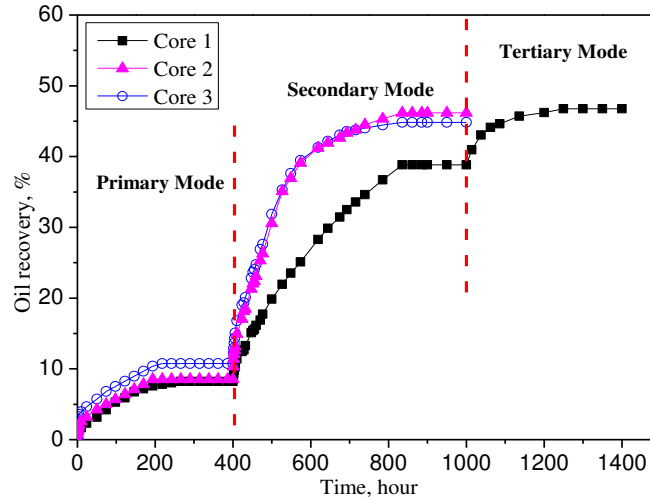
Figure 4-15 Impacts of NPs on oil recovery in spontaneous imbibition tests

Table 4-2 Details of imbibition tests

Cores	Diameter, in.	Length, in.	Imbibition sequence	Total oil recovery, %
1	1.02	2.619	0.2 wt.% KCl	8.23
			1000 mg/L HCS	38.83
			1000 mg/L HCS + 2000 mg/L LUDOX SM-30	46.74
2	1.02	2.781	0.2 wt.% KCl	8.52
			1000 mg/L HCS + 2000 mg/L LUDOX SM-30	46.19
3	1.03	2.749	0.2 wt.% KCl	10.76
			1000 mg/L HCS + 2000 mg/L LUDOX TM-50	44.82

Higher oil production efficiency was obtained by integrating nonionic surfactant with

hydrophilic SiNPs. 2000 mg/L KCl only recovered 8.0 ~ 11.0 % of the original oil from the Berea

sample (Cores 1 ~ 3), and the subsequent spontaneous imbibition using 1000 mg/L MERPOL HCS

surfactant solution alone in secondary mode could extract 30.6 % OOIP additional oil over imbibition test using KCl solution. Spontaneous imbibition tests on Core 2 using 1000 mg/L MERPOL HCS + 2000 mg/L LUDOX SM-30 nanofluid yielded 46.19 % OOIP oil recovery, which is 37.67 % OOIP higher than KCl brine imbibition. Another nanofluid (1000 mg/L MERPOL HCS + 2000 mg/L LUDOX TM-50) imbibition test on Core 3, which is also in secondary mode, produced additional 34.06 % OOIP oil. The better performance of LUDOX SM-30 over LUDOX TM-50 may be ascribed to its higher efficiency in reducing surfactant adsorption, lowering IFT and altering wettability. Moreover, when used in the tertiary recovery mode, 1000 mg/L MERPOL HCS surfactant + 2000 mg/L LUDOX SM-30 SiNP system was able to produce additional 7.91 % OOIP oil over imbibition test using 1000 mg/L MERPOL HCS surfactant solution. In summary, hydrophilic SiNPs exhibit great potentials to increase nonionic surfactant's efficiency in oil recovery and the proposed water-based nanofluids have great opportunities in both the secondary and the tertiary oil production process.

4. Summary

(1) Surfactant adsorption density on NP surfaces significantly decreased with increasing $c(SiNP)/c(surfactant)$ ratio. When 1000 mg/L MERPOL HCS surfactant was mixed with 2000 mg/L SiNPs, the adsorption densities were around 0.50 mg/mg and 0.21 mg/mg for LUDOX SM-30 and LUDOX TM-50 SiNPs, respectively.

(2) The surface charge of SiNPs decreases with increasing adsorption of nonionic surfactant and reaches a plateau of around -10.0 mV when $c(SiNP)/c(surfactant)$ ratio was 0.05. However, no aggregation or sedimentation was observed thanks to the contribution of steric repulsion imposed by surfactant micelles.

(3) Surfactant adsorption decreased when SiNPs existed in the system, and SiNPs with smaller size and higher concentration demonstrated higher efficiency.

(4) Nonionic surfactant MERPOL HCS and hydrophilic LUDOX SiNPs showed noticeable synergistic effects on oil-water interfacial tension reduction and wettability alteration.

(5) Hydrophilic SiNPs exhibited great potentials to increase nonionic surfactant's efficiency in oil recovery. More than 34.0 % OOIP and over 4.0 % OOIP additional oil was recovered compared with 2000 mg/L KCl imbibition and pure surfactant imbibition, respectively.

CHAPTER V

ENHANCED OIL RECOVERY IN HIGH SALINITY AND ELEVATED TEMPERATURE
CONDITIONS WITH ZWITTERIONIC SURFACTANT AND SILICA NANOPARTICLES
ACTING IN SYNERGY

1. Introduction

The gap between increasing energy demand and decreasing energy production rate calls for urgent innovations in recovery technologies (Zheng et al., 2018a, 2018b; Zeng et al.; 2018; Hendraningrat et al., 2013a; Kazempour et al., 2018). In recent decades, nanotechnology has gained considerable interest and gradually developed into the leading-edge enhanced oil recovery (EOR) technology for the exploitation of reservoirs with small pores and narrow pore throats (Nwidee et al., 2017; Li et al., 2017a; Chen et al., 2018; Xu et al., 2015; Roustaei and Bagherzadeh, 2015; Franco et al., 2017; Jung et al., 2018; Li et al., 2018). SiO_2 nanoparticles (NPs) are cost-effective, widely accessible and can be easily fabricated and functionalized (Metin et al, 2014; Almahfood and Bai, 2018), hence, are perfect options for engineering purposes. NPs fulfill the EOR purpose mainly through the mechanisms of interfacial tension (IFT) reduction and wettability alteration (Hendraningrat et al., 2013a; Nwide et al., 2017; Roustaei and Bagherzadeh, 2015). However, hydrophilic SiO_2 NPs terminated by hydroxyl groups (SiO_2-OH) hardly have any impacts on IFT (Metin et al., 2016) and in most cases, relatively high particle concentration (≥ 1.0 wt.%) is required to induce noticeable wettability change (Jiang et al., 2017; Jang et al., 2018). According to Yuan's (2017) research, even when the applied NPs have super good dispersity in the dispersant, the permeability reduction caused by NPs adsorption and straining was huge, and the adverse effects were more significant at higher NPs concentrations.

105

Surfactant-SiO2 NP augmented systems have attracted much attention due to increased particle stability, reduced NP dosage, decreased surfactant adsorption loss and enhanced efficiency. The synergistic effects between anionic, cationic or nonionic surfactants and SiO2 NPs have been widely studied (Kuang et al., 2018; Zhong et al., 2019b). Ahmed (2017) found that the addition of anionic surfactants IOS$_{19-23}$ could stabilize SiO2 NPs in 3.5 wt.% NaCl brine and induce further IFT reduction. Cheraghian (2017) recovered another 13.0 % OOIP heavy oil compared with SDS (a anionic surfactant) by SiO2 NPs-SDS mixture at 70 ℃ and 2.0 wt.% synthetic brine. Zhao (2018) obtained additional 8.0 % OOIP by using nonionic surfactant TX-100 with SiO2 NPs at 80 ℃ and 3.0 wt.% NaCl. By integrating SiO2 NPs with CTAB (cationic surfactant), Roustaei (2014) extracted 10.0 % additional oil after CTAB imbibition at room temperature and 6.8 wt.% synthetic brine. Most researches were carried out at either room temperature or low salinity conditions without much attention being paid to the size or stability change. However, the EOR efficiency of surfactant-SiO2 NP formula is highly depend on surfactant and NP stability as well as other properties, which can be sensitive to the solution environment such as pH, salinity, temperature, etc. To prepare an effective and stable surfactant-SiO2 NP system suitable for hostile reservoir conditions, the commonly used unstable anionic, cationic or nonionic surfactants can be replaced by mild zwitterionic surfactants with high tolerance towards salts and elevated temperature, good biodegradability and excellent interfacial properties (Nieto-Alvarez et al., 2014). But the stability of SiO2 NPs is still a great concern. Elevated temperature would intensify the Brownian motion and increase the possibility of particle collision, while the oppositely charged ions present in solution may limit the electrostatic repulsion between particles and promote particle flocculation, and the adverse effects of divalent cations (Ca^{2+}, Mg^{2+}…) are more prominent than monovalent cations (Na^+, K^+…) (Hamad et al., 2016; Metin et al., 2011). Using surfactants or polymers alone

as stabilizers to increase the electrostatic repulsion (Songolzadeh and Moghadasi, 2017; Zhu et al., 2014) or adding hydrochloric acid to form H^+ protection layers (Sofla et al., 2018) only demonstrated limited effects and were generally invalid when confronted with elevated temperature and concentrated brines with multiple types of cations. To cater for harsher conditions like API brine (8.0 wt.% NaCl + 2.0 wt.% $CaCl_2$), steric repulsion between particles is necessary (Worthen et al., 2016). Though covalently connected copolymers onto SiO_2 NPs surfaces can achieve long-term colloidal stability at a salinity as high as 12.0 wt.% at 90 °C, the complexity of particle-synthesis process and the non-negligible particle growth when connecting high molecular weight polymers would increase the investment and the possibility of pore plugging (Ranka et al., 2015). Based on the classic concept proposed by Napper (1983), attaching a ligand to the particle surface can also provide steric stabilization as long as it has good solubility in the solvent. Hence, low molecular weight ligands that could be connected to SiO_2 NPs surfaces via a facile process are in demand. GLYMO, produced by acid-catalyzed ring opening of (3-glycidyloxypropyl) trimethoxysilane is therefore a good choice because it is soluble in API brine at up to 120 °C, neutral pH condition (Worthen et al., 2016) and can be connected to SiO_2 NPs through the highly versatile silylation reaction.

In this study, SiO_2 NPs co-stabilized by low molecular weight GLYMO (steric stabilization) and zwitterionic surfactant cocamidopropyl hydroxysultaine (electrostatic stabilization) were prepared and tested to against aggregation and precipitation when confronted with concentrated brine and elevated temperatures. Different from the betaine-type zwitterionic surfactant, cocamidopropyl hydroxysultaine (CAPHS) can maintain a zwitterionic form whatever solution pH is (Cullum, 1994). The developed nanofluid displayed higher EOR efficiency at 60 °C, API brine conditions. Additional oil was recovered from the Berea sandstone cores by the augmented system

after surfactant or pure NP flooding in the tertiary recovery mode. In addition, thanks to the weak interactions between surfactant CAPHS and surface modified SiO_2 NPs, flexible adjustments can be made to their concentration ratios to customize the desirable nanofluid formulas intended for specific applications.

2. Experimental Section

2.1. Materials.

Nexil 6, a 16.9 wt.% silica colloid with particle size and specific surface area around 6.0 nm and 445.0 m^2/g, respectively, was obtained from Nyacol Nano Technologies. The ligand (3-glycidyloxypropyl) trimethoxysilane (GPS) was purchased from Sigma-Aldrich. Zwitterionic surfactant CAPHS, with structure being presented in Figure 5-1, was provided by Stepan Company and was used directly without further purification. Sodium chloride (NaCl), potassium chloride (KCl), calcium chloride ($CaCl_2 \cdot 2H_2O$) and magnesium chloride ($MgCl_2 \cdot 6H_2O$) of analytical grade were purchased from VWR International. In this study, crude oil with a density of 0.81 g/cm^3 and a dynamic viscosity of 2.0 mPa·s at 25 °C was used.
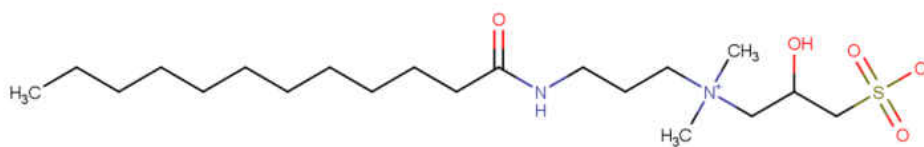
Figure 5-1 Structure of zwitterionic surfactant CAPHS

2.2. Critical Micelle Concentration (CMC) of CAPHS.

The CMCs of CAPHS in distilled water and API brine were measured separately through surface tension method using a Du Noüy ring tensiometer. Surface tension first decreases dramatically with increasing surfactant concentration and then gradually reaches a plateau or even shows an increasing trend when surfactant addition increases further. The turning point is defined

as surfactant CMC.

2.3. Synthesis of SiO$_2$-GLYMO NPs.

SiO$_2$-GLYMO NPs were synthesized following the previous works (Griffith and Daigle, 2018; Worthen et al., 2016), and the resultant ligand coverage was around 2.9 μmol/m^2. GPS first went through a ring opening process in hydrochloric acid (HCl) solution to form GLYMO (Scheme 5-1) and the pH was adjusted to 10.0 with concentrated NaOH solution before being added dropwise into the silica suspension. A small amount of methanol was also added to prevent GLYMO oligomers from precipitating out during the reaction. The SiO$_2$-OH concentration in the reaction mixture was 10.0 wt.%. Once the silylation reaction was completed after 24.0 hrs stirring at 60 ℃ (Scheme 5-2), methanol was removed by evaporation. SiO$_2$-GLYMO NPs were collected after three times water wash using centrifuge filters (3.0 k MWCO, 6000 rpm). Large aggregates were eliminated by syringe filters (0.45 μm) and the ultimate SiO$_2$-GLYMO NPs concentration was determined by weighing the mass of solid after water evaporation.
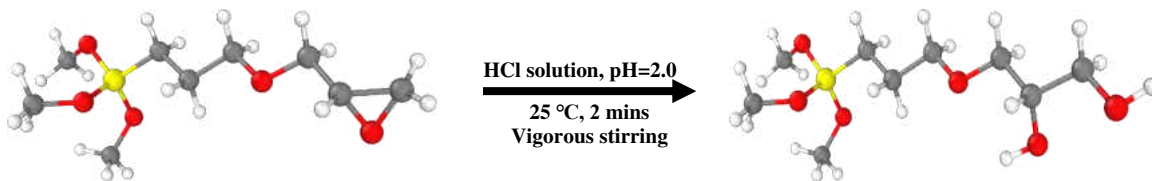
Scheme 5-1 Ring opening of GPS at acid condition to form GLYMO. Atom color code: Si, yellow; O, red; C, grey; H, white.
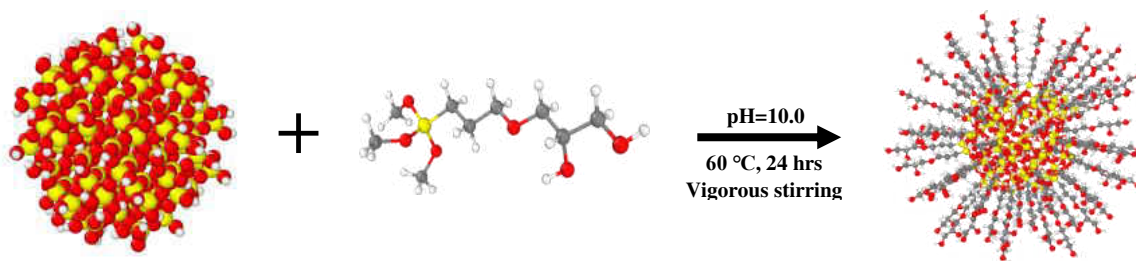
Scheme 5-2 Silylation reaction between SiO$_2$ NP and GLYMO to form SiO$_2$-GLYMO NP.

2.4. Preparation of Surfactant-Nanoparticle Augmented System.

SiO_2-GLYMO NPs were mixed vigorously with surfactant CAPHS solution (API brine, pH=7.0±0.5) under sonification to prepare homogeneous nanofluids. The concentrations of SiO_2-GLYMO NPs and CAPHS were 0 ~ 4000 mg/L and 0 ~ 1000 mg/L, respectively.

2.5. Selection of Surfactant-Nanoparticle Formula.

In this part, a systematic study on interfacial properties including IFT, contact angle and adsorption behavior were conducted to screen out a promising EOR formula. Herein, the IFTs between different fluids and crude oil were obtained through a spinning drop tensiometer (M6500, Grace Instrument). Contact angles were measured by a contact angle device in the sessile drop mode on pretreated oil-wet rock substrates and the standard deviation was around ±3.0° based on replicate measurements. The impacts of SiO_2-GLYMO NPs on the static adsorption behavior of zwitterionic surfactant on the crushed Berea rock sample were studied through UV/vis spectroscopy (Lambda 1050, PerkinElmer).

2.6. Long-Time Stability.

The tolerance of CAPHS/SiO_2-GLYMO NP nanofluid towards monovalent (Na^+, K^+) cations, divalent (Ca^{2+}, Mg^{2+}) cations as well as its long-time stability at high salinity and elevated temperature conditions was investigated based on particle size measurement by a dynamic light scattering Zetasizer (Malvern).

2.7. EOR Potential.

Core flooding experiments were implemented on the Berea sandstone cores with air permeability about 50.0±1.6 mD and porosity around 16.7±0.50 % to evaluate the EOR performance of CAPHS/SiO_2-GLYMO NP formula.

2.7.1. Rock Characterization.

The surface morphology of Berea sample was studied based on SEM images (HITACHI SU 8010). A polished Berea slice was mounted rigidly on the sample holder using a conductive adhesive such as carbon tape. Rock is generally nonconductive, so sample coating is necessary to eliminate scanning faults. XDR analysis (Rigaku Smartlab) was also conducted to study rock compositions.

2.7.2. Core Flooding Experiment.

Before the experiment, core plugs with standard size of 1.5 in. in diameter and 3.0 in. in length were cleaned by Soxhlet extraction apparatus and then were saturated with crude oil using a vacuum saturator. In the experiment, saturated Berea core plugs (Kocurek Industries, Inc., USA) were loaded into a Hassler core holder under the confining pressure of ~ 2000 psi (60 ℃). The displacing fluid was injected at a constant injection rate of 0.50 mL/min. The volume of produced oil as well as differential pressure ΔP ($\Delta P = P_1\text{-}P_2$) along the injection process was recorded. The schematic diagram of the experimental apparatus is shown in Figure 5-2.

In this part, API brine flooding was carried out first to yield the primary recovery, then 2.0 PV (Pore Volume) CAPHS solution or SiO_2-GLYMO NP suspension was applied to get the secondary oil recovery. Tertiary oil recovery was obtained by injecting 2.0 PV CAPHS/SiO_2-GLYMO NP nanofluid to see its additional effects over surfactant or pure SiO_2-GLYMO NPs. The slug size of 2.0 PV for testing fluid was used to ensure that all the recoverable oil by a certain testing fluid can be fully recovered, so the further increment in oil recovery when surfactant-NP system was applied can be totally attributed to its pure effects.
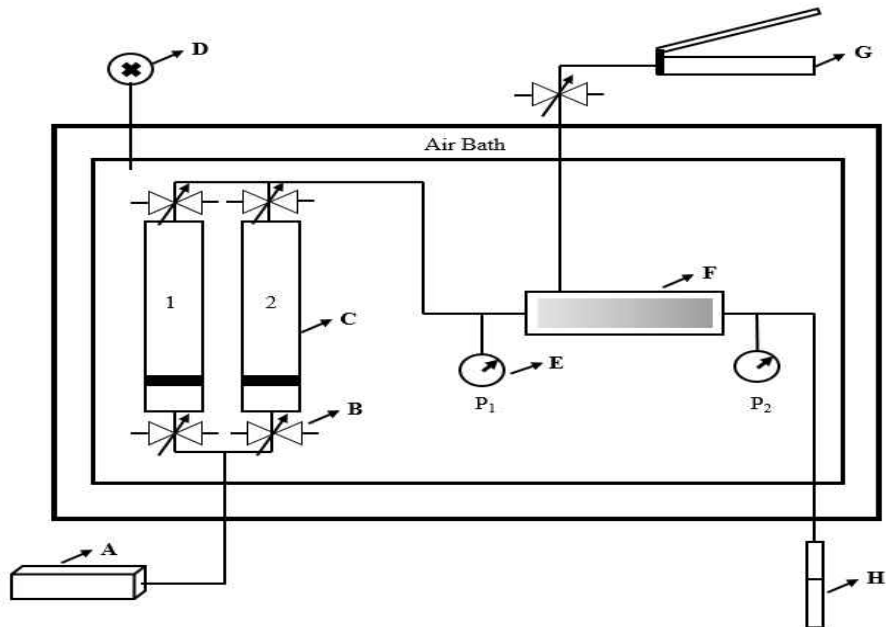
Figure 5-2 Schematic of the core flooding setup. A, constant-flux pump; B, valve; C, piston accumulator; D, temperature control; E, pressure gage; F, Hassler core holder; G, hand pump (confining pressure); H, volumetric cylinder.

3. Results and Discussions

3.1. CMC Measurement of Surfactant CAPHS.

The relationships between surface tension and CAPHS concentration at different situations were presented in Figure 5-3. The CMC of CAPHS in distilled water was 179.0 mg/L, compared to a decreased value of around 100.0 mg/L in API brine when large amount of salts presents.

3.2. Characterization of SiO_2-GLYMO NPs.

The size and zeta potential of SiO_2-OH NPs in distilled water were around 5.3±0.4 nm and -48.9±3.1 mV (pH=7.2±0.2), respectively. When SiO_2-OH NPs surfaces were covalently connected with GLYMO molecules, the zeta potential increased to -33.5±1.4 mV, accompanied by a small increase of 1.5 nm in particle hydrodynamic diameter, as presented in Figure 5-4.

Meanwhile, the surface chemistry of SiO_2-OH and SiO_2-GLYMO NPs were compared by FTIR analysis and the surface modification could be confirmed through the variations in the spectra (Figure 5-5). Peaks at ~800 cm^{-1}, ~1100 cm^{-1} and ~3600 cm^{-1} in both spectra were ascribed to the stretching vibration of C-C, Si-O-Si and -OH, separately. The new peaks at ~1470 cm^{-1} and ~2800-2950 cm^{-1} were generated by the stretching vibration of -CH, indicating the presence of GLYMO. However, due to the multiplicity of absorption bands, the adsorption peak of epoxy group (736~864, 863~950, and ~1260 cm^{-1}) is usually hard to be distinguished.

(a)   (b)
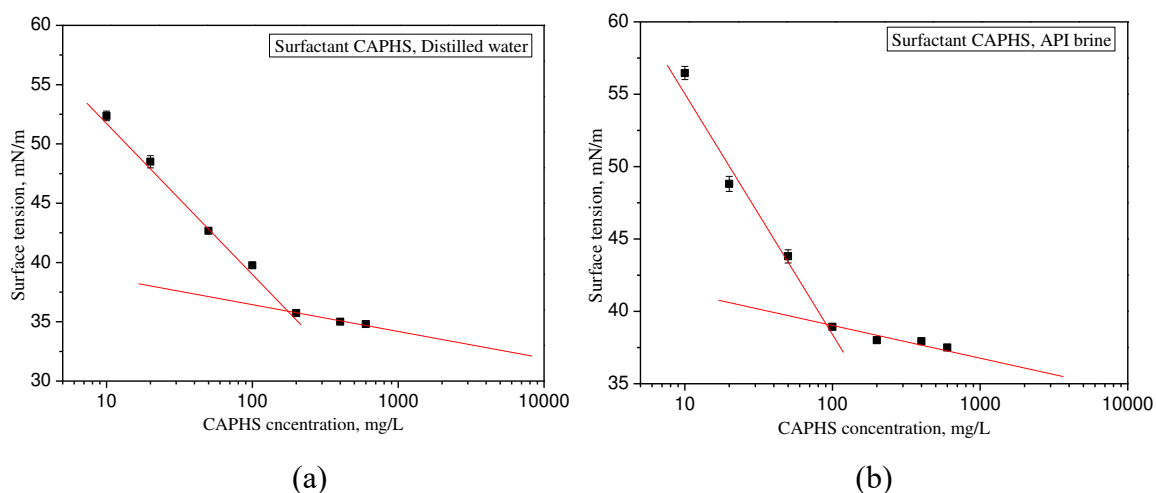
Figure 5-3 CAPHS CMCs at different conditions. (a) Distilled water. (b) API brine.

(a)   (b)
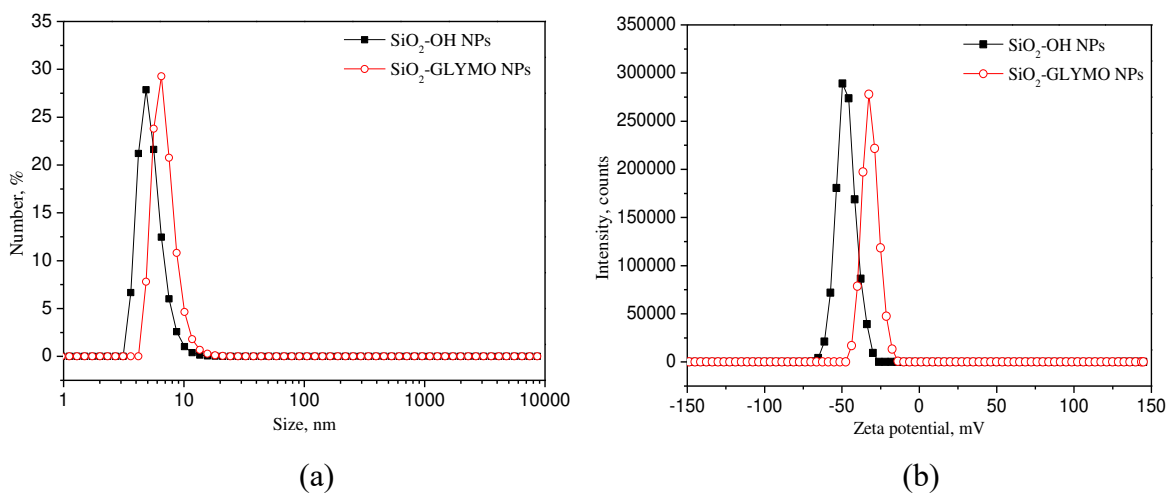
Figure 5-4 Basic properties of SiO_2-OH NPs and SiO_2-GLYMO NPs. (a) Size distribution. (b) Zeta potential.

113
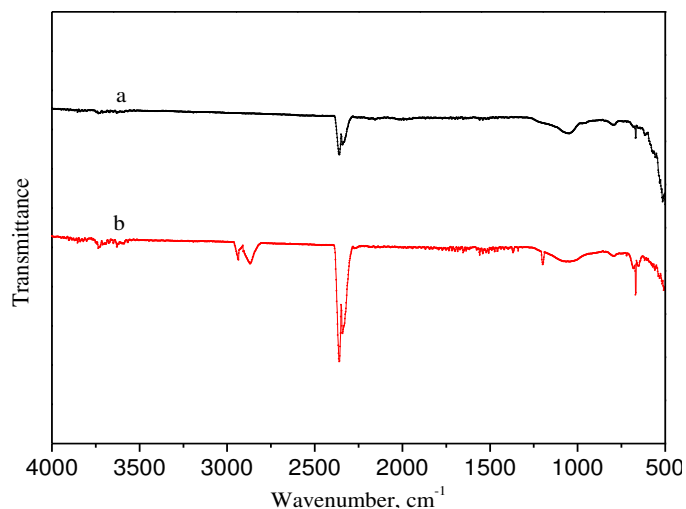
Figure 5-5 FTIR spectra of SiO$_2$-OH NPs (a) and SiO$_2$-GLYMO NPs (b).

3.3. Interactions between Surfactant CAPHS and SiO$_2$-GLYMO NPs.

The interactions between surfactant CAPHS and SiO$_2$-GLYMO NPs were investigated mainly through zeta potential measurement. API brine was used to prepare the nanofluids. The presence of salts severely compressed the diffuse electric double layer on SiO$_2$-GLYMO NPs surfaces and resulted in a huge variation in zeta potential from -33.5±1.4 mV to -1.96±0.80 mV, indicating a great reduction in intraparticle electrostatic repulsion. The chelate effects of zwitterionic surfactant with cations might mitigate the adverse effects. However, the concentration ratio between surfactant and NP matters when preparing an augmented system, especially when different interactions coexist in the system ((Songolzadeh and Moghadasi, 2017; Worthen et al., 2014)). Electrostatic and steric repulsions are favorable for particle stability while hydrophobic tails being exposed onto NPs surfaces may possibly promote particle aggregation. In this study, nanofluids with a wide range of CAPHS/SiO$_2$-GLYMO NPs concentration ratio from 1:40 to 10:1 were prepared and no precipitation was observed for all formulas within one day at room temperature. According to Figure 5-6, particle size remained nearly unchanged at around 10.0 nm when CAPHS concentration was no higher than 800 mg/L (1:2.5), while when the addition of

114

CAPHS increased, particle size would grow to 24.2 nm at a ratio of 1:2 and to 96.2 nm at 10:1.
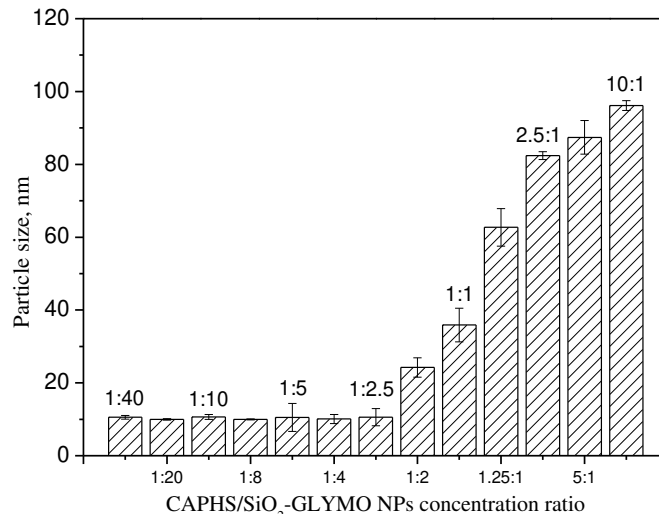
Figure 5-6 Particle size at different CAPHS/SiO$_2$-GLYMO NP concentration ratios.

3.4. Interfacial Properties of CAPHS/ SiO$_2$-GLYMO NPs System.

3.4.1. Interfacial Tension.

The interfacial tension between crude oil and API brine was 17.3±0.13 mN/m, and only a small reduction of 2.23 mN/m was observed when 2000 mg/L SiO$_2$-GLYMO NPs were added. To better clarify the IFT differences between surfactant system (γ_1) and surfactant-nanoparticle augmented system (γ_2), reduction ratio ($R = \frac{\gamma_1 - \gamma_2}{\gamma_1}$) was used. A larger R value corresponds to a greater variation. Figure 5-7 indicated that for pure CAPHS system, the IFT showed a first decrease and then increase trend, and the minimum value of 0.08 mN/m was achieved at the concentration of 100 mg/L. The most noticeable synergistic effects between CAPHS and SiO$_2$-GLYMO NPs in reducing IFT occurred when surfactant concentration was lower than 100 mg/L. When 10 mg/L CAPHS was mixed with 2000 mg/L SiO$_2$-GLYMO NPs, the IFT dropped sharply from 6.99±0.24 mN/m to 0.15±0.02 mN/m, while when CAPHS concentration increased to 100 mg/L, the difference was only 0.03 mN/m.
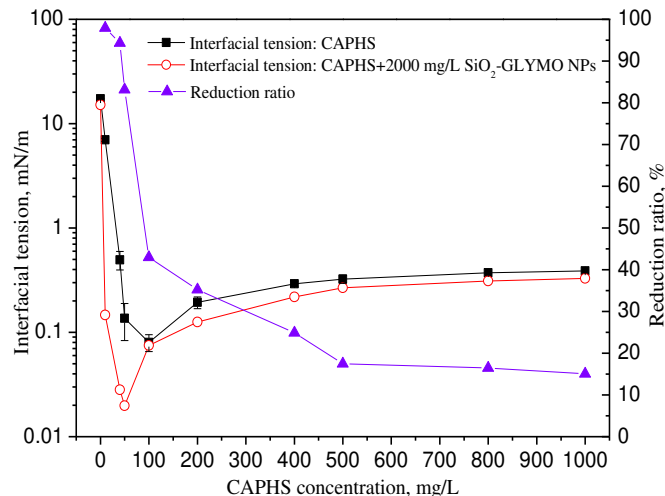
Figure 5-7 Impacts of CAPHS concentration on oil/aqueous interfacial tension.

In order to figure out the exact SiO_2-GLYMO NPs concentration needed for different CAPHS systems to achieve the lowest IFT value, different amounts of nanoparticle (0~4000 mg/L) were added. Herein, CAPHS concentrations have been divided into three levels according to its CMC, 1) lower than CMC (10 mg/L, 50 mg/L), 2) CMC (100 mg/L) and 3) higher than CMC (200 mg/L, 800 mg/L), as demonstrated in Figure 5-8. When CAPHS concentration was 10 mg/L, the decrease in IFT nearly stagnated at 1000 mg/L SiO_2-GLYMO NPs, with values staying in the region below 0.10 mN/m. When CAPHS concentration increased to 50 mg/L, only 100 mg/L surface-modified SiO_2 NPs were required to achieve the same result. When CAPHS concentration reached 100 mg/L, all the studied formulas either with or without SiO_2-GLYMO NPs can achieve relatively low IFTs of 0.03~0.08 mN/m. When CAPHS proportion increased further to over 100 mg/L, the overall IFTs showed an increasing trend and the effects of NPs became weaker, the reduction ratios for 200 mg/L and 800 mg/L CAPHS were only 36.9 % and 16.7 % in the presence of 4000 mg/L NPs, compared to 99.4 % and 82.8 % for systems with 10 mg/L and 50 mg/L CAPHS, respectively.

116
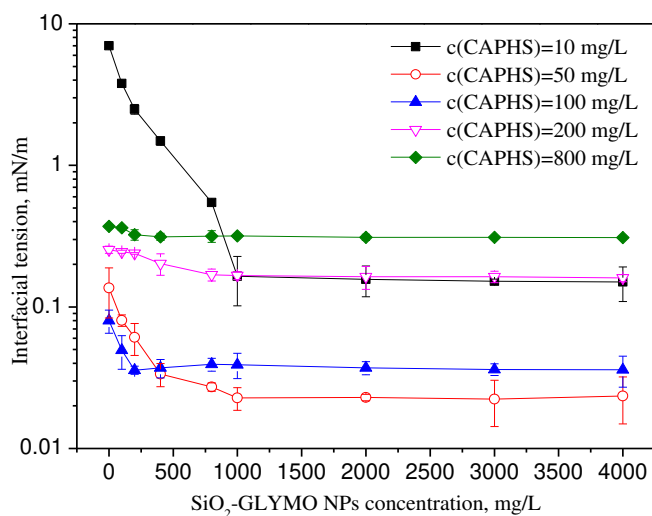
Figure 5-8 Impacts of SiO$_2$-GLYMO NPs concentration on oil/aqueous interfacial.

Molecular dynamics (MD) simulation performed with LAMMPs software was applied to explore the reason for further decrease in IFT when SiO$_2$-GLYMO NPs were introduced into the zwitterionic surfactant solution. In this study, OPLS all-atom force-field parameters (Jorgensen et al., 1996) were used for the oil phase and the GLYMO ligand, while single point charge/extended (SPC/E) model (Berendsen et al., 1987) was applied for the water phase. The periodic boundary condition was applied in all three directions. Herein, SiO$_2$-OH NP and SiO$_2$-GLYMO NP fully coated with GLYMO ligands (consistent with the Experimental results) were fabricated for comparison. Initially, both NPs were forced to locate at the oil-water interface, as the simulation going forward, SiO$_2$-OH NP gradually moved into the water phase, showing a huge reduction in occupied interfacial areas. While the SiO$_2$-GLYMO NP remained stably staying at the interface (Figure 5-9). The possible explanation can be that, compared with the totally hydrophilic SiO$_2$-OH NPs which prefer to stay entirely in the aqueous phase, the coexistence of hydrophilic part and hydrophobic part on SiO$_2$-GLYMO NPs surfaces offers them higher affinity to the oil/water interface. At low surfactant concentrations, CAPHS molecules were loosely and irregularly packed at the oil-water interface, leaving huge available interfacial area for SiO$_2$-GLYMO NPs. Once

117

those extra spaces were occupied by NPs, synergistic effects would emerge to further decrease the oil-water interfacial tension (Vu et al., 2019). However, since few interfacial spaces were left for NPs to absorb at higher surfactant concentrations, the combined effects therefore showed a descending trend. In this paper, the developed CAPHS/SiO$_2$-GLYMO NP augmented system was able to produce a wide range of IFTs, and the formulas could be tailored simply by adjusting the concentration ratios to satisfy the requirements for different applications as diverse as food preparation, detergency (Calzolari et al., 2012) and oil industry.

<center>(a)　　　　　　　(b)　　　　　　　(c)　　　　　　　(d)</center>
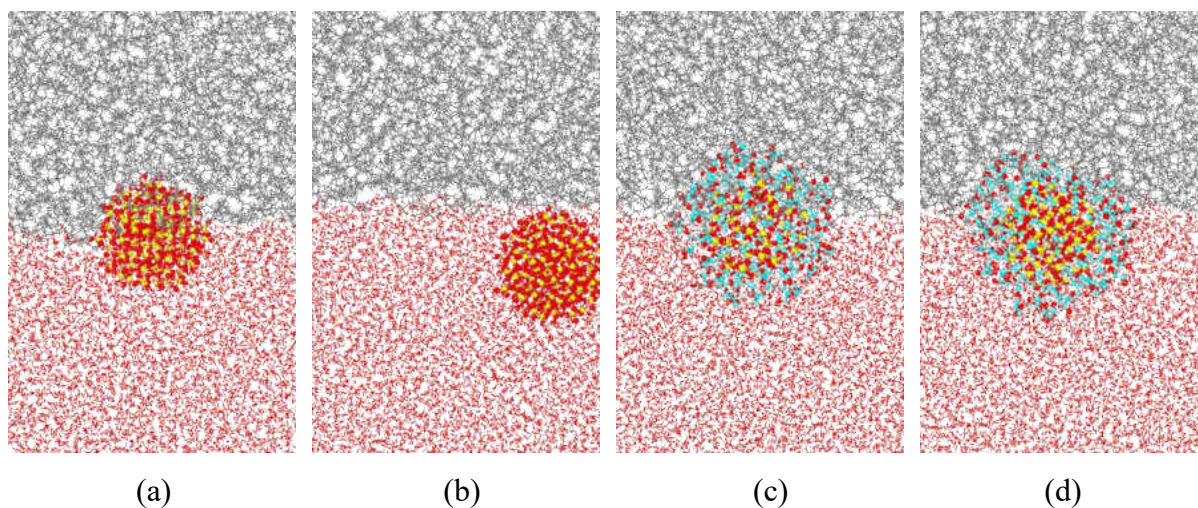
Figure 5-9 Snapshots of the oil-water interface with different SiO$_2$ NPs. Upper layer-oil, Lower layer-water. (a) SiO$_2$-OH NP, Initial state. (b) SiO$_2$-OH NP, Equilibrium state. (c) SiO$_2$-GLYMO NP, Initial state. (d) SiO$_2$-GLYMO NP, Equilibrium state.

3.4.2. Contact Angle.

The oil detaching capability of different treating fluids was evaluated by three-phase contact angle measurement. Water contact angle at air/aqueous/rock interface and oil contact angle at oil/aqueous/rock interface were measured separately. The air/aqueous/rock (θ_1) and oil/aqueous/rock (θ_2) contact angles of the pretreated glass were 89.0° and 34.0°, respectively. Figure 5-11 shows that when in the absence of NPs, 800 mg/L zwitterionic surfactant CAPHS

itself can reduce θ_1 to 46.5° and increase θ_2 to 75.0°. A strengthened effect emerged when 2000 mg/L SiO$_2$-GLYMO NPs were added, where θ_1 was witnessed to decrease further to 24.0° and θ_2 increased to 102.0°, resulting in a more water-wet condition beneficial for additional oil recovery.
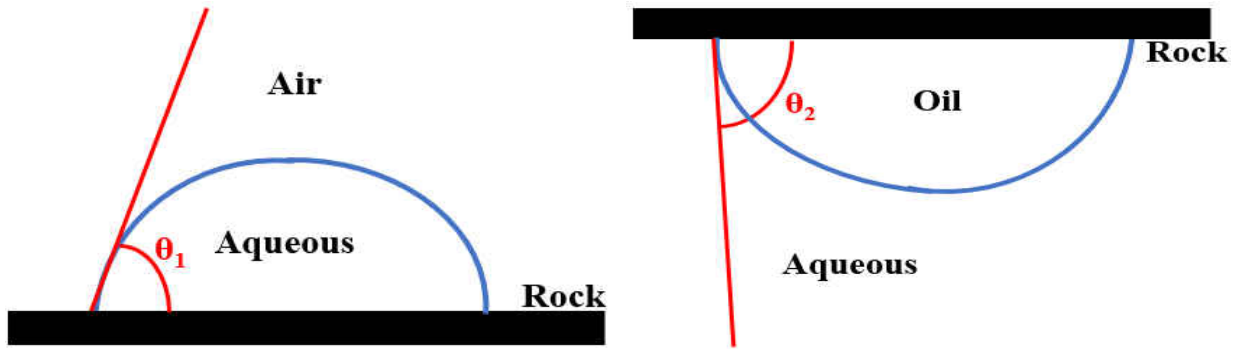
Figure 5-10 Schematic diagram of different contact angles.
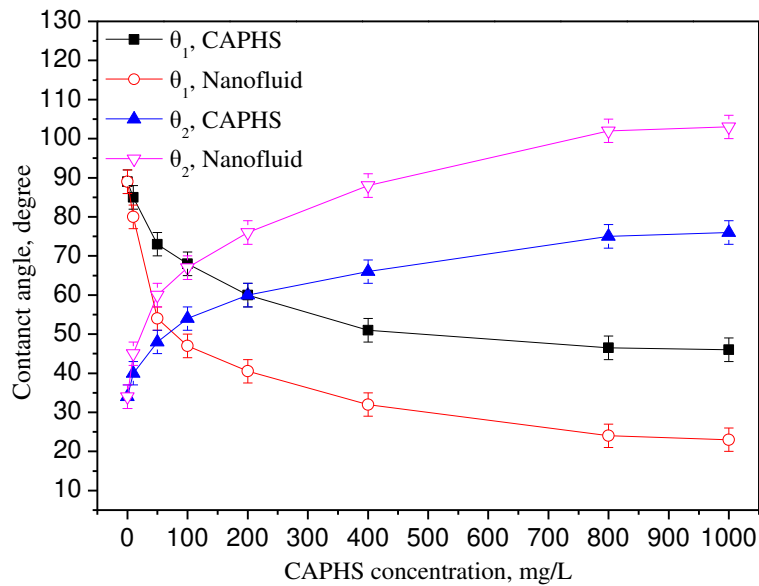
Figure 5-11 Impacts of different treating fluids on contact angles.

3.4.3. Static Adsorption.

The static adsorption behavior of zwitterionic surfactant on crushed Berea sample (≤125 μm) was studied at a liquid/solid ratio of 10:1 through batch equilibrium tests. In each test, 2.0 g (*M*) rock powders were soaked in 20.0 mL (*V*) treating fluid. The testing fluids were 200 ~ 1000

mg/L CAPHS (c_i) with or without 2000 mg/L SiO₂-GLYMO NPs prepared by API brine. After 24 hrs of fully interactions, rock powders were removed by centrifugation and the residual CAPHS concentration (c_e) was analyzed with a UV/vis spectrometer. Surfactant adsorption density (Γ_e) was then calculated by Equation 5-1.

$$\Gamma_e = \frac{(c_i - c_e)V}{M} \tag{5-1}$$
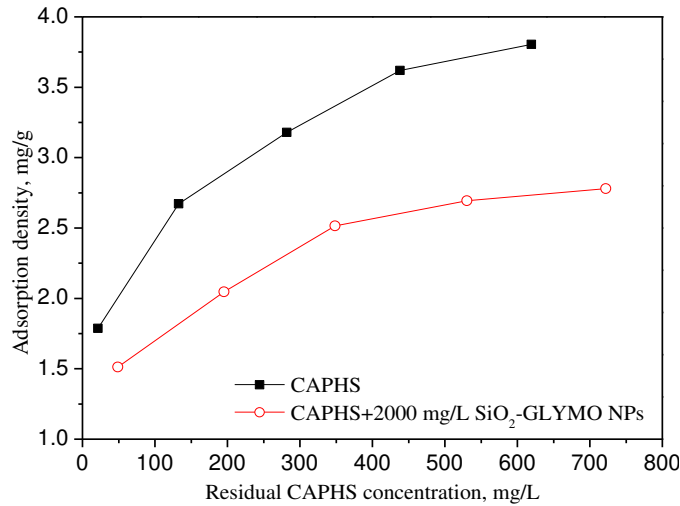
Figure 5-12 Static adsorption of surfactant CAPHS on crushed Berea sample.

Figure 5-12 illustrated that the adsorption density of surfactant CAPHS has been generally reduced when SiO₂-GLYMO NPs were added. The adsorption density of 200 mg/L CAPHS was 1.79 mg/g without NPs and a reduction of around 16.0 % was observed when 2000 mg/L SiO₂-GLYMO NPs presented. In addition, the influences of NPs in lowering surfactant adsorption were more prominent when initial CAPHS concentration was higher. For example, when CAPHS concentration was 800 mg/L, the original adsorption was 3.62 mg/g and could be lowered to 2.69 mg/g when 2000 mg/L SiO₂-GLYMO NPs were added.

3.5. Selection of CAPHS/ SiO₂-GLYMO NPs Formula.

Wettability alteration is believed to be a main EOR mechanism especially when formations are characterized as intermediate-wet or oil-wet (Alvarez, 2017). Meanwhile, stable emulsion

formed at low IFTs can have adverse impacts on the oil production process in most low-permeability reservoirs due to permeability damage and increase the difficulty of crude oil demulsification process (Kiani et al., 2019). Hence, we mainly focused on the surfactant-NP augmented system with specifications of 800 mg/L CAPHS and 2000 mg/L SiO$_2$-GLYMO, which displayed good wetting ability and an IFT around 0.31 mN/m.

3.6. Long-Time Stability.

The tolerance of the selected formula towards monovalent cations and divalent cations, long-time stability at room temperature (25 °C) as well as elevated temperature (60 °C) was systematically evaluated. Particle size measurement showed that the selected CAPHS/SiO$_2$-GLYMO NP nanofluid exhibited excellent stability in different brines at room temperature. When Na$^+$ concentration increased to 25.0 wt.%, the hydrodynamic radius of NPs only increased by 1.54 nm, and the impacts of K$^+$ were even more negligible. Given the smaller solvation area and the higher exchange capacity of divalent cations compared with monovalent cations (Nieto-Alvarez et al., 2014), NPs showed slightly larger sizes when divalent cations exist, as shown in Figures 5-12(a) and 5-12(b). The size of freshly prepared nanofluid in API brine was 8.24±0.78 nm, after 60 days aging at room temperature, particles size increased slightly to 9.69±0.44 nm. While at 60 °C, due to more aggressive molecular motion and particle collision, NP stability decreased, where particle size remained around 10.0 nm within 4 weeks and increased to 34.6±3.27 nm after 8 weeks.
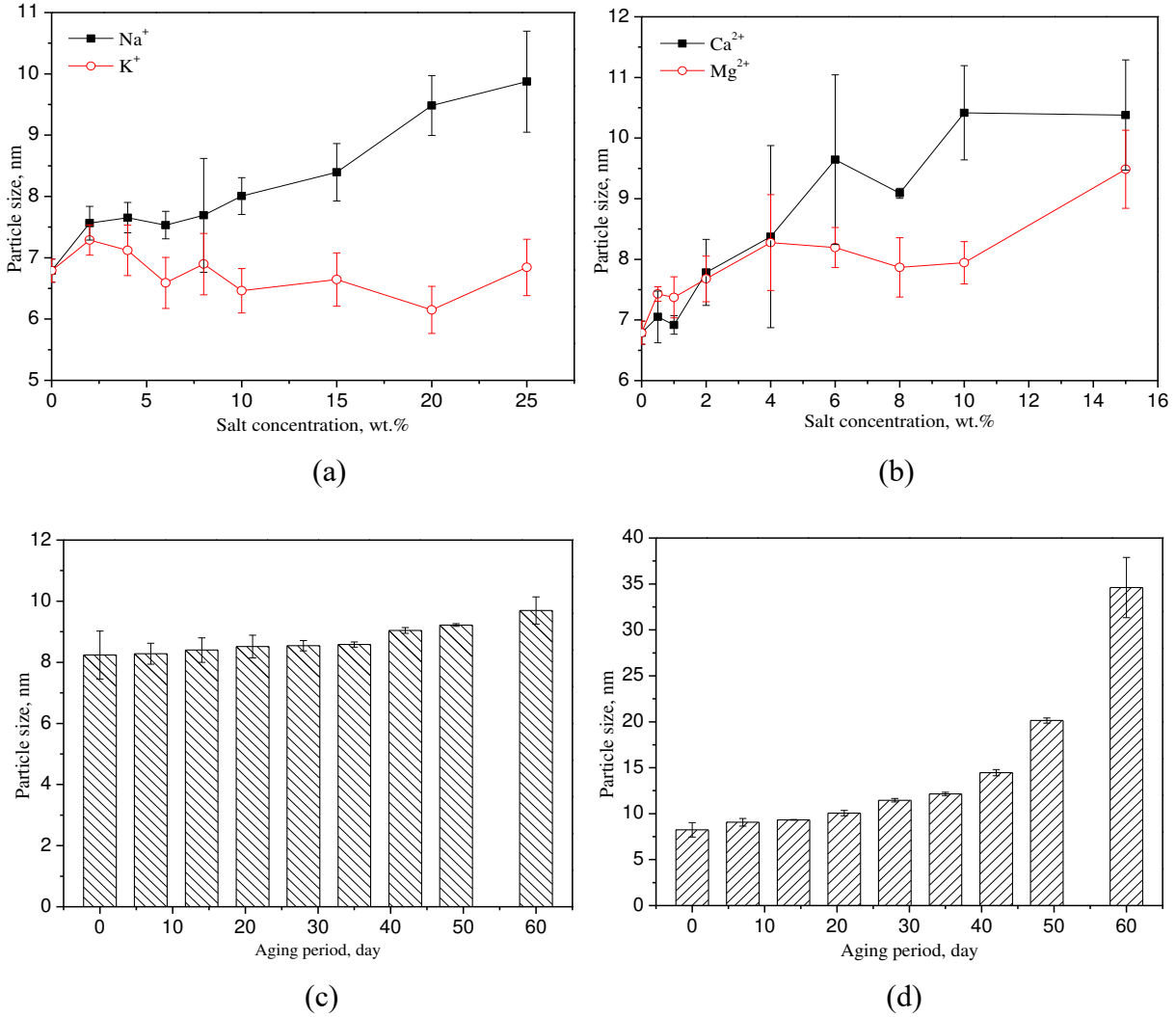
Figure 5-13 Stability test of CAPHS/SiO$_2$-GLYMO NP nanofluid. (a) Effects of monovalent cations, 25 ℃, 24 hrs. (b) Effects of divalent cations, 25 ℃, 24 hrs. (c) API brine, 25 ℃. (d) API brine, 60 ℃.

3.7. EOR Potential.

3.7.1. Rock Characterization.

Berea rock is composed of 70. 9 % quartz, 13.7 % feldspar, 8.6 % kaolinite and illite, 2.3 % dolomite and a small fraction of other minerals. The SEM image in Figure 5-13(a) shows that there were many intergranular pores of micron order and micron size intragranular dissolved pores in

Berea sample. According to the one-third- to one-seventh-arch principles (Franco et al., 2017), the prepared nanofluid was able to pass through the pore throat smoothly and could induce inner rock properties change as long as the system was free of severe aggregation.

3.7.2 Core Flooding Experiment.

The primary oil recovery of Core 1 and Core 2 yielded by API brine flooding was 25.47 % and 24.29 % respectively, as demonstrated in Figure 5-15. In the secondary oil recovery stage, 800 mg/L surfactant CAPHS flooding recovered additional 7.05 % OOIP from Core 1 and 2000 mg/L SiO_2-GLYMO NPs flooding only recovered 1.46 % additional oil from Core 2. CAPHS/SiO_2-GLYMO NP nanofluid was used as an EOR agent for tertiary oil recovery in this study. Subsequent surfactant-NP flooding increased the oil recovery of Core 1 by another 3.12 % and resulted in a recovery factor of 35.65 %. Similar performance was observed in Core 2, where additional 5.39 % OOIP was extracted.
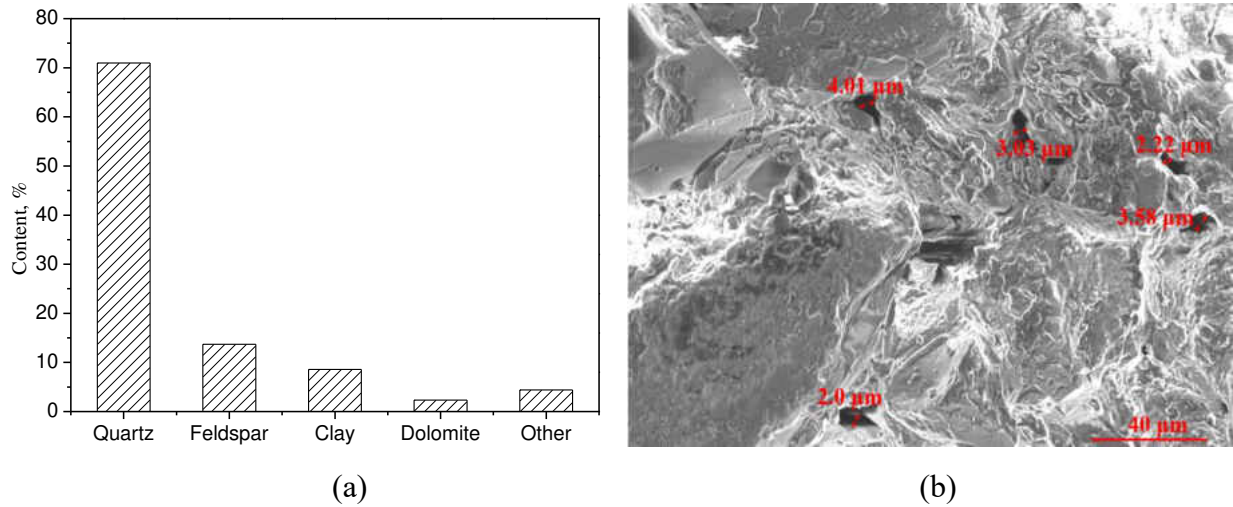
Figure 5-14 Physico-chemical properties of Berea sample. (a) Mineral composition. (b) Surface morphology.
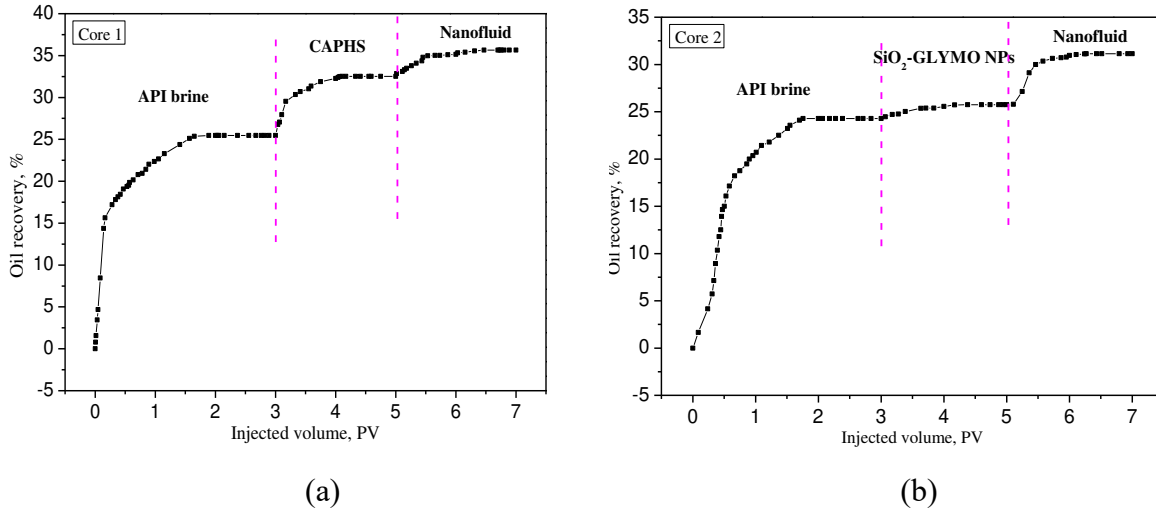
Figure 5-15 EOR potential of CAPHS/SiO$_2$-GLYMO NP nanofluid. (a) Core 1. (b) Core 2.

4. Summary

(1) SiO$_2$-GLYMO NPs demonstrated higher surface charge when mixed with zwitterionic surfactant CAPHS because surfactant molecules can adsorb on NPs and weaken the interactions between NPs and cations by chelate effects.

(2) The concentration ratio between surfactant CAPHS and SiO$_2$-GLYMO NPs should be maintained below 1:2.5 to ensure the small particle size of around 10.0 nm.

(3) The developed surfactant-nanoparticle augmented system showed great tolerance towards salts and elevated temperature, where particle size remained around 10.0 nm in API brine within 8 weeks at 25 °C and 4 weeks at 60 °C.

(4) Zwitterionic surfactant CAPHS and SiO$_2$-GLYMO NPs showed synergistic effects in reducing IFT and the combined effects were more noticeable at lower CAPHS concentration.

(5) CAPHS/SiO$_2$-GLYMO NP flooding recovered another 5.39 % OOIP after SiO$_2$-GLYMO NPs flooding and 3.12 % OOIP after surfactant CAPHS flooding in the tertiary recovery mode, indicating its great potential to be eligible EOR agent for sandstone reservoirs with high salinity and elevated temperature.

CHAPTER VI

CONCLUSIONS AND RECOMMANDATIONS

The goal of this dissertation was to investigate the adsorption behaviors of surfactants and the synergistic effects between surfactant and nanoparticles in enhanced oil recovery for sandstone reservoirs. In this research, two surfactant-nanoparticle augmented systems were developed, nonionic surfactant-hydrophilic silica nanoparticles system prepared by low salinity brine (0.2 wt.% KCl) and zwitterionic surfactant-GLYMO modified silica nanoparticle system prepared by API brine (8.0 wt.% NaCl + 2.0 wt.% CaCl$_2$). Both of which were stable at elevated temperatures ($\leq$ 60 °C). The addition of hydrophilic silica nanoparticles could further reduce the oil-water interfacial tension compared with high concentration (> CMC) nonionic surfactant alone, while combined effects of zwitterionic surfactant and GLYMO-modified silica nanoparticles in reducing oil-water interfacial tension were more noticeable at low surfactant concentration cases. For both systems, nanoparticles showed the capability to decrease surfactant adsorption loss and to alter rock wettability to a more water-wet condition, both of which are beneficial for water imbibition and the oil recovery process. For detailed conclusions, the readers are suggested to refer to each chapter which elaborated the motivations, methods, results and innovation findings for every specific topic.

However, the long-term stability of nanofluids has always been a huge concern. The pore plugging effects of nanoparticles and permeability damage become more significant especially when particle size becomes large, particle concentration becomes high and nanoparticle aggregation occurs. In order to extend the application of nanofluids to unconventional reservoirs that usually have high temperature and high salinity, the research on developing novel nanomaterials should be continued. Meanwhile, it is worth mentioning that surfactant-nanoparticle

augmented systems, if prepared by surfactants with varying structures and different types of nanoparticles, difference size and different surface modification, the final results can be different. Therefore, deeper insight into the functional mechanisms is required and is of key importance.

REFERENCES

Adil, M.; Zaid, H. M.; Chuan, L. K.; Latiff, N. R. A. 2016. Effect of dispersion stability on electrorheology of water-based ZnO nanofluids. Energy Fuels, 30(7), 6169–6177.

AfzaliTabar, M.; Alaei, M.; Khojasteh, R. R.; et al. 2017. Preference of multi-walled carbon nanotube (MWCNT) to single-walled carbon nanotube (SWCNT) and activated carbon for preparing silica nanohybrid pickering emulsion for chemical enhanced oil recovery (C-EOR). J. Solid State Chem., 245, 164–173.

Agista, M. N.; Guo, K.; Yu, Z. 2018. A state-of-the-art review of nanoparticles application in petroleum with a focus on enhanced oil recovery. Appl. Sci., 8(6), 871.

Ahmadi, M. A.; Shadizadeh, S. R. 2012. Adsorption of novel nonionic surfactant and particles mixture in carbonates: enhanced oil recovery implication. Energy Fuels, 26, 4655–4663.

Ahmadi, M. A.; Habibi, A.; Pourafshary, P.; Ayatollahi, S. 2013. Zeta-potential investigation and experimental study of nanoparticles deposited on rock surface to reduce fine migrations. SPE J., 18(3). SPE Paper 142633.

Ahmadi, M. A.; Shadizadeh, S. R. 2013. Experimental investigation of adsorption of a new nonionic surfactant on carbonate minerals. Fuel, 104, 462–467.

Ahmed, A.; Saaid, I. M.; Tunio, A. H.; et al. 2017. Investigation of dispersion stability and IFT reduction using surface modified nanoparticle: Enhanced oil recovery. J. Appl. Environ. Biol. Sci., 7(4S), 56–62.

Al-Anssari, S.; Arif, M.; Wang, S.; et al. 2016. Wettability alteration of oil-wet carbonate by silica nanofluid. J. Colloid Interface Sci., 461, 435–442.

Al-Anssari, S.; Arif, M.; Wang, S.; et al. 2018. Wettability of nanofluid-modified oil-wet calcite at reservoir conditions. Fuel, 211, 405–414.

Almahfood, M.; Bai, B. 2018. The synergistic effects of nanoparticle-surfactant nanofluids in EOR applications. J. Pet. Sci. Eng., 171, 196–210.

Alnarabiji, M. S.; Yahya, N.; Shafie, A.; et al. 2016. The influence of hydrophobic multiwall carbon nanotubes concentration on enhanced oil recovery. Procedia Engineering, 148, 1137–1140.

Alomair, O. A.; Matar, K. M.; Alsaeed, Y. H. 2015. Experimental study of enhanced heavy oil recovery in Berea sandstone cores by use of nanofluids applications. SPE Reservoir Evaluation & Engineering, 18(03). SPE Paper 171539.

Alvarea, J. O.; Saputra, I. W. R.; Schechter, D. S. 2017. Potential of improving oil recovery with surfactant additives to completion fluids for the Bakken. Energy Fuels, 31(6), 5982–5994.

Alvarez, O. 2017. Wettability Alteration Using Surfactants to Improve Oil Recovery from Unconventional Liquid Reservoirs. Doctoral dissertation, Texas A & M University.

Amirianshoja, T.; Junin, R.; Idris, A. K.; Rahmani, O. A. 2013. A comparative study of surfactant adsorption by clay minerals. J. Pet. Sci. Eng., 101, 21–27.

Anderson, W. G. 1986. Wettability literature survey-part 1: rock/oil/brine interactions and the effects of core handling on wettability. J. Petrol. Technol., 38(10), 1246–1262.

Archer, R.; Borthwick, K.; Travers. M.; Ruschena, L. 2012. WHS: a Management Guide, third ed., Australia.

Ball, B.; Fuerstenau, D. W. 1971. Thermodynamics and adsorption behaviour in the quartz/aqueous surfactant system. Discuss. Faraday Soc., 52, 361–371.

Bai, Y.; Lin, D.; Wu, F.; et al. 2010. Adsorption of Triton X-series surfactants and its role in stabilizing multi-walled carbon nanotube suspensions. Chemosphere, 79(4), 362–367.

Bayat, A. E.; Junin, R.; Samsuri, A.; et al. 2014. Impact of metal oxide nanoparticles on enhanced oil recovery from limestone media at several temperatures. Energy Fuels, 28(10), 6255–6266.

Bayford, R.; Rademacher, T.; Roitt, I.; Wang, S. X. 2017. Emerging applications of nanotechnology for diagnosis and therapy of disease: a review. Physiol. Meas., 38, 8.

Bazazi, P.; Gates, I. D.; Nezhad, A. S.; Hejazi, S. H. 2017. Silica-based nanofluid heavy oil recovery a microfluidic approach. In Proceedings of SPE Canada Heavy Oil Technical Conference; Calgary, Alberta, February 15-16. SPE Paper 185008.

Berendsen, H. J. C.; Grigera, J. R. and Straatsma, T. P. 1987. The missing term in effective pair potentials. J. Phys. Chem., 91 (24), 6269–6271.

Betancur, S.; Carrasco-Marín, F.; Franco, C. A.; Cortés, F. B. 2018. Development of composite materials based on the interaction between nanoparticles and surfactants for application in chemical enhanced oil recovery. Ind. Eng. Chem. Res., 57(37), 12367–12377.

Binks, B. P.; Desforges, A.; Duff, D. G. 2007. Synergistic stabilization of emulsions by a mixture of surface-active nanoparticles and surfactant. Langmuir, 23(3), 1098–1106.

Calzolari, D. C. E.; Pontoni, D.; Deutsch, M.; et al. 2012. Nanoscale structure of surfactant-induced nanoparticle monolayers at the oil-water interface. Soft Matter, 8, 11478–11483.

Cassagnau, P. 2015. 3-Rheology of carbon nanoparticle suspensions and nanocomposites. Rheology of non-spherical particle suspensions, 59–75.

Cerqueira, M. A.; Pinheiro, A. C.; Ramos, O. L.; et al. 2017. Chapter Two -Advances in food nanotechnology. Emerg. Nanotechnologies Food Sci., 11–38.

Chandran, K. A/P. 2013. Multiwall carbon nanotubes (MWNT) fluid in EOR using core flooding method under the presence of electromagnetic waves. Bachelor Dissertation, Universiti Teknologi PETRONAS.

Chang, H.; Chang, Y. 2008. Fabrication of Al_2O_3 nanofluid by a plasma arc nanoparticles synthesis system. J. Mater. Process. Technol., 207, 193–199.

Chen, L; Zhu, X.; Wang, L.; et al. 2018. Experimental study of effective amphiphilic graphene oxide flooding for an ultralow-permeability reservoir. Energy Fuels, 32(11), 11269–11278.

Cheraghian, G.; Neshad, S. S. K.; Kamari, M.; et al. 2014. Adsorption polymer on reservoir rock and role of the nanoparticles, clay and SiO_2. Int. Nano. Lett., 4, 114.

Cheraghian, G. 2016a. Effects of titanium dioxide nanoparticles on the efficiency of surfactant flooding of heavy oil in a glass micromodel. J. Pet. Sci. Technol., 34(3), 260–267.

Cheraghian, G. 2016b. Effect of nano titanium dioxide on heavy oil recovery during polymer flooding. J. Pet. Sci. Technol., 34(7), 633–641.

Cheraghian, G.; Kiani, S.; Nassar, N. N.; et al. 2017. Silica nanoparticle enhancement in the efficiency of surfactant flooding of heavy oil in a glass micromodel. Ind. Eng. Chem. Res., 56(30), 8528–8534.

Choi, S. K.; Son, H. A.; Kim, H. T.; Kim, J. W. 2017. Nanofluid enhanced oil recovery using hydrophobically associative zwitterionic polymer-coated silica nanoparticles. Energy Fuels, 31(8), 7777–7782.

Cote, L. J.; Kim, J.; Tung, V. C.; et al. 2010. Graphene oxide as surfactant sheets. Pure Appl. Chem., 83 (1), 95–110.

Cullum, D. C. 1994. Introduction to surfactant analysis. Springer, Dordrecht, Netherlands. ISBN 978-94-011-1316-8. pp. 23–24.

Cui, G.; Wang, Y.; Chen, B.; et al. 2018a. Assessing the combined influence of fluid–rock interactions on reservoir properties and injectivity during CO_2 storage in saline aquifers. Energy, 155, 281–296.

Cui, G.; Ren, S.; Ezekiel, J.; et al. 2018b. The influence of complicated fluid–rock interactions on the geothermal exploitation in the CO_2 plume geothermal system. Appl. Energy, 227. 49–63.

Cygan, R. T.; Liang, J.; Kalinichev, A. G. 2004. Molecular models of hydroxide, oxyhydroxide, and clay phases and the development of a general force field. J. Phys. Chem. B, 108 (4), 1255–1266.

Da, C.; Alzobaidi, S.; Jian, G.; et al. 2018. Carbon dioxide/water foams stabilized with a zwitterionic surfactant at temperatures up to 150 °C in high salinity brine. J. Pet. Sci. Eng., 16, 880–890.

Dai, C.; Wang, X.; Li, Y.; et al. 2017. Spontaneous imbibition investigation of self-dispersing silica nanofluids for enhanced oil recovery in low-permeability cores. Energy Fuels, 31(3), 2663–2668.

Dasgupta, N.; Ranjan, S. and Ramalingam, C. 2017. Applications of nanotechnology in agriculture and water quality management. Environ. Chem. Lett., 15(4), 591–605.

Deri, M.; Ellafi, A.; Ofori, B.; et al. 2019. Successful implementation of high viscosity friction reducers from laboratory to field scale: Middle Bakken case study. In Proceedings of Unconventional Resources Technology Conference; Denver, Colorado, July 22–24. URTeC Paper 447.

Duncan, T. V.; Singh, G. 2017. Nanomaterials in food products: a new analytical challenge. Nanotechnologies Food, 143–177.

Duran–Alvarez, A.; Moldonado-Dominguez, M; Gonzalez-Antonio, O.; et al. 2016. Experimental-theoretical approach to the adsorption mechanisms for anionic, cationic, and zwitterionic surfactants at the calcite-water interface. Langmuir, 32(11), 2608–2616.

Ehtesabi, H.; Ahadian, M. M.; Taghikhani, V.; Ghazanfari, M. H. 2014. Enhanced heavy oil recovery in sandstone cores using TiO_2 nanofluids. Energy Fuels, 28(1), 423–430.

Ehtesabi, H.; Ahadian, M. M.; Taghikhani, V.; Ghazanfari, M. H. 2015. Enhanced heavy oil recovery using TiO_2 nanoparticles: investigation of deposition during transport in core plug. Energy Fuels, 29(1), 1–8.

Elmouwahidi, A.; Bailón-García, E.; Pérez-Cadenas, A. F. 2017. Activated carbons from KOH and $H_3PO_4^-$ activation of olive residues and its application as supercapacitor electrodes. Electrochimica Acta, 229, 219–228.

Feng, Z. C. 2012. Handbook of zinc oxide and related materials: Volume Two, Devices and Nano-engineering, vol. 2 CRC press.

Franco-Aguirre, M.; Zabala, R. D.; Lopera, S. H.; et al. 2018. Interaction of anionic surfactant-nanoparticles for gas–wettability alteration of sandstone in tight gas-condensate reservoirs. Journal of Natural Gas Science and Engineering, 51, 53–64.

Franco, C. A.; Zabala, R.; Cortés, F. B. 2017. Nanotechnology applied to the enhancement of oil and gas productivity and recovery of colombian fields. J. Pet. Sci. Eng., 157, 39–55.

Ge, J.; Wang, Y. 2015. Surfactant enhanced oil recovery in a high temperature and high salinity carbonate reservoir. J. Surfact. Deterg., 18(6), 1043–1050.

Giraldo, J.; Benjumea, P.; Lopera, S.; et al. 2013. Wettability alteration of sandstone cores by alumina-based nanofluids. Energy Fuels, 27(7), 3659–3665.

Goresy, A. E.; Chen, M.; Dubrovinsky, L. et al. 2001. An ultradense polymorph of rutile with seven-coordinated titanium from the Ries crater. Science, 293(5534), 1467–1470.

Griffith, C.; Daigle, H. 2018. Manipulation of Pickering emulsion rheology using hydrophilically modified silica nanoparticles in brine. J. Colloid Interface Sci., 509, 132–139.

Guo, K.; Li, H.; Yu, Z. 2016. In-situ heavy and extra-heavy oil recovery: A review. Fuel, 185, 886–902

Guo, S.; Wang, H.; Shi, J.; et al. 2015. Synthesis and properties of a novel alkyl-hydroxyl-sulfobetaine zwitterionic surfactant for enhanced oil recovery. J. Petrol. Explor. Prod. Technol., 5, 321–326.

Gupta, R.; Mohan, K.; Mohanty, K. K. 2009. Surfactant screening for wettability alteration in oil-wet fractured carbonates. In Proceedings of SPE Annual Technical Conference and Exhibition; New Orleans, Louisiana, October 4-7. SPE Paper 124822.

Halt, S. K.; Moulik, S. P. 2001. Determination of critical micelle concentration (CMC) of nonionic surfactants by donor-acceptor interaction with Iodine and correlation of CMC with

hydrophile-lipophile balance and other parameters of the surfactants. J. Surf. Deterg., 4, 303.

Hamad, M. A.; Sultan, A.; Khan, S.; et al. 2016. Challenges for extending the application of nanoparticles in high salinity reservoirs. In Proceedings of SPE Kingdom of Saudi Arabia Annual Technical Symposium and Exhibition; Dammam, Saudi Arabia, April 25-28. SPE Paper 182838.

Haroun, M. R.; Alhassan, S.; Ansari, A. A.; et al. 2012. Smart nano-EOR process for Abu Dhabi carbonate reservoirs. In Proceedings of SPE Abu Dhabi International Petroleum Conference and Exhibition; Abu Dhabi, UAE, November 11–14. SPE Paper 162386.

Hashemi, R.; Nassar, N. N.; Almao, P. P. 2013. Enhanced heavy oil recovery by in situ prepared ultradispersed multimetallic nanoparticles: A study of hot fluid flooding for Athabasca bitumen recovery. Energy Fuels, 27(4), 2194–2201.

Hendraningrat, L.; Engeset, B.; Suwarno, S. and Torsæter, O. 2012. Improved oil recovery by nanofluids flooding: An experimental study. In Proceedings of SPE Kuwait International Petroleum Conference and Exhibition, Kuwait City, Kuwait, December 10-12. SPE Paper 163335.

Hendraningrat, L.; Li, S.;Torsater, O. 2013a. A coreflood investigation of nanofluid enhanced oil recovery in low-medium permeability Berea sandstone. In Proceedings of SPE International Symposium on Oilfield Chemistry; Woodlands, Texas, April 8-10. SPE Paper 164106.

Hendraningrat, L.; Li, S.; Torsater, O. 2013b. Effect of some parameters influencing enhanced oil recovery process using silica nanoparticles: an experimental investigation. In Proceedings of SPE Reservoir Characterization and Simulation Conference and Exhibition; Abu Dhabi, UAE, September 16-18. SPE Paper 165955.

Hendraningrat, L.; Li, S.; Torsæter, O. 2013c. A coreflood investigation of nanofluid enhanced oil recovery. J. Petrol. Sci. Eng., 111, 128–138.

Hendraningrat, L.; Torsæter, O. 2014. Unlocking the potential of metal oxides nanoparticles to enhance the oil recovery. In Proceedings of Offshore Technology Conference–Asia; Kuala Lumpur, Malaysia, March 25-28. SPE Paper 24696.

Hendraningrat, L.; Torsæter, O. 2015. Metal oxide-based nanoparticles: Revealing their potential to enhance oil recovery in different wettability systems. Appl. Nanosci., 5, 181–199.

Hernández-Battez, A.; González, R.; Viesca, J. L.; et al. 2008. CuO, ZrO_2 and ZnO nanoparticles as antiwear additive in oil lubricants. Wear, 265(3–4), 422–428.

Hernando, E.; Castillo, R. R. Rodrguez, N.; et al. 2014. Copper-catalyzed mild nitration of protected anilines. Chem. Eur. J., 20, 13854–13859.

Hirasaki, G.; Zhang, D. L. 2004. Surface chemistry of oil recovery from fractured, oil-wet, carbonate formations. SPE J., 9(02). SPE paper 88365.

Hockney, R. W.; Eastwood, J. W. 1989. Computer simulation using particles. CRC Press: Adam Hilger, New York.

131

Hoover, W. Q.; Ladd, A. J. C.; Moran, B. 1982. High-strain-rate plastic flow studied via nonequilibrium molecular dynamics. Phys. Rev. Lett., 48, 26–28.

Huang, T.; Evans, B. A.; Crews, J. B.; Belcher, C. K. 2010. Field case study on formation fines control with nanoparticles in offshore applications. In Proceedings of SPE Annual Technical Conference and Exhibition; Florence, Italy, September 19-22. SPE Paper 135088.

IOP. Institute of Physics, Scientists delve deeper into carbon nanotubes, IOP, UK, 2013.

Jahangirian, H.; Lemraski, E. G.; Webster, T. J.; et al. 2017. A review of drug delivery systems based on nanotechnology and green chemistry: green nanomedicine. Int. J. Nanomedicine. 12, 2957–2978.

Jang, H.; Lee, W.; Lee, J. 2018. Nanoparticle dispersion with surface-modified silica nanoparticles and its effect on the wettability alteration of carbonate rocks. Colloids and Surfaces A: Physicochemical and Engineering Aspects, 554(5), 261–271.

Jian, G.; Puerto, M.; Wehowsky, A.; et al. 2018. Characterizing adsorption of associating surfactants on carbonates surfaces. J. Colloid Interface Sci., 513(1), 684–692.

Jian, G.; Puerto, M. C.; Wehowsky, A.; et al. 2016. Static adsorption of an ethoxylated nonionic surfactant on carbonate minerals. Langmuir, 32(40), 10244–10252.

Jiang. L.; Li, S.; Yu, W.; et al. 2016. Interfacial study on the interaction between hydrophobic nanoparticles and ionic surfactants. Colloids and Surfaces A: Physicochemical and Engineering Aspects, 488, 20–27.

Jiang, L.; Sun, G.; Zhou, Z.; et al. 2005. Size-controllable synthesis of monodispersed SnO_2 nanoparticles and application in electrocatalysts. J. Phys. Chem. B, 109(18), 8774-8778.

Jiang, R.; Li, K. and Horne, R. 2017. A Mechanism Study of Wettability and Interfacial Tension for EOR Using Silica Nanoparticles. In Proceedings of SPE Annual Technical Conference and Exhibition; San Antonio, Texas, October 9-11. SPE Paper 187096.

Johannessen, A. M. and Spildo, K. 2013. Enhanced oil recovery (EOR) by combining surfactant with low salinity injection. Energy Fuels, 27(10), 5738–5749.

Joonaki, E. and Ghanaatian, S. 2014. The application of nanofluids for enhanced oil recovery: effects on interfacial tension and coreflooding process. J. Pet. Sci. Technol., 32(21), 2599–2607.

Jorgensen, W. L.; Maxwell, D. S. and Tirado-Rives, J. 1996. Development and testing of the OPLS all-atom force field on conformational energetics and properties of organic liquids. J. Am. Chem. Soc., 118, 11225–11236.

Kadhum, M. J.; Swatske, D. P.; Chen, C.; et al. 2015. Propagation of carbon nanotube hybrids through porous media for advancing oilfield technology. In Proceedings of SPE International Symposium on Oilfield Chemistry; The Woodlands, Texas, April 13-15. SPE Paper 173781.

Kamal, M. S.; Sultan, A. S.; Al; Mubaiyedh, U. A.; et al. 2015. Rheological properties of thermoviscosifying polymers in high-temperature and high-salinity environments. Can. J. Chem. Eng., 93(7), 1194–1200.

Kamal, M. S.; Hussein, I. A.; Sultan, A. S. 2017. Review on surfactant flooding: phase behavior, retention, IFT, and field applications. Energy Fuels, 31(8), 7701–7720.

Kamal, M. S.; Hussain, S. M. S.; Fogang, L. T. 2018. A zwitterionic surfactant bearing unsaturated tail for enhanced oil recovery in high-temperature high-salinity reservoirs. J. Surfact. Deterg., 21, 165–174.

Kandiban, M.; Vigneshwaran, P.; Potheher, I. V. 2015. Synthesis and characterization of MgO nanoparticles for photocatalytic applications.

Kanj, M. Y.; Rashid, M. H.; Giannells, E. 2011. Industry first field trial of reservoir nanoagents. In Proceedings of SPE Middle East Oil and Gas Show and Conference; Manama, Bahrain, September 25-28. SPE Paper 142592.

Karimi, A.; Fakhroueian, Z.; Bahramian, A.; et al. 2012. Wettability alteration in carbonates using zirconium oxide nanofluids: EOR implications. Energy Fuels, 26(2), 1028–1036.

Kiani, S.; Samimi, A.; Rashidi, A. 2016a. Novel one-pot dry method for large-scale production of nano γ-Al_2O_3 from gibbsite under dry conditions. Monatsh. Chem., 1–7.

Kiani, S.; Zadeh, M. M.; Khodabakhshi, S.; et al. 2016b. Newly prepared Nano gamma alumina and its application in enhanced oil recovery: an approach to low-salinity waterflooding. Energy Fuels, 30(5), 3791–3797.

Kiani, M.; Hsu, T.; Roostapour, A.; et al. 2019. A Novel Enhanced Oil Recovery Approach to Water Flooding in Saskatchewan's Tight Oil Plays. Proceedings of the Unconventional Resources Technology Conference; Denver, Colorado, July 22–24. URTeC Paper 419.

Kim, I.; Taghavy, A.; DiCarlo, D.; Huh, C. 2015. Aggregation of silica nanoparticles and its impact on particle mobility under high-salinity conditions. J. Pet. Sci. Eng., 133, 376–383.

Kong, X.; Ohadi, M. 2010. Applications of micro and nano technologies in the oil and gas industry-an overview of the recent progress. In Proceedings of SPE Abu Dhabi International Petroleum Exhibition and Conference; Abu Dhabi, UAE, November 1-4. SPE Paper 138241.

Koopal, L. K.; Lee, E. M.; Bohmer, M. R. 1995. Adsorption of cationic and anionic surfactants on charged metal oxide surfaces. J. Colloid Interface Sci., 170(1), 85–97.

Kothari, N.; Raina, B.; Chandak, K. B.; et al. 2010. Application of ferrofluids for enhanced surfactant flooding in IOR. In Proceedings of SPE EUROPEC/EAGE Annual Conference and Exhibition; Barcelona, Spain, June 14-17. SPE Paper 131272.

Kumar, A.; Mandal, A. 2017. Synthesis and physiochemical characterization of zwitterionic surfactant for application in enhanced oil recovery. J. Mol. Liq., 243, 61–71.

Kumar, A.; Mandal, A. 2018. Characterization of rock-fluid and fluid-fluid interactions in presence of a family of synthesized zwitterionic surfactants for application in enhanced oil recovery. Colloids and Surfaces A: Physicochemical and Engineering Aspects, 549, 1–12.

Kumar, K.; Dao, E. K.; Mohanty, K. K. 2005. Atomic force microscopy study of wettability alteration by surfactants. SPE J., 13(2). SPE Paper 93009.

Langmuir, I. 1916. The adsorption of gases on plane surfaces of glass, mica and platinum. J. Am. Chem. Soc., 38, 2221–2295.

Lara, L. S.; Rigo, V. A.; Miranda, C. R. 2016. Functionalized silica nanoparticles within multicomponent oil/brine interfaces: a study in molecular dynamics. J. Phys. Chem. C, 120(12), 6787–6795.

Latiff, N. R. A.; Yahya, N.; Zaid, H. M.; Demiral, B. 2011. Novel enhanced oil recovery method using dielectric zinc oxide nanoparticles activated by electromagnetic waves. In Proceedings of National Postgraduate Conference (NPC).

Lefever, J.; Martiniuk, C.; Dancsok, E.; Mahnic, P. 1991. Petroleum potential of the Middle Member, Bakken Formation, Williston Basin. Sixth International Symposium, October 7, (SP11), 74–94.

Le, N. Y. T.; Pham, D. K.; Le, K. H.; Nguyen, P. T. 2011. Design and screening of synergistic blends of SiO_2 nanoparticles and surfactants for enhanced oil recovery in high-temperature reservoirs. Advances in Natural Sciences: Nanoscience and Nanotechnology, 2 (3).

Li, H.; Hart, B.; Dawson, M.; Radjef, E. 2015a. Characterizing the Middle Bakken: laboratory measurement and rock typing of the Middle Bakken Formation. In Proceedings of Unconventional Resources Technology Conference; San Antonio, Texas, July 20-22. URTeC Paper 2172485.

Li, N.; Zhang, G.; Ge, J.; et al. 2011. Adsorption behavior of betaine-type surfactant on quartz sand. Energy Fuels, 25(10), 4430–4437.

Li, R.; Jiang, P.; Gao, C.; et al. 2017. Experimental investigation of silica-based nanofluid enhanced oil recovery: the effect of wettability alteration. Energy Fuels, 31(1), 188–197.

Li, R.; Hirasaki, G.; Masaimeh, S. K. 2012. Wettability alteration and foam mobility control in a layered, 2D heterogeneous sandpack. SPE J., 17(04); SPE Paper 141462.

Li, S.; Torsæter, O. 2015. Experimental investigation of the influence of nanoparticles adsorption and transport on wettability alteration for oil wet berea sandstone. In Proceedings of SPE Middle East Oil & Gas Show and Conference; Manama, Bahrain, March 8-11. SPE Paper 172539.

Li, S. 2016. An experimental investigation of enhanced oil recovery mechanisms in nanofluid injection process. PhD Thesis, Norwegian University of Science and Technology, Trondheim, Norway.

Li, S.; Genys, M.; Wang, K.; Torsæter, O. 2015b. Experimental study of wettability alteration during nanofluid enhanced oil recovery process and its effect on oil recovery. In

Proceedings of SPE Reservoir Characterisation and Simulation Conference and Exhibition; Abu Dhabi, UAE, September 14-16. SPE Paper 175610.

Li, S.; Hadia, N. J.; Lau, H. C.; et al. 2018. Silica nanoparticles suspension for enhanced oil recovery, stability behavior and flow visualization. In Proceedings of SPE Europec featured at 80th EAGE Conference and Exhibition; Copenhagen, Denmark, June 11-14. SPE Paper 190802.

Li, Y.; Dai, C.; Zhou, H.; et al. 2017a. A novel nanofluid based on fluorescent carbon nanoparticles for enhanced oil recovery. Ind. Eng. Chem. Res., 56(44), 12464–12470.

Li, Y.; Dai, C.; Zhou, H.; et al. 2017b. Investigation of spontaneous imbibition by using a surfactant-free active silica water-based nanofluid for enhanced oil recovery. Energy Fuels, 32(1), 287–293.

Lian, B.; Deng, J.; Leslie, G.; et al. 2017. Surfactant modified graphene oxide laminates for filtration. Carbon, 116, 240–245.

Lu, T.; Li, Z.; Zhou, Y.; Zhang, C. 2017. Enhanced oil recovery of low-permeability cores by SiO_2 nanofluid. Energy Fuels, 31(5), 5612–5621.

Luo, D.; Wang, F.; Zhu, J.; et al. 2016. Nanofluid of graphene-based amphiphilic Janus nanosheets for tertiary or enhanced oil recovery: high performance at low concentration. PNAS, 113 (28), 7711–7716.

Lv, W.; Bazin, B.; Ma, D.; et al. 2011. Static and dynamic adsorption of anionic and amphoteric surfactants with and without the presence of alkali. J. Pet. Sci. Eng., 77 (2), 209-218.

Jha, N. K.; Iglauer, S.; Barifcani, A.; et al. 2019. Low-salinity surfactant nanofluid formulations for wettability alteration of sandstone: role of the SiO_2 nanoparticle concentration and divalent cation/SO_4^{2-} ratio. Energy Fuels, 33(2), 739–746.

Jung, H. Y.; Onishi, T.; Datta-Gupta, A. 2018. Numerical simulation of EOR from wettability alteration in tight oil reservoir with multiple hydraulic fractures. In Proceedings of SPE Annual Technical Conference and Exhibition; Dallas, Texas. September 24-26. SPE Paper 191409.

Kazempour, M.; Kiani, M.; Nguyen, D.; et al. 2018. Boosting oil recovery in unconventional resources utilizing wettability altering agents: successful translation from laboratory to field. Proceedings of the Society of Petroleum Engineers (SPE) Improved Oil Recovery Conference; Oklahoma, USA, April 14-18. SPE Paper 190172.

Kuang, W.; Saraji, S.; Piri, M. 2018. A systematic experimental investigation on the synergistic effects of aqueous nanofluids on interfacial properties and their implications for enhanced oil recovery. Fuel, 220, 849–870.

Ma, X.; Lee, N. H.; Oh, H.; et al. 2010. Surface modification and characterization of highly dispersed silica nanoparticles by a cationic surfactant. Colloids and Surfaces A: Physicochemical and Engineering Aspects, 358(1–3), 172–173.

Maghzi, A.; Kharrat, R.; Mohebbi, A.; Ghazanfari, M. H. 2014. The impact of silica nanoparticles on the performance of polymer solution in presence of salts in polymer flooding for heavy oil recovery. Fuel, 123, 123–132.

MeElfresh, P. M. Holcomb, D. L; Ector, D. 2012a. Application of nanofluid technology to improve recovery in oil and gas wells. In Proceedings of SPE International Oilfield Nanotechnology Conference and Exhibition; Noordwijk, The Netherlands. June 12-14. SPE Paper 154827.

MeElfresh, P. M. Wood, M.; Ector, D. 2012b. Stabilizing nano particle dispersions in high salinity, high temperature downhole environments. In Proceedings of SPE International Oilfield Nanotechnology Conference and Exhibition; Noordwijk, The Netherlands. June 12-14. SPE Paper 154827.

Metin, C. O.; Lake, L. W.; Miranda, C. R.; Nguyen, Q. P. 2011. Stability of aqueous silica nanoparticle dispersions. J. Nanopart. Res., 13, 839–850.

Metin, C. O.; Baran, J. R.; Nguyen, Q. P. 2012. Adsorption of surface functionalized silica nanoparticles onto mineral surfaces and decane/water interface. J. Nanopart. Res., 14, 1246.

Metin, C. O.; Bonnecaze, R. T.; Lake, L. W.; et al. 2014. Aggregation kinetics and shear rheology of aqueous silica suspensions. Applied Nanoscience, 4(2), 169–178.

Miranda, C. R.; Lara, L. S.; Tonetto, B. C. 2012. Stability and mobility of functionalized silica nanoparticles for enhanced oil recovery applications. In Proceedings of SPE International Oilfield Nanotechnology Conference and Exhibition; Noordwijk, The Netherlands. June 12-14. SPE Paper 157033.

Mohajeri, M.; Hemmati, M.; Shekarabi, A. S. 2015. An experimental study on using a nanosurfactant in an EOR process of heavy oil in a fractured micromodel. J. Petrol. Sci. Eng., 126, 162–173.

Monfared, A. D.; Ghazanfari, M. H.; Jamialahmadi, M.; Helalizadeh, A. 2016. Potential application of silica nanoparticles for wettability alteration of oil-wet calcite: A mechanistic study. Energy Fuels, 30(5), 3947–3961.

Moslan, M. S.; Wan Sulaiman, W. R.; Ismail, A. R.; et al. 2016. Wettability alteration of dolomite rock using nanofluids for enhanced oil recovery. Materials Science Forum, 864, 194–198.

Murray, B. S.; Ettelaie, R. 2004. Foam stability: proteins and nanoparticles. Curr. Opin. Colloid Interface Sci., 9(5), 314–320.

Naje, A. N.; Norry, A. S.; Suhail, A. M. Preparation and characterization of SnO_2 nanoparticles. 2013. Int. J Innovative Res. Sci., Eng. Technol., 2(12), 7068–7072.

Napper, D. H. 1983. Polymeric stabilization of colloidal dispersions. Academic Press, New York.

Nassar, N. N.; Al-Jabari, M. E.; Husein, M. M. 2008. Removal of asphaltenes from heavy oil by nickel nano and micro particle adsorbents. In Proceedings of the IASTED International Conference NANOTECHNOLOGY AND APPLICATIONS (NANA 2008); Crete, Greece. September 29-October 1.

Negin, C.; Ali, S.; Xie, Q. 2016. Application of nanotechnology for enhancing oil recovery-A review. Petroleum, 2, 324–333.

Nguyen, A.; Schulze, H. J. Colloidal science of flotation. 2003. New York: Marcel Dekker, pp. 80–105.

Nieto-Alvarez, D. A.; Zamudio-Rivera, L. S.; Luna-Rojero, E. E.; et al. 2014. Adsorption of zwitterionic surfactant on limestone measured with high-performance liquid chromatography: micelle-vesicle influence. Langmuir, 30 (41), 12243–12249.

Nieto-Alvarez, D. A.; Marn-Leon, A.; Luna-Rojero, E. E.; et al. 2018. Nonquilibrium and equilibrium stationary states of zwitterionic surfactant dynamic adsorption on limestone cores at oil-reservoir conditions. Ind. Eng. Chem. Res., 57(6), 2075–2082.

Nourafkan, N.; Hu, Z.; Wen, D. 2018. Nanoparticle-enabled delivery of surfactants in porous media. J. Colloid Interface Sci., 519, 44–57.

Nosé, S. A. 1984. A unified formulation of the constant temperature molecular dynamics methods. J. Chem. Phys., 81, 511–519.

Nwidee, L. N.; Al-Anssari, S.; Barifcani, A.; et al. 2016. Nanofluids for enhanced oil recovery processes: wettability alteration using zirconium oxide. In Proceedings of Offshore Technology Conference Asia; Kuala Lumpur, Malaysia, March 22-25. OTC Paper 26573.

Nwidee, L. N.; Al-Anssari, S.; Barifcani, A.; et al. 2017. Nanoparticles influence on wetting behaviour of fractured limestone formation. J. Petrol. Sci. Eng., 149, 782–788.

Ogolo, N. A.; Olafuyi, O. A.; Onyekonwu, M. O. 2012. Enhanced oil recovery using nanoparticles. In Proceedings of SPE Saudi Arabia Section Technical Symposium and Exhibition; Al-Khobar, Saudi Arabia, April 8-11. SPE Paper 160847.

Omurlu, C.; Pham, H.; Straatsma, T. P. 2016. Interaction of surface-modified silica nanoparticles with clay minerals. Appl. Nanosci., 6, 1167–1173.

Onyekonwu, M. O.; Ogolo, N. A. 2010. Investigting the use of nanoparticles in enhancing oil recovery. In Proceedings of the Nigeria Annual International Conference and Exhibition, Tinapa-Calabar, Nigeria, July 31-August 7. SPE Paper 140744.

Paria, S.; Kartic, C. K. 2004. A review on experimental studies of surfactant adsorption at the hydrophilic solid-water interface. Adv. Colloid Interface Sci., 110, 75–95.

Park, B. J.; Pantina, J. P.; Furst, E. M.; et al. 2008. Direct measurements of the effects of salt and surfactant on interaction forces between colloidal particles at water-oil interfaces. Langmuir, 24(5), 1686–1694.

Parrinello, M.; Rahman, A. 1981. Polymorphic transitions in single crystals: A new molecular dynamics method. J. Appl. Phys., 52, 7182–7190.

Patil, G. E.; Kajale, D. D.; Gaikwad, V. B.; Jain, G. H. 2012. Preparation and characterization of SnO_2 nanoparticles by hydrothermal route. Int Nano Lett., 2, 17.

Patil, P. D.; Rohilla, N.; Katiyar, A.; et al. 2018. Surfactant based EOR for tight oil reservoirs through wettability alteration: novel surfactant formulations and their efficacy to induce

spontaneous imbibition. In Proceedings of SPE EOR Conference at Oil & Gas West Asia; Muscat, Oman, March 26-28. SPE Paper 190397.

Peng, C.; Guo, J.; Yang, W.; et al. 2016. Synthesis of three-dimensional flower-like hierarchical ZnO nanostructure and its enhanced acetone gas sensing properties. J. Alloys Compd., 654, 371–378.

Plimpton, S. 1995. Fast parallel algorithms for short-range molecular dynamics. J. Comp. Phys., 117, 1–19.

Pope, G. A. Recent developments and remaining challenges of enhanced oil recovery. 2011. J. Pet. Technol., 63 (7), 65–68.

Prajapati, R. R.; Bhagwat, S. S. Effect of foam boosters on Krafft temperature. 2012. J. Chem. Eng. Data, 57(3), 869–874.

Puerto, M.; Hirasaki, G. J.; Miller, C. A.; Barnes, J. R. 2010. Application of internal olefin sulfonates and other surfactants to EOR. Part 1: Structure-performance relationships for selection at different reservoir conditions. In Proceedings of SPE Improved Oil Recovery Symposium; Tulsa, Oklahoma, April 24-28. SPE Paper 129766.

Qiu, F. 2010. The potential applications in heavy oil EOR with the nanoparticle and surfactant stabilized solvent–based emulsion. In Proceedings of Canadian Unconventional Resources and International Petroleum Conference; Calgary, Alberta, October 19-21. SPE Paper 134613.

Radnia, H.; Rashidi, A.; Nazar, A. R. S.; et al. 2018. A novel nanofluid based on sulfonated graphene for enhanced oil recovery. J. Mol. Liq., 2018, 271, 795–806.

Randviir, E. P.; Banks, C. E. 2017. Graphene and graphene oxide for energy storage. Nanotechnol. Energy Sustain, 725–744.

Ranka, M.; Brown, P.; Hatton, T. A. 2015. Responsive stabilization of nanoparticles for extreme salinity and high-temperature reservoir applications. ACS Appl. Mater. Interfaces, 7(35), 19651–19658.

Ravera, F.; Santini, E.; Loglio, G.; et al. 2006. Effect of nanoparticles on the interfacial properties of liquid/liquid and liquid/air surface layers. Phys. Chem. B, 110, 19543–19551.

Ravera, F.; Ferrari, M.; Liggieri, L.; et al. 2008. Liquid-liquid interfacial properties of mixed nanoparticle-surfactant systems. Colloids and Surfaces A: Physicochemical and Engineering Aspects, 323(1–3), 99–108.

Rellegadla, S.; Bairwa, H. K.; Kumari, M. R.; et al. 2018. An effective approach for enhanced oil recovery using nickel nanoparticles assisted polymer flooding, Energy Fuels, 32(11), 11212–11221

Rezvani, H.; Khalilnezhad, A.; Ganji, P.; Kazemzadeh, Y. 2018. How ZrO_2 nanoparticles improve the oil recovery by affecting the interfacial phenomena in the reservoir conditions? J. Mol. Liq., 252, 158–168.

Rosen, M. J. Surfactants and interfacial phenomena, 2nd ed. 1989. John Wiley & Sons, Inc.: New York, pp. 33–63.

Roustaei, A. 2014. An evaluation of spontaneous imbibition of water into oil-wet carbonate reservoir cores using nanofluid. Petrophysics, 55(01). Paper SPWLA-2014-v55n1a3.

Roustaei, A.; Bagherzadeh, H. 2015. Experimental investigation of SiO_2 nanoparticles on enhanced oil recovery of carbonate reservoirs. J. Pet. Explor. Prod. Technol., 2, 27–33.

Rui, Z.; Cui, K.; Wang, X.; et al. 2018. A quantitative framework for evaluating unconventional well development. J. Pet. Sci. Eng., 166, 900–905.

Ryckaert, J. P.; Ciccotti, G.; Berendsen, H. J. C. 1977. Numerical integration of the cartesian equations of motion of a system with constraints: molecular dynamics of n-alkanes. J. Comput. Phys., 23, 327–341.

Sagala, F.; Montoya, T.; Hethnawi, A.; et al. 2019. Nanopyroxene-based nanofluids for enhanced oil recovery in sandstone cores at reservoir temperature. Energy Fuels, 33(2), 877–890.

Saha, R.; Uppaluri, R. V. S.; Tiwari, P. 2018. Silica nanoparticle assisted polymer flooding of heavy crude oil: emulsification, rheology, and wettability alteration characteristics. Ind. Eng. Chem. Res., 57(18), 6364-6376.

Sedaghat, M. H.; Mohammadi, H.; Razmi, R. 2015. Application of SiO_2 and TiO_2 nano particles to enhance the efficiency of polymer-surfactant floods. Journal of Energy Sources, Part A: Recovery, Utilization, and Environmental Effects, 38(1), 22–28.

Shah, D. O.; Schechter, R. S. 2012. Improved oil recovery by surfactant and polymer flooding. Elsevier: New York.

Shah, R. D. 2009. Application of nanoparticle saturated injectant gases for EOR of heavy oils. In Proceedings of SPE Annual Technical Conference and Exhibition; New Orleans, Louisiana, October 4-7. SPE Paper 129539.

Sharma, K.; Aswal, V. K.; Kumaraswamy, G. 2010. Adsorption of nonionic surfactant on silica nanoparticles: structure and resultant interparticle interactions. J. Phys. Chem. B, 114(34), 10986–10994.

Sharma, T.; Iglauer, S.; Sangwai, J. S. 2016. Silica nanofluids in an oilfield polymer polyacrylamide: interfacial properties, wettability alteration, and applications for chemical enhanced oil recovery. Ind. Eng. Chem. Res., 55(48), 12387–12397.

Shekhawat, D. S.; Aggarwai, A.; Agarwai, S.; Imtiza, M. 2016. Magnetic recovery–injecting newly designed magnetic fracturing fluid with applied magnetic field for EOR. In Proceedings of SPE Asia Pacific Hydraulic Fracturing Conference; Beijing, China, August 24–26. SPE Paper 181853.

Shokriu, Y. H.; Babadagli, T. 2011. Transportation and interaction of nano and micro size metal particles injected to improve thermal recovery of heavy-oil. In Proceedings of SPE Annual Technical Conference and Exhibition; Denver, Colorado, October 30-November 2. SPE Paper 146661.

Sierra-Fernandez, A.; Gomez-Villalba, L. S.; Rabanal, M. E.; Fort, R. 2017. New nanomaterials for applications in conservation and restoration of stony materials: a review. Materiales de Construcción, 67 (325), 107.

Sis, H. and Birinci, M. 2009. Effect of nonionic and ionic surfactants on zeta potential and dispersion properties of carbon black powders. Colloids and Surfaces A: Physicochemical and Engineering Aspects, 341, 60–67.

Sofla, S. J. D.; James, A. A., Zhang, Y. 2018. Insight into the stability of hydrophilic silica nanoparticles in seawater for enhanced oil recovery implications. Fuel, 216, 559–571.

Song, B.; Hu, X.; Shui, X.; et al. 2016. A new type of renewable surfactants for enhanced oil recovery: Dialkylpolyoxyethylene ether methyl carboxyl betaines. Colloids and Surfaces A: Physicochemical and Engineering Aspects, 489, 433–440.

Songolzadeh, R.; Moghadasi, J. 2017. Stabilizing silica nanoparticles in high saline water by using ionic surfactants for wettability alteration application. Colloid. Polym. Sci., 295, 145–155.

Sonnenberg, S. A.; Vickery, J.; Theloy, C.; Sarg, J. F. 2011. Middle Bakken facies, Williston Basin, USA: a key to prolific production. In Proceedings of AAPG Annual Convention and Exhibition; Houston, Texas, April 10-13. SPE Paper 50449.

Standnesm D. C.; Austad, T. 2000. Wettability alteration in chalk: mechanism for wettability alteration from oil-wet to water-wet using surfactants. J. Pet. Sci. Eng., 28(3), 123–143.

Stukowski, A. 2010. Visualization and analysis of atomistic simulation data with OVITO-the open visualization tool. Modelling Simul. Mater. Sci. Eng., 18(1), 015012.

Suleimanov, B. A.; Ismailov, F. S.; Veliyev, E. F. 2011. Nanofluid for enhanced oil recovery. J. Pet. Sci. Eng., 78, 431–437.

Sun, Q.; Li, Z.; Li, S.; et al. 2014. Utilization of surfactant-stabilized foam for enhanced oil recovery by adding nanoparticles. Energy Fuels, 28(4), 2384–2394.

Sun, X.; Zhang, Y.; Chen, G.; et al. 2018. Wettability of hybrid nanofluid-treated sandstone/heavy oil/brine systems: Implications for enhanced heavy oil recovery potential. Energy Fuels, 32(11), 11118–11135.

Sun, X.; Zhang, Y.; Chen, G.; Gai, Z. 2017. Application of nanoparticles in enhanced oil recovery: a critical review of recent progress. Energies, 10(3), 345.

Tajmiri, M.; Mousavi, S. M.; Ehsani, M. R.; et al. 2015. Wettability alteration of sandstone and carbonate rocks by using zno nanoparticles in heavy oil reservoirs. Iranian J. Oil Gas Sci. Technol., 4(4), 50–66.

Thammachart, M.; Meeyoo, V.; Risksomboon, T.; Osuwan, S. 2001. Catalytic activity of CeO_2-ZrO_2 mixed oxide catalysts prepared via Sol-gel technique: CO oxidation. Catal. Today, 63, 53–61.

Thomas, S. 2008. Enhanced oil recovery - an overview. Oil Gas Sci. Technol., 63, 9–19.

Tsuzuki, T.; McCormick, P. G. 2004. Mechanochemical synthesis of nanoparticles. J. Mater. Sci., 39, 5143–5146.

Ugwekar, R. P.; Lakhawat, G. P. 2014. Synthesis and characterization of nano-sized copper oxide by X-ray diffraction & scanning electron microscopy. International Journal of Scientific & Engineering Research, 5(2).

Villamizar, L. C.; Lohateeraparp, P.; Harwell, J. H.; et al. 2010. Interfacially active SWNT/silica nanohybrid used in enhanced oil recovery. In Proceedings of SPE Improved Oil Recovery Symposium; Tulsa, Oklahoma, April 24-28. SPE Paper 129901.

Vu, T. V.; Papavassiliou, D. V. 2019. Synergistic effects of surfactants and heterogeneous nanoparticles at oil-water interface: insights from computations. J. Colloid Interface Sci., 553(1), 50–58.

Wan, Y.; Shi, Y.; Zhao, D. 2007. Designed synthesis of mesoporous solids via nonionic-surfactant-templating approach. Chem. Commun., 9, 897–926.

Wang, D.; Liu, C.; Wu, W.; Wang, G. 2010. Novel surfactants that attain ultra-low interfacial tension between oil and high salinity formation water without adding alkali, salts, co-surfactants, alcohols and solvents. In Proceedings of SPE EOR Conference at Oil & Gas West Asia; Muscat, Oman, April 11-13. SPE Paper 127452.

Wang, D. M.; Butler, R.; Liu, H.; Ahmed, S. 2011. Surfactant formulation study for Bakken shale imbibition. In Proceedings of SPE Annual Technical Conference and Exhibition; Denver, Colorado, October 30-November 2. SPE Paper 145510.

Wang, X.; Hou, J.; Song, S.; et al. 2018. Combining pressure-controlled porosimetry and rate-controlled porosimetry to investigate the fractal characteristics of full-range pores in tight oil reservoirs. J. Pet. Sci. Eng., 171, 353–361.

Wang, Y.; Ge, J.; Zhang, G.; et al. 2015. Adsorption behavior of dodecyl hydroxypropyl sulfobetaine on limestone in high salinity water. RSC Adv., 5, 59738–59744.

Wang, Y.; Ma, C.; Sun, X.; Li, H. 2002. Preparation and characterization of SnO_2 nanoparticles with a surfactant–mediated method. Nanotechnology, 13, 565–569.

Wei, B.; Li, Q.; Jin, F.; et al. The potential of a novel nanofluid in enhancing oil recovery. Energy Fuels, 2016, 30, 2882–2891.

Wijayanto, T.; Kurihara, M.; Kurniawan, T.; Muraza, O. 2019. Experimental investigation of aluminosilicate nanoparticles for enhanced recovery of waxy crude oil. Energy Fuels, 33(7), 6076–6082.

Worthen, A. J.; Foster, L. M.; Dong, J. N.; et al. 2014. Synergistic formation and stabilization of oil-in-water emulsions by a weakly interacting mixture of zwitterionic surfactant and silica nanoparticles. Langmuir, 30(4), 984–994.

Worthen, A. J.; Tran, V.; Cornell, K. A.; et al. 2016. Steric stabilization of nanoparticles with grafted low molecular weight ligands in highly concentrated brines including divalent ions. Soft Matter, 12, 2025–2039.

Wu, Y.; Chen, W.; Dai, C.; et al. 2017. Reducing surfactant adsorption on rock by silica nanoparticles for enhanced oil recovery. J. Pet. Sci. Eng., 153, 283–287.

Wu, Y.; Iglauer, S.; Shuler, P.; et al. 2010. Branched alkyl alcohol propoxylated sulfate surfactants for improved oil recovery. Tenside, Surfactants, Deterg., 47 (3), 152–161.

Wu, Y.; Shuler, P. J.; Bianco, M; et al. 2008. An experimental study of wetting behavior and surfactant EOR in carbonates with model compounds. SPE J., 13(01). SPE Paper 99612.

Xu, D.; Bai, B.; Meng, Z.; et al. 2018. A novel ultra-low interfacial tension nanofluid for enhanced oil recovery in super-low permeability reservoirs. In Proceedings of SPE Asia Pacific Oil and Gas Conference and Exhibition; Brisbane, Australia, October 23-25. SPE Paper 192113.

Xu, K.; Zhu, P.; Huh, C.; Balhoff, M. T. 2015. Microfluidic investigation of nanoparticles' role in mobilizing trapped oil droplets in porous media. Langmuir, 31(51), 13673–13679.

Xu, K.; Agrawal, D.; Darugar, Q. 2018. Hydrophilic nanoparticle-based enhanced oil recovery: microfluidic investigations on mechanisms. Energy Fuels, 32(11), 11243–11252.

Xu, Z.; Yang, X.; Yang, Z. 2008. On the mechanism of surfactant adsorption on solid surfaces: free–energy investigations. J. Phys. Chem. B, 112(44), 13802–13811.

Xue, Z.; Foster, E.; Wang, Y.; et al. 2014. Effect of grafted copolymer composition on iron oxide nanoparticle stability and transport in porous media at high salinity. Energy Fuels, 28(6), 3655–3665.

Yahya, N.; Kashif, M.; Nasir, N.; et al. 2012. Cobalt ferrite nanoparticles: an innovative approach for enhanced oil recovery application. Journal of Nano Research, 17, 115–126.

Yan, Q.; Gozin, M.; Zhao, F.; et al. 2016. Highly energetic compositions based on functionalized carbon nanomaterials. Nanoscale, 8, 4799–4851.

Youssif, M. I.; El-Maghraby, R. M.; Saleh, S. M.; ElgibalyA. A. 2018. Sol-gel tailored synthesized nanosilica for enhanced oil recovery in water-wet and oil-wet benthemier sandstone. Energy Fuels, 32(12), 12373–12382.

You, Y.; Jin, X.; Wen, X.; et al. 2018. Application of graphene oxide membranes for removal of natural organic matter from water. Carbon, 129, 415–419.

Yu, J.; Berlin, J. M.; Lu, W.; et al. 2010. Transport study of nanoparticles for oilfield application. In Proceedings of SPE International Conference on Oilfield Scale; Aberdeen, UK, May 26-27. SPE Paper 131158.

Yu, J.; Cheung, K. W.; Yan, W.; et al. 2017. High-sensitivity low-power tungsten doped niobium oxide nanorods sensor for nitrogen dioxide air pollution monitoring. Sensors Actuators B Chem., 238, 204–213.

Yuan, B.; Wang, W.; Moghanloo, R. G.; et al. 2017. Permeability reduction of Berea cores owing to nanoparticle adsorption onto the pore surface: mechanistic modeling and experimental work. Energy Fuels, 31(1), 795–804.

Zaid, H. M.; Yahya, N.; Latiff, N. R. A. 2012. The effect of nanoparticles crystallite size on the recovery efficiency in dielectric nanofluid flooding. J. Nano Res., 21, 103–108.

Zallaghi, M.; Kharrat, R.; Hashemi, A. 2018. Improving the microscopic sweep efficiency of water flooding using silica nanoparticles. J. Pet. Explor. Prod. Technol., 8(1), 259–269.

Zargartalebi, M.; Barati, N.; Kharrat, R. 2014. Influences of hydrophilic and hydrophobic silica nanoparticles on anionic surfactant properties: interfacial and adsorption behaviors. J. Pet. Sci. Eng., 119, 36–43.

Zargartalebi, M.; Kharrat, R.; Barati, N. 2015. Enhancement of surfactant flooding performance by the use of silica nanoparticles. Fuel, 143, 21–27.

Zeng, T.; Miller, C. S.; Mohanty, K. 2018. Application of surfactants in shale chemical EOR at high temperatures. Proceedings of the Society of Petroleum Engineers (SPE) Improved Oil Recovery Conference; Oklahoma, USA, April 14-18. SPE Paper 190318.

Zeyghami, M.; Kharrat, R.; Ghazanfari, M. H. 2014. Investigation of the applicability of nano silica particles as a thickening additive for polymer solutions applied in EOR processes. Energy Source Part A, 36, 1315–1324.

Zhang, Q.; Cai, B.; Gang, H.; et al. 2014. A family of novel bio-based zwitterionic surfactants derived from oleic acid. RSC Adv., 4, 38393–38396.

Zhao, J.; Dai, C.; Ding, Q.; et al. 2015. The structure effect on the surface and interfacial properties of zwitterionic sulfobetaine surfactants for enhanced oil recovery. RSC Adv., 5, 13993–14001.

Zhao, G.; Khin, C. C.; Chen, S. B.; Chen, B. 2005. Nonionic surfactant and temperature effects on the viscosity of hydrophobically modified hydroxyethyl cellulose solutions. J. Phys. Chem. B, 109(29), 14198–14204.

Zhao, L.; Li, A.; Chen, K.; et al. 2012. Development and evaluation of foaming agents for high salinity tolerance. J. Pet. Sci. Eng., 81, 18–23.

Zhao, M.; Lv, W.; Li, Y.; et al. 2018. Study on the synergy between silica nanoparticles and surfactants for enhanced oil recovery during spontaneous imbibition. J. Mol. Liq., 26, 373–378.

Zheng, R.; Li, S.; Li, X. 2018a. Study on the relations between controlling mechanisms and dissociation front of gas hydrate reservoirs. Appl. Energ., 215, 405–415.

Zheng, R.; Li, S.; Li, X. 2018b. Sensitivity analysis of hydrate dissociation front conditioned to depressurization and wellbore heating. Mar. Petrol. Geol., 91, 631–638.

Zhong, X.; Pu, H.; Zhou, Y.; Zhao, J. X. 2019a. Comparative study on the static adsorption behavior of zwitterionic surfactants on minerals in Middle Bakken Formation. Energy Fuels, 33(2), 1007–1015.

Zhong, X.; Li, C.; Pu, H.; et al. 2019b. Increased nonionic surfactant efficiency in oil recovery by integrating with hydrophilic silica nanoparticle. Energy Fuels, 33(9), 8522–8529.

Zhong, X.; Pu, H.; Zhou, Y.; Zhao, J. X. 2018. Static adsorption of surfactants on Bakken rock surfaces in high temperature, high salinity conditions. In Proceedings of the SPE

International Conference on Oilfield Chemistry; Galveston, Texas, April 8-9. SPE Paper 193589.

Zhu, D.; Wei, L.; Wang, B.; Feng, Y. 2014. Aqueous hybrids of silica nanoparticles and hydrophobically associating hydrolyzed polyacrylamide used for EOR in high-temperature and high-salinity reservoirs. Energies, 7(6), 3858–3871.

Zhu, L.; Li, Y.; Zeng, W. 2018. Hydrothermal synthesis of hierarchical flower-like ZnO nanostructure and its enhanced ethanol gas-sensing properties. Appl. Surf. Sci., 427(Part B), 281–287.

Zuniga, C. A.; Goods, J. B.; Cox, J. R.; et al. 2016. Long-term high-temperature stability of functionalized graphene oxide nanoplatelets in Arab-D and API Brine. ACS Appl. Mater. Interfaces 8(3), 1780–1785.